POLITECNICO
MILANO 1863

SCUOLA DI INGEGNERIA INDUSTRIALE
E DELL'INFORMAZIONE

First Approach to a Model-based Control System for Optimal Microaeration in Anaerobic Digestion

Tesi di Laurea Magistrale in
Chemical Engineering - Ingegneria Chimica

Author: **Federico Rocca**

Student ID: 970819
Advisor: Prof. Giulia Luisa Bozzano
Co-advisors: Ing. Federico Moretta
Academic Year: 2021-22

Abstract

During the 21st century, the most significant challenge the world is facing is the fight against climate change. The exploitation of biomass for energy production represents a practical solution to reduce the carbon dioxide emission impact (i.e., decarbonization). *Anaerobic digestion* transforms organic material into biogas by microbiological reactions in the absence of oxygen. This process is widespread today, but the lack of a detailed engineering approach constrains its further deployment. In addition, the purity of the produced biogas has high standard requirements. Among the pollutants, the most appendant is hydrogen sulfide, a highly toxic for humans and an inhibiting agent for microorganisms. However, it is possible to inject a small amount of oxygen into the digester to convert H_2S to elemental sulfur, which is much easier to remove, being solid. This solution is named *microaeration* and can positively impact the sulfide removal process. This work proposes a model-based control system to minimize oxygen injection while ensuring efficient and sufficient sulfide removal.

The control algorithm lays its basis on a lumped model capable of predicting the sulfate reduction and the microaerobic oxidation mechanism. Consequently, the *Anaerobic Digestion Oxygen Control System* (ADOCS) model is developed and further validated with literature data and an industrial case. The model provides a good compromise between accuracy and complexity and can be efficiently employed in practical contexts. The model efficacy for a control action is later evaluated by applying it in a complete control algorithm. The outcomes confirm that a preventive oxygen injection based on predictive model results efficiently avoids excessive sulfide concentration in the biogas.

Keywords: anaerobic digestion, modeling, microaeration, control, predictive

Abstract in lingua italiana

Nel corso del XXI secolo, la sfida più importante che il mondo sta affrontando è la lotta al cambiamento climatico. Le biomasse sono risorse molto promettenti per ridurre l'impatto delle emissioni di anidride carbonica derivanti dalla produzione di energia. Il processo di digestione anaerobica trasforma il materiale organico in biogas, mediante reazioni microbiologiche in assenza di ossigeno.Questo processo è oggi molto diffuso, ma la mancanza di un approccio ingegneristico dettagliato ne limita l'ulteriore diffusione. Inoltre, la purezza del biogas prodotto ha requisiti di standard elevati. Tra gli inquinanti, il più importante è l'idrogeno solforato, altamente tossico per l'uomo e inibitore dei microrganismi. Tuttavia, è possibile iniettare una ridotta quantità di ossigeno nel digestore per convertire efficacemente l'acido solfidrico in zolfo elementare, molto più semplice da rimuovere essendo solido. Questa soluzione prende il nome di *microaerazione* e può semplificare il processo di rimozione dei solfuri. Questo lavoro propone lo sviluppo di un sistema di controllo basato su un modello matematico in grado di minimizzare l'iniezione di ossigeno, garantendo al contempo una sufficiente rimozione dei solfuri. L'algoritmo di controllo si basa su un modello a parametri concentrati in grado di prevedere la riduzione dei solfati e il meccanismo di ossidazione microaerobica. In primo luogo, viene sviluppato il modello *Anaerobic Digestion Oxygen Control System* (ADOCS), confrontandolo con dati presenti in letteratura e con un caso industriale. I risultati ottenuti permettono di dimostrare che il modello proposto offre un buon compromesso tra accuratezza e complessità, permettendo una sua applicazione in contesti pratici. L'efficacia del modello in un'azione di controllo viene poi valutata applicandolo a un completo algoritmo di controllo. I risultati confermano che un'iniezione preventiva di ossigeno, basata sui risultati del modello predittivo, è efficace nell'evitare un'eccessiva concentrazione di solfuri nel biogas.

Parole chiave: digestione anaerobica, modellazione, microaerazione, controllo, predittivo

Contents

Introduction

During the 21st century, the world is facing the issue of climate change and sustainable transition. A broad range of new technologies, processes, and opportunities are already arising and will keep increasing, both in number and effectiveness, helping face these challenges. Biomass is considered one of this era's most valuable raw materials. It is intrinsically capable of reducing the impacts of CO_2 emissions in various sectors. Indeed, biomass can be converted to a variety of bio-fuels which are less impacting than their fossil counterpart from a double perspective. Firstly, their combustion releases fewer pollutants. Secondly, the carbon dioxide emitted during the final stage derives from that absorbed by the organic matter during its growth.

The most common utilization of biomass for energy purposes consists of biogas production by anaerobic digestion. This microbial-mediated process converts organic materials into a gaseous mixture mainly composed of methane and carbon dioxide, with other minor gases as impurities. The process in the last year is well-established in its practical terms. However, a large margin for optimization is still present due to the complexity of the reactions involved and the consequent difficulties in its mathematical modeling. The varieties of substrates and feedstock utilized only sometimes reflect the optimal choice regarding process efficiency and add additional complexity to the system control.

Biogas is typically used in combined heat and power plants (CHPs), which are burnt in combustion engines to recover energy. This gas can be applied in all of these contexts where fossil fuel methane is now employed, dramatically reducing the associated environmental impact. However, worthy of interest are some higher-value applications of more recent development. These include upgrading biogas to biomethane, where the CH_4 content is more than 95%.

Raw biogas usually contains a large share of methane (50-75%), with the remaining fraction mainly composed of carbon dioxide (25-50%) and other impurities (less than 5%). Among these contaminants, some do not affect the product quality, such as water vapor or oxygen traces, while others can have a significant impact. It is the case of hydrogen sulfide, H_2S, produced from the digestion of sulfur-containing substrates such as proteins.

This toxic, poisonous, and odorous compound produces sulfur oxides if burnt in a combustion engine. Furthermore, it rapidly corrodes any metallic equipment with which it comes in contact, leading to a life-shortening of the pieces of equipment employed if no adequate removal is performed.

The most widespread methods for sulfide removal include physical, chemical, or chemical-physical treatments. These are usually expensive, space, and energy-consuming. A possible solution for H_2S removal is to use another family of bacteria that intervene in an anaerobic digestion system under certain circumstances. This microbial family, named sulfide-oxidizing bacteria (SOBs), can convert the gaseous hydrogen sulfide into solid elemental sulfur, greatly simplifying its removal. However, SOBs are aerobic bacteria and thus require oxygen to live and perform their metabolic reactions, opposite to the environment of biogas production systems which is, by definition, anaerobic.

The condition of adding a limited amount of oxygen in an anaerobic digestion system is known as *microaeration*. It is proven effective in improving such processes in different stages. Indeed, a minimal quantity of oxygen is helpful in hydrolysis enhancement, reactor stabilization, and, as mentioned, sulfide removal. Microaeration has been applied at different scales and for various primary purposes. This solution has been mainly performed with a lack of rigorous scientific basis and limited assessment of its effects. To be a helpful technique and be effectively applied at an industrial scale, there is the need for standardized methods to assess microaeration impact and eventually provide solutions for optimal oxygen injection timing and quantity.

The present work aims at defining a first estimation of a model-based control system to dynamically optimize the microaeration for sulfide removal in an anaerobic digestion system. Such a system is hypothesized as inserted within a complete control algorithm based on the dynamic model of anaerobic digestion also presented. The resulting method triggers a control action whenever, according to the simulated results, an excessive amount of hydrogen sulfide results from the anaerobic digestion of a given influent feedstock. Moreover, a predictive algorithm is also defined to preventively increase the oxygen injection rate when a critical sulfide content is supposed to be reached.

The most critical part of the control algorithm is that it depends on a simulative mathematical representation of the process, and accuracy is thus fundamental. The model should also be flexible to changes in the influent and operating conditions to be applicable in various situations. This work presents a new lumped model that accounts for the effect of oxygen and sulfate reduction processes and is used in the control algorithm. The overall model produced is named ADOCS (Anaerobic Digestion Oxygen Control Systems)

to highlight its feature regarding control purposes. It is derived from the Anaerobic Digestion Model No. 2 (AM2), also referred to as AMOCO from the name of the organization within it has been developed. This latter is considered to be the *state-of-the-art* within models applicable for control purposes in anaerobic digestion since it depends on a few parameters estimable from experimental data.

The work starts by presenting an overview of the transition that the world has to face and the regulatory framework, along with the role that biomass, and bioenergies, in particular, can have. The subsequent chapters present the general features of anaerobic digestion and its mathematical modeling, which is the foundation upon which a dynamic control system should be built. Chapter four presents a potential improvement in the parameter calibration of the AM2 model. Subsequently, chapter five presents the ADOCS model, describing the added reactions and processes. The results are presented within a base-case scenario used as an explicative example, with a final application in an industrial case study. Finally, a preliminary dynamic optimization based on the model mentioned above is performed to show the potential for an application at a full-scale level to achieve a successful microaeration-based sulfide removal. This last chapter also compares a model-predictive and not control system, highlighting the first's potential to avoid excessive sulfide in the resulting biogas.

1 | The Sustainable Transition of the XXI Century

The major challenge of the present century is undoubtedly the struggle against climate change and its consequences, with global warming among all. Although the scientific community has issued numerous warnings since the late 1900s, it has only been in the last decade that the majority of the general population has become aware of the significance and urgency of the issue [1]. Thanks to the divulgation by magazines, newspapers, and

Figure 1.1: Cover page of *Time* magazine special issue on global warming (Apr. 03, 2006) [2].

televisions, a *technical* topic came into the lives of the people, who finally got the intrinsic importance of the message. Today climate change is a fact: it is recognized unanimously

by the scientific community, and many people are involved in the fight against it.

The second decennium of the 2000s has been a game-changing period, with the mass manifestations favoring climate and the environmental issue as a pillar of most governments' agendas. In 2015, under the supervision of the United Nations (UN), two historical treaties were to make effective the sustainable transition: the Paris Agreement [3] and the 2030 Sustainable Development Agenda [4]. These two agreements are interconnected but aim at two different targets: the first is dedicated to climate change, with exact figures to respect to limiting global warming, while the latter has a broader perspective, posing the concrete aspects of developing and improving the living standards of all the people of the world by respecting the planet.

1.1. The Paris Agreement

Every year since 1995, in the scheme provided by the United Nations Framework Convention on Climate Change (UNFCCC), an annual conference is held to evaluate the progress against global warming: the Conference of the Parties (COP). These meetings are those where the world's leaders have reached the most relevant results for environmental issues. Indeed, during COP3, held in Kyoto, Japan, in 1997, the Kyoto Protocol was signed, marking the first international climate awareness milestone. This convention has been subsequently amended in Doha during COP18 (2012) and set the bases for the most ambitious agreement regarding climate: the Paris Agreement. This historic and legally binding international agreement was adopted at COP21, which took place in Paris in December 2015 [3], and is intended to serve as the blueprint for combating climate change in the early years of this century. Announcing the treaty, then-President of the United States Barack Obama stated that its target was to *"leave to our children a world that is safer and more secure, more prosperous, and freer"* [5]. In fact, despite the appearance that this most recent treaty solely replaces the Kyoto Protocol, it may be different. The older agreement focused on developing countries reducing their greenhouse gas (GHG) emissions. Conversely, the Paris Agreement mandates that all nations take action to combat climate change in its broadest sense, keeping the average temperature rise below two degrees Celsius above pre-industrial levels and continuing to work toward limiting it to 1.5 °C. The treaty poses dedicated deadlines and a regulatory framework on how the more vulnerable countries may get the help that they need from the more developed ones, along with measures related to market and financial systems [6]. By 2020, all the nations propose their plans for emissions reduction, named Nationally Determined Contributions (NDCs), and their Long-Term Low greenhouse gas Emission Development

Strategies (LT-LEDS). These documents should finally assess the progress made in emissions and actions taken, with insights on the help received or provided, if it is the case. Moreover, a key aspect regards the emissions control system. It has been defined as making the countries respect their commitments by reporting every five years on their status. This procedure, called Global stocktake, will start in 2023 and consists of the confluence of all the countries' Enhanced Transparency Framework (ETF). [7].

1.2. The 2030 Agenda for Sustainable Development

The result of the UN General Assembly of September 2015 as the framework for a global transition in the upcoming years is the 2030 Agenda for Sustainable Development [4], [8]. This resolution is a universal call for action which aims at universal and sustainable growth toward a peaceful and prosperous planet facing poverty and environmental harm. Indeed, it implies the participation and the shared responsibility of all the 193 countries' signatories, which commonly pledged to *leave no one behind*. The*Agenda* defines five main areas of relevant importance for sustainable growth which inspire the plan:

People End hunger and poverty, ensuring that all people can live in dignity, equality, and health;

Planet Guarantee the respect of the planet against degradation, supporting the needs of the present and future generations by employing sustainable production and consumption policies. Urge actions against climate change;

Prosperity Ensure prosperous lives for everybody, with adequate and environmentally-friendly technological, social, and economic progress;

Peace Promote peaceful, just, and inclusive societies without fear or violence. It is considered the necessary but not sufficient condition for sustainable development.;

Partnership Implement the *Agenda* has to be in a spirit of global solidarity, focusing on a common response to the needs of the poorest and most vulnerable.

These dimensions, also known as the 5Ps, are at the center of the Sustainable Development Goals (SDGs), the real focus of the 2030 Agenda.

1.2.1. The Sustainable Development Goals

The UN established 17 common goals to meet the requirements of the 2030 Agenda to provide a clearer perspective and idea of the topics that must be addressed [9]. These goals, which include 169 additional specific targets, were created to succeed in the Millenium

Development Goals, which, even though they have not yet been fully attained, can be seen as the first joint effort towards a shared sense of sustainability. Each of the 17 goals, presented in Figure 1.2, is integrated and interconnected with the others and typically has 8-12 targets, divided into "outcome targets" or "means of implementation." Indeed, not all the indicators can be quantitatively measured. Such an approach has been used to guarantee better achievability in most countries, adopting measures of various sectors. To facilitate monitoring of the progress of the various signatories: data and information from each region are collected and processed by the UN System to produce annually an SDG Progress Report based on a global framework of 232 indicators. Moreover, to facilitate the access of the general public to these data, an online *SGDs tracker* is available from 2018 [10]. The SDG Report 2022 [11] provides insight into how quickly it is necessary to

Figure 1.2: UN 17 Sustainable Development Goals [9].

act to meet the goals by their deadline. The cause of this is the number of interconnected crises, including COVID-19, climate change, and wars, which have come to a head while undoing years' progress. The pandemic's effects have increased the number of people living in poverty and reduced the ability of sanitary systems to prevent the spread of previously curable diseases like malaria and tuberculosis. With the Russian invasion of Ukraine sparking one of the worst crises in recent memory, consequences are also seen in the forced migration of refugees due to the growing poverty in conflict-ridden nations. Furthermore, rising interest rates and inflation make it more challenging for many countries to transition to more sustainable energy sources, which is why they have

difficulty meeting their climate change and greenhouse gas emission goals. The focus on sustainable development should be increased in light of the current challenges. In contrast, a more robust coordinated response to the crisis is required if the 2030 Agenda becomes a reality and results in significant advancements for both people and the environment.

1.3. The European Green Deal

The European Union (EU) is undoubtedly one of the prominent actors in the international geopolitical scheme and is one of the leading advocates and parties of the Paris Agreement. This role implies extensive responsibilities since the Union represents most western economies and their people. Indeed, European countries are at the center of what is considered to be the new industrial revolution, which will lead the world toward a more sustainable and efficient economy. The European Union and its organisms have taken the challenge from the beginning, defining the ecological transition as a fundamental issue of the present and setting it as a priority of the new legislative actions for the upcoming years. [12].

The future roadmap for the European Union has been defined by the European Commission in the European Green Deal [13], an ambitious set of policies approved between 2019 and early 2020, with the primary objective of making the EU climate neutral by 2050. This framework poses the bases for building a competitive, sustainable, resource-efficient, and environmentally friendly continent, able to lead the world in the fight against climate change under the Paris Agreement of 2015. Indeed, the primary purpose of the Green Deal is to turn Europe into the first climate-neutral continent in the world. To do so, more and less ambitious targets have been set as milestones for the years up to 2050, with the ultimate goal of reaching net zero impact in terms of greenhouse gas emissions by that date. European countries agreed to reduce, by 2030, by at least 55% compared to the 1990s level. These pledges are pretty ambitious and must be accompanied by concrete actions at all levels of governance and in different sectors of everyone's lives.

The abandonment of fossil fuels and oil-based products is one of the significant challenges that every country which intends to decrease its impact on the planet needs to face. After the COVID-19 pandemic outbreak, the European Union delivered the NextGenerationEU Recovery Plan [14], an instrument defining measures to recover from the social and economic crisis caused by the actions adopted to fight against the virus. This legislative package is, however, more than just a stimulus to restore the pre-existing *status quo*. The Green Deal, which was modified to operate in the new post-pandemic framework, will continue to be at the core of the European ecological transition. Indeed, it is a turning

point in European history, being the most extensive package ever approved, with more than 2 trillion euros available. It aims at developing a stronger Europe, which will be *greener, more digital, and more resilient* [15]. Although the current laws have not been abandoned, they will most likely benefit from the more considerable funds provided by NextGenerationEU to accomplish their objectives.

The transition to a green economy without leaving anyone behind involves numerous intermediate steps for the EU to accomplish the targets for 2050. The 55% reduction of greenhouse gases by 2030 is undoubtedly the significant and more widespread milestone set, which includes a set of legislative actions grouped as *Fit for 55*, presented by the Commission in 2021 and generally approved by the European Council on June 2022 [16], [17]. This legislative package includes all the policies governments are willing to take to respect the final target of having a fair transition toward a green and competitive Union. The central principles of this body of legislation are an increase in energy efficiency for both buildings and industries, new viewpoints on cars and transportation systems, a higher percentage of energy coming from renewable sources, and the development of sustainable management of the agricultural system and carbon sinks. Additionally, it includes steps to adjust markets to the new era, such as an upgrade to the Emissions Trading System (ETS), new vehicle and transportation laws, and a reformed product taxation system to account for all factors that have an impact on the environment. In terms of percentages, the Members of the European Union committed to a target of 40% of energy from renewable sources by 2030 to achieve the target of greenhouse gas emissions reduction set by this regulation.

The year 2022, with the Russian invasion of Ukraine, forced the international governments to change plans regarding their geopolitical settlements. The consequences are also reflected in the energy market, and the European Union is no exception. The Commission persuaded all the members to accelerate the transition by reducing their dependence on Russian fuel sources, namely oil and natural gas, with the latter accounting for almost four-tenths of all the European gas imports. Therefore, to allow for the continent's energy independence while pursuing the ecological transition, the European Commission devised a new action plan to be included within the larger context of the Green Deal. This new strategic policy set, named *REPowerEU*, looks even closer to the other programs previously mentioned since it has been developed to efficiently tackle an imminent external cause [18]. Despite this, the highlights reflect those that have been settled by the *Green Deal*, eventually looking forward to more ambitious targets [19]. Indeed, with the *REPowerEu* program, the renewable share to be reached by 2030 is raised at 45%, updating the figures set by *Fit for 55* plan just after two years. The discussion on details of this

new body of measures is still a matter of debate within the Council and in the European Parliament. However, surely there will be many efforts needed by both the governments and the scientific world, with research in the broad matter of renewable energies will be the principal focus of the present decade, and the European Union will be a lead actor in this process. [20].

1.3.1. The Italian Situation

Italy is the largest beneficiary of the funds from the NextGenerationEU Recovery Plan, being the first and probably the heaviest hit country in Europe by COVID-19. These investments are an enormous opportunity for a country with delays and below-the-average indicators regarding digitalization, efficiency, and investments in research and education. Thanks to the plan, Italy is supposed to enormously increase its level of digital skills in crucial roles, such as public administration and businesses, along with enhancements in the scholar, healthcare, and social inclusion [21], [22]. The other central pillar of Italy's recovery and resilience plan - Piano Nazionale di Ripresa e Resilienza (PNRR) - ecological transition, shows measures for a share of 37% of the total funds.

The environmental part of the PNRR shows actions that will foster those presented in the *Piano Nazionale integrato per l'Energia e il Clima* (PNEC), the national proposal to fulfill the requirements of the Green Deal, presented in 2019 [23]. As requested by the legislators, the document's key points involve reforms to increase the share of renewables, decarbonization, and energy efficiency. It satisfies the European requirements for these topics. In particular, Italy pledges to reach a 33% greenhouse-gas reduction and the 30% of totally consumed coming from renewable sources, which will be the summary of 55% in the electric sector, 33,9% in the thermal and 22% in transportation.

1.4. The Role of Biomass

The term "biomass" can describe various organic fractions, including algae, agricultural and urban waste, trees, and plants. In the ecological transition, bioresources will be crucial for materials and energy. Indeed, biomass is currently the largest renewable energy source in the EU, accounting for almost 60% of total energy consumption. This value rises even further considering the heat and cooling sector only because bioenergy—defined as energy derived from biological resources—outperforms all other renewable sources, making up 75% of the total. This large share is because most nations where those resources are much use forestry and other solid biofuels as their primary heating sources on a large scale. Despite having clear advantages over other traditional options, it is essential

to emphasize that biomass is not a replacement for a greenhouse gas-free solution [24]. Indeed, bioenergies play and will play a significant role in the energy transition towards the European targets, in particular to the closest ones [25]. However, the central policies suggest that their use should be prioritized for high-value-added applications, leaving other greener alternatives, such as wind or solar, the central roles of energy production. In this way, bioenergy could be used in those sectors where decarbonization is difficult or lagging, like parts of transportation, such as shipping and aviation. Moreover, biobased solutions have great potential to replace many petroleum-based commodities and compounds, such as many alcohols.

Biomass must adhere to a few sustainability-related requirements outlined in the Green Deal to fully play its relevant part in the transition [26]. The woody materials must originate from nations with legislation that complies with the requirements for proper forestation and soil consumption and effective harvesting systems to be used as an energy source. Because forests are such effective carbon sinks, proper ecosystem management can ensure more significant benefits in terms of emissions. Policies that prioritize the value of biomass in its total capacity as a potential carbon-negative actor in the current system should be used to enforce this. These policies should aim to preserve and enhance the biodiversity that biomass can guarantee in most places. Consequently, the planet's resources will be optimized if the principles of the circular economy and cascading, or usage in hierarchical and sequential phases, are fully recognized and utilized.

1.5. Biogas and Biomethane in the Energy Transition

Biogas is a mixture of methane (CH_4) and carbon dioxide (CO_2) in different percentages, usually with a prevalence of the first (50-70%). Such gas is typically obtained from different sources, such as agricultural wastes, sewage sludge, or animal and vegetal by-products, by a natural process of biomass degradation in the absence of oxygen, named anaerobic digestion (AD) Ṫhe dedicated chapter will give a detailed description of both the product and the operations. Currently, exploitation of biogas is for the majority in plants that generate both electricity and heat simultaneously - CHP (Combined Heat and Power). A more recent, attractive exploitation is the so-called biogas upgrading to biomethane. Such a process consists in increasing the fraction of methane to obtain a product similar to natural gas, which can thus be directly injected into the grid or as vehicle fuel [27].

The development of a biogas production system started in Europe in the 90s and has constantly been growing at a high pace, reaching more than 10 GW of installed capacity

in recent years, as shown in Figure 1.3. Nowadays, countries like Germany, Italy, France, the Czech Republic, Austria, and Sweden are leading the market of biogas technology and are among the most significant worldwide developers of upgrading solutions [28].

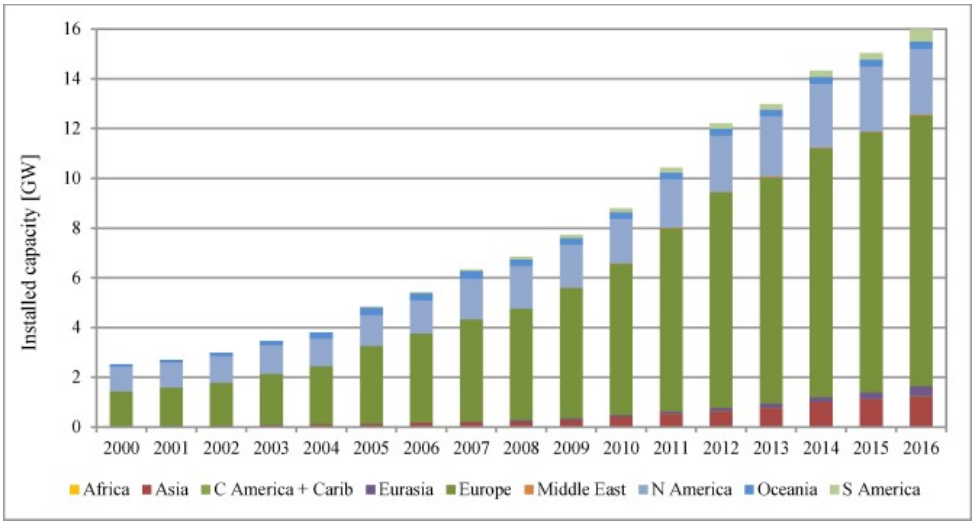

Figure 1.3: Installed capacity of biogas plants in the world [29].

Biofuels, including biomethane and biogas, release GHG during combustion but do not increase the overall amount in the atmosphere because they come from sources that, during their growth, have, directly or indirectly, absorbed CO_2. The sum allows for a closed carbon cycle, potentially generating zero or negative net emissions. Biogas has been shown to reduce GHG emissions by up to 240%. This value might be inflated, given the strict assumptions about the substrate and technology. In general, it is possible to state that both biogas and biomethane, when used to replace fossil fuels, can guarantee an emissions reduction of at least 80% [30], [31]. The counts for carbon dioxide are just one of the advantages of these bioenergies. Indeed, after upgrading, the product is one of the most flexible energy carriers. Production does not depend on seasonality and does not require any modification to the existing grid. In addition, it is relevant to consider that the production process accounts for two main by-products: the digestate during the anaerobic digestion and a CO_2-rich stream obtained along with biomethane during the upgrading. These two by-products have considerable potential, being able to be utilized as fertilizers, in the case of the digestate, or as valuable raw material for many chemical processes in the case of carbon dioxide. As discussed later, bioenergies production enables smart management of various resources that would otherwise be disposed of as waste, leading to the development of waste-to-energy (WtE) solutions, another important tenet of the sustainable transition. Additional advantages are also present, such as lessening the harmful effects of other activities by avoiding their direct emissions, as in the case of

agricultural manure [27], [32].

1.5.1. Bioenergies and Sustainability Targets

Above is a summary of a few advantages that could aid in expanding the bioenergy sector. These and other factors were taken into consideration by policymakers, which enacted and recommended crucial measures to successfully implement sustainable sources to meet the challenges of the energy transition.

European Commission significantly sets the role that biogas can have in the RePowerEU plan, recognizing the potentialities in energy security, sustainability, and economics [33]. Indeed, apart from all the considerations regarding emissions reduction, biomass sources are widely available in European countries at a constant and reasonable price. Indeed the final cost of biogas and biomethane is estimated to be between € 40 and € 120 per MWh, with the relevant benefit of not being subjected to the large market fluctuations of natural gas prices that Europe has realized recently [27]. The Commission defined some key points, and other high-level associations have introduced more to give bioenergies the necessary and deserved role in profitably combining with other renewables for decarbonization. This series of steps should maximize the benefits of biogas and its conversion into biomethane, setting up the conditions for a long-term supply of this fuel and its introduction into the grid. The final goal is to fully exploit the biomethane potential to reach a production of 35 *bcm* (billions of cubic meters) by 2030, as clearly outlined in the RePowerEU, and 95 *bcm* by 2050. These figures are relevant considering that EU nowadays consumption is around 400 *bcm*, 155 of which were imported from Russia and will thus have to be almost eliminated, standing to the RePowerEU guidelines. That large production is coherent with the feedstock available in European countries and could be further expanded using more advanced sources and technologies. The challenge is relevant, considering that today EU production is almost half what it should be by 2030, with the whole industry producing almost 18 *bcm*, divided by 15 *bcm* of biogas and three *bcm* of biomethane [34]. The incentive for the improvement will need to favor the demand side in the use of biobased sources over natural gas, for example, in transportation or grid injection, as well as the supply side. Regarding the latter, the plant capacities should be fully exploited with non-limited contracts and better investments, along with dedicated national and shared strategies to guarantee feedstock sustainability and the needed support for industrial partnerships. Regarding the sources, one relevant measure is already in sight at the European level: from 2024, all the organic waste will have to be collected separately and processed in a dedicated facility which, in many cases, will be a biogas production plant [33], [35].

Although Europe is the largest biogas producer, this source can provide considerable advantage to the transition on a global scale. Indeed, this industry can benefit all the three areas which define the *triple bottom line* of sustainable development: social, environmental, and economical. It should not surprise that biogas can have a direct and quantifiable impact on global targets, such as the SDGs, given that the concepts of bio-economy and circularity are acknowledged to be among the foundational elements of the green transition. The SDG most affected by an enhancement of biogas production will be *SDG 7: Affordable and Clean Energy*, but, as already said, a cleaner source is not the only advantage that bioenergies can offer. Many other benefits can be undoubtedly related to this technology, and most of them can significantly impact those areas most in need of development. It is possible to fully capitalize on the WtE capacity of these processes to reach significant milestones connected to waste management (*SDG 11: Sustainable cities and communities*) and wastewater utilization and treatment (*SDG 6: Clean water and sanitation*). Expanding the lens to include the entire supply chain can also emphasize sustainable biofuel production's benefits on agriculture and soil (*SDG 15: Life on land*). Indeed, an adequately grown biomass, after serving as a carbon sink throughout its life, acts as both a food source (*SDG 2: Zero hunger*) and a substrate for anaerobic digestion or other biobased processes [36], [37].

Above is just a brief description of what biogas and biobased solution can help accomplish in the future. These resources have much potential, and even though their issues are not entirely resolved, they should be included in the range of strategies used to combat climate change and build a fair and sustainable world for future generations.

2 | Anaerobic Digestion

Anaerobic digestion is a biological process in which microorganisms degrade organic matter without oxygen. Such process may occur naturally, in the soil or some water basins, or dedicated facilities: the anaerobic digesters. The metabolism of the bacteria involved biomass transformation in two major products of interest: biogas and digestate. The first contains a high content of methane (CH_4, 50-70 &vol) and carbon dioxide (CO_2, 30-50 %), with traces of byproducts, like H_2S and water vapour. The digestate represents the nutrient-rich solid residue and part of the liquid fraction, commonly used as fertilizer.

2.1. The Process of Anaerobic Digestion

AD is regarded as one of the most cost-effective and environmentally benign methods of converting biomass, particularly organic wastes, into renewable energy. Compared to other bioenergy production technologies, the AD process is relatively simple and affordable, with a lower carbon footprint and a higher net energy return. Furthermore, it provides a wide range of applications from its core products, broadening the field for a circular economy within the waste management discipline.

2.1.1. The Metabolic Reactions

Anaerobic digestion relies on a complex microbial consortium consisting of interdependent biochemical steps. In general, it is possible to recognize four main phases: *hydrolysis, acidogenesis, acetogenesis* and *methanogenesis*. A previous step, named *disintegration*, may be relevant in the case of complex feedstocks, which have to be broken down into simpler organic polymers.

Hydrolysis In this phase, the long polymeric chains, which constitute the biomass, carbohydrates, lipids, and proteins, are *hydrolized* into their smaller constituents: monomers or oligomers. These reactions refer to the cleavage of the covalent bonds by water, by which sugars, amino acids, and lipids are formed. The involvement of the protons of water can involve the release of cations and anions, which may affect the pH of the solution,

Figure 2.1: Aerial view of a biogas production facility, including basins for post-digestion and feedstock storage basins, [38].

which usually decreases at this moment. This step is necessary since the latter compounds are directly soluble and thus available for other bacteria to perform the subsequent steps of digestion. It is relevant to say that this phase is the slowest and can be considered as the *Rate Determining Step* of the whole process. The reaction rate can be enhanced by performing some pretreatments, such as milling, grinding, and contact with high temperatures or chemicals. Moreover, this process is usually catalyzed by extracellular enzymes secreted by the microorganisms which will utilize the products. There are four main families of enzymes, classified according to which polymer they will work on: *cellulase, amylases, proteases* and *lipases*.

Acidogenesis This set of reactions involves the transformation of hydrolysis products into fatty acids. The most relevant products are the volatile fatty acids (VFA) : those with a C4 carbon backbone, such as valeric and butyric acids, and the C5 propionic acid. This phase is performed by the *acidogenic* bacteria, a family able to tolerate acidic conditions and with fast growth kinetics. Along with the desired products, it is possible to have a production of secondary metabolites in this phase, including long-chain fatty acids (LCFA) as well as carbon dioxide, hydrogen, and acetic acid, as well as other minor by-products (ethanol, lactic acid, or H_2S). CO_2, H_2, and acetic acid are valuable products for the later stages since they are the growth source for methanogens microorganisms. Indeed, the primary purpose of this phase is to provide metabolites for the subsequent bacteria, which will then produce the acetate needed in methanogenesis. This phase and the subsequent one are sometimes generally referred to as fermentation.

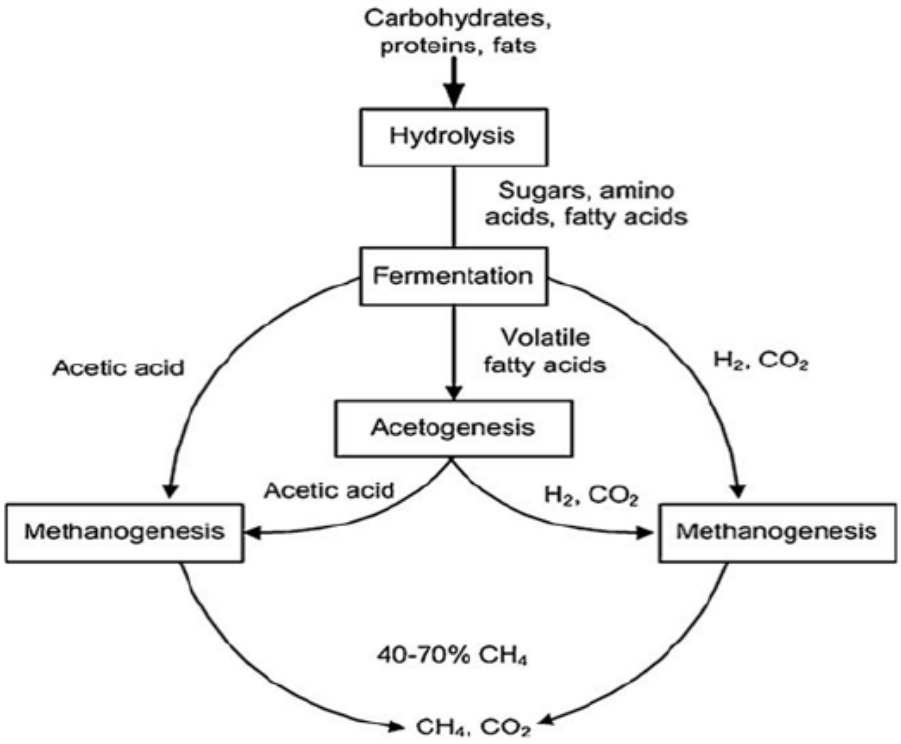

Figure 2.2: Scheme of main phases and intermediates of anaerobic digestion [39].

Acetogenesis This phase produces the primary substrate for methane producers: acetic acid (CH_3COOH). This molecule is produced either directly by fermentative reduction of VFA or subsequently from the other main product of that reaction, H_2, which is also an inhibitor for some acetogenic species. This second pathway reduces the CO_2 to CH_3COOH, utilizing part of the by-products produced during the acidogenesis.

Methanogenesis The last and most crucial step of the AD process when the main product is obtained. Here strictly anaerobic strains of bacteria and archaea can convert part of the molecules previously produced into CH_4 and CO_2, the significant components of biogas. This is possible thanks to two principal pathways: carbon, the final electron acceptor, and oxygen's role in respiration.

One family of methanogens, the *Hydrogenotrophic*, grows utilizing hydrogen and carbon dioxide as substrate (R1), and commonly are the most abundant strain inside the reactor.

$$CO_2 + 4\,H_2 \longrightarrow CH_4 + 2\,H_2O \tag{R1}$$

The other strain of methanogens is represented by the *Acetoclastic* microorganisms. These are less abundant, but despite this, they can usually provide the majority of the total

methane by converting acetic acid, as reported in (R2).

$$CH_3COOH \longrightarrow CH_4 + CO_2 \tag{R2}$$

A last, smaller apart of methane can be produced, depending on the fermenter conditions. by ethanol decarboxylation (R3). This pathway also gives acetic acid, which can be exploited accordingly to (R2).

$$2\,CH_3CH_2OH + CO_2 \longrightarrow CH_4 + 2\,CH_3COOH \tag{R3}$$

2.1.2. The Feedstock

Along with the production of valuable fuel, AD has a significant advantage that does not need any *fresh* raw material to be performed. Indeed it almost relies on wastes as feedstock, which, however, can have different natures and thus different properties.

In general, it is possible to identify four macro-categories of source for AD: manure, agricultural waste, organic waste, and sludge. They are all by-products of other sectors, which can fully exploit their value thanks to AD. This can surely be a positive point from a global perspective, but as long as it is considered just the process of digestion, there are some specific properties to consider. Indeed, even though almost any organic compound can be digested, every source has its *putrescibility* to define its possibility to be anaerobically degraded. From a chemical point of view, this means considering the oxidative state of carbon found in the feedstocks. The more reduced the carbon is, the higher will be the methane potential [40]. The other key parameter regards the feedstock composition, which optimally should have a carbon-to-nitrogen ratio (C/N) of 20-30. Typically, this is not the case: manure ranges around 10, agricultural wastes about 50, and sludge and organic wastes between 10 and 20. To overcome this issue, adopting co-digestion is becoming common practice, blending different available feeds to maximize the methane potential [41], [42]. Other relevant parameters for AD are the Biochemical Oxygen Demand (BOD) and the Chemical Oxygen Demand (COD). The first is a measure of the biodegradable organics in sludge that can be used as a metric for the overall efficacy of an anaerobic digester. It indicates dissolved oxygen microbial metabolism levels in a specific sludge sample. Similarly, COD measures the amount of oxygen in a sample of sludge that can be consumed in a reaction with oxidizing agents. It generally indicates the number of organics contained in sludge and provides for the evaluation of process efficiency in AD: COD decrease can reveal the amount of degradation occurring within

an anaerobic digester since it reflects organics consumption [43].

The value of the feedstock has a significant impact also on the sustainability of the whole AD process. Indeed, as presented in the previous chapter, a plant should rely on local or proximate feedstocks, possibly without any possibility of being utilized in higher-value applications. Moreover, the whole supply chain impacts the life-cycle-assessment of an AD facility, considering that crops and other biomass should be cultivated sustainably and securely.

2.1.3. The Products

The main products of interest of AD are two: biogas and digestate. In addition to those, there is also the residual liquid phase, constituted by the residual moisture of the feedstock and by the water produced by microbial reactions during the process.

Biogas constitutes the most relevant product, a renewable energy source with a vast potential for application. It is composed for the major part by methane and carbon dioxide, with some pollutants as by-products, as reported in Table 2.1. It can be used directly to produce electricity and heat, after a natural purification, in the cogenerative heat and power (CHP) plants or for more practical applications after further treatments. In particular, the reduction of the H_2S amount is of great importance, which, in the presence of moisture, quickly corrodes the equipment and mechanical parts with which it gets in contact. Its uses can vary from the mentioned energy generation by burning in boilers or via CHP units. It can also be used as a feedstock for advanced chemical processing, for example, in syngas. Suppose the biogas is *upgraded*, increasing its CH_4 content above 95%. The H_2S should be as low as possible and generally at most 10-20 ppm. In that case, it is possible to inject the product directly, named biomethane, into the existing grid or use it in the form of compressed natural gas (CNG) as a transportation fuel. A strictly controlled amount of pollutants is also required in these latter cases.

Digestate is the second relevant product of AD and can be considered as the residual from the feedstock. While most of the carbon and hydrogen are converted to gas, the effluent is rich in minerals such as nitrogen, potassium, and phosphorous, making it valuable as a fertilizer to increase the activity of soil microbes. Digestate nature varies accordingly to the feedstock, giving rise to a variety of effluents both in terms of state and composition. Indeed, raw materials with a high cellulose content will provide a very fibrous effluent, which direct application in the soil can be complex. In this case, some post-treatments may be applied, such as pyrolysis, to reduce the recalcitrant nature of carbon and produce bio-char or bio-oil without wasting the heating potential. In the opposite case, naming an

Compound	*Formula*	*Quantity*	*Unit*
Methane	CH_4	50-75	% vol/vol
Carbon Dioxide	CO_2	25-50	% vol/vol
Nitrogen	N_2	0-6	% vol/vol
Water	H_2O	0-5	% vol/vol
Oxygen	O_2	0-10	% vol/vol
Hydrogen	H_2	0-1	% vol/vol
Hydrogen Sulfide	H_2S	0-4000	ppm
Ammonia	NH_3	< 100	ppm
Siloxanes	$(OSiH_2)_n$	80-500	ppm

Table 2.1: Typical ranges of biogas composition [39], [40], [44]

effluent with a high-liquid content usually requires a dewatering procedure, consequently requiring further proper wastewater management.

2.1.4. The Operating Conditions

Anaerobic digestion systems traditionally rely on well-established technologies, and from a reactor perspective, it is difficult to see significant differences among different reactor classes and operating parameters. However, some generalities are presented below. It is important to note that the unique parameter is pressure, which is usually considered atmospheric. Complete digestion is frequently performed in two reactors to optimize the operating conditions for each digestion phase.

T he most common design for AD reactors resembles those of the CSTR (Continuous Stirred Tank Reactor). It is known for its reliability and easiness of operation. Usually, it has a double phase, and a continuous or intermittent impeller gives the mixing. The main drawbacks are related to microbial biomass, which may suffer damage from the stirring effect and is lost with the outlet flow of sludge.

Alternatives have been dedicated to developing solutions to retain the valuable biomass inside the reactor and fully exploit its potential. Some technological solutions can be seen in the fluidized bed reactors, from which the UASB reactor has been developed (Upflow Anaerobic Sludge Blanket Reactor) and with the fixed film reactors [45].

T he temperature of operation is defined according to the microorganism which has to grow inside the digester and, consequently, on the type of feedstock utilized.

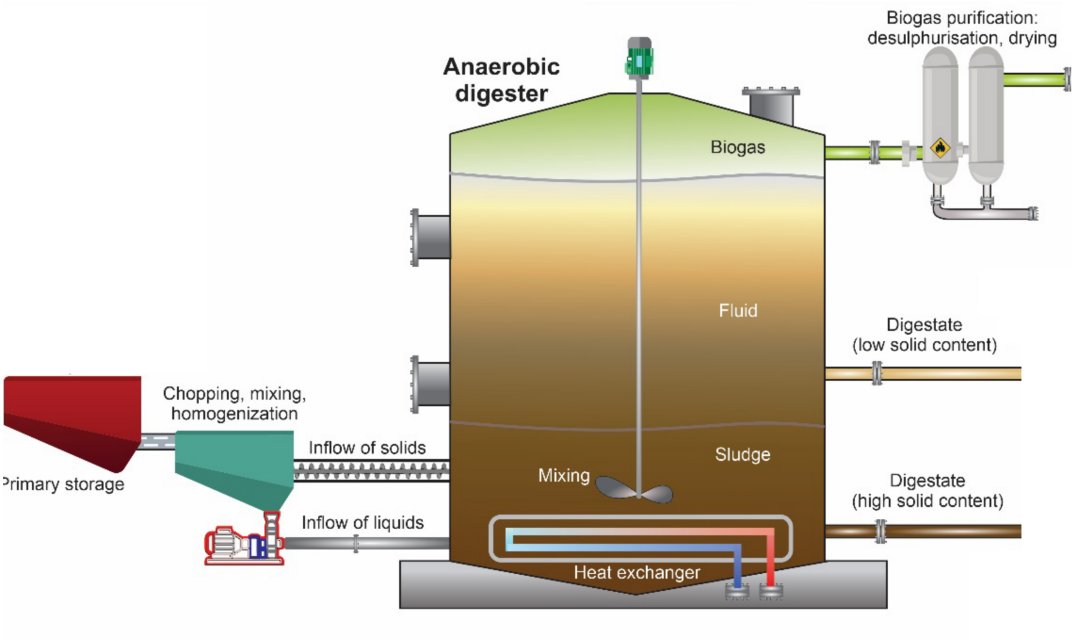

Figure 2.3: Schematic view of a CSTR anaerobic digester [46]

It is possible to define two ranges of operating conditions: *mesophilic* within 35-45 °C and *thermophilic* above 55 °C. The latter has a rate advantage due to increased kinetics concerning lower temperatures, potentially resulting in higher biogas yields. However, this is commonly not the best solution since these conditions stimulate the production of acids as by-products, reducing the final product globally. Moreover, the energy needed to reach thermophilic conditions is only sometimes justified by the results. A commonly accepted standard temperature is 37 °C [47].

I t is the amount of time necessary to complete the decay of organic materials. It can be associated with microbial growth and process conditions, including reactor design. Moreover, it is related to the global organic loading rate (OLR) , using it as a way to define the plant flow rate.

Generally, two main definitions are the most relevant: HRT (Hydraulic Retention Time) and SRT (Solid Retention Time). . The first refers to the residence reactor time of the reactor, and it is defined as follows: $HRT = V/Q$, where V is the digester volume and Q is the inlet liquid flow rate. The SRT parameters refer instead to the average time that the bacteria spend inside the digester and can be equal or different from the HRT according to the reactor design and performances requested.

An effective HRT, necessary for substrate degradation, depends on feedstock composition and OLR, but generally, it is between 15-30 days. Lower times will yield higher VFA

accumulation, whereas a higher time will be unnecessary [48].

T he operating pH has a direct impact on the digestive process and products. The optimal pH range for AD has been reported to be in the neutral range of pH 6.8-7.4. Indeed, each of the subphases of anaerobic digestion has its optimum window, and a trade-off between them has to be assessed. The hydrolysis phase strictly depends on the type of substrate and operative enzymes, but in most cases, it lowers the system pH by releasing protons. Conversely, acidogenesis and methanogenesis depend on the optimum of their microbial communities. The first performs better when carried out at slightly more acid conditions, with pH levels around 6. On the contrary, literature ranges for pH for methanogenesis stand between 6.6 and 8, with a sizeable kinetic decrease when the value drops below [48].

2.1.5. Biogas Sulfur Chain

Among the many compounds present during the anaerobic digestion of biomass, sulfur-related compounds are critical. They interact in many aspects of AD, the most notable being the limitation of methane yield. Sulfates are commonly found in feedstocks and participate in various metabolic reactions, the most common of which are sulfate reductions (SR) mediated by specific bacterial families. In these reactions, organic electron donors such as propionate, butyrate, acetate, and hydrogen are commonly used. As a result, sulfate-reducing bacteria (SRB) and methanogens competed for substrates, explaining why CH_4 formation is reduced. Sulfates are converted into sulfides due to these reactions, [49]. These compounds are inhibitory for the biochemical processes already at low concentrations (0.05 - 0.43 $kg\,S\,m^{-3}$) and will further limit microbial activity. This inhibition is usually associated with the sulfate concentration in the influent, which is more easily determined. Severe inhibition is not seen when the SO_{42}^{-}: COD is below 0.1, or when the COD concentration is so high that makes sulfur conversion not significantly relevant [50]. However, in some cases, such as vinasses, algae, protein-rich substrates, or specific wastewaters, this value can be significantly higher, leading to a significant impact of sulfur contents in the overall process [49], [51], [52]. As seen in Figure 2.4, Sulfides impact more than just the production of liquid products. The gas phase of H_2S is a significant pollutant of biogas, causing problems in the machines and lowering the product value. As a result, the sulfur chain must be monitored and investigated to avoid any problems during AD's reactive and purification stages.

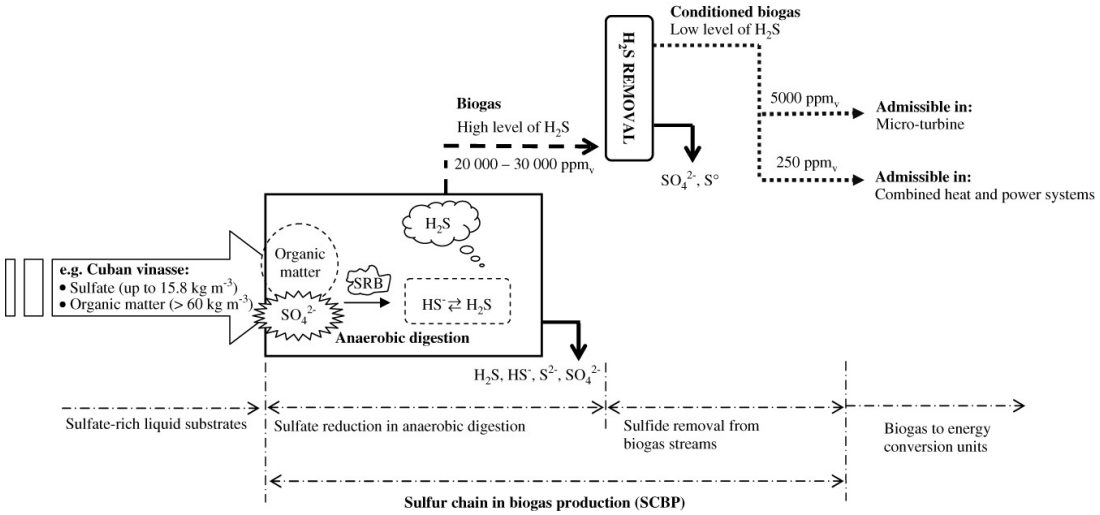

Figure 2.4: Representation of the sulfur-chain in anaerobic digestion [49]

2.2. Biogas Purification

As mentioned previously, depending on the type of feedstock, there can be a range of various compounds which can be detected in biogas as impurities. Those usually are non-desirable for different reasons, particularly corrosion of components and reduced heat exchange. Consequently, when biogas is intended to be burnt for electricity and heat generation purposes, it is essential to consider the potential presence of undesired elements carefully. In the case of upgrading to biomethane, the requirements of purity are even stricter, leading to the necessity of minimizing the pollutants present in the final product. Purifying undesired components should be done in two key moments: efficiently removing them during the upgrading process and avoiding unnecessary production during the anaerobic digestion phase by tuning the process feedstock and parameters. Biogas purity is fundamental since strict requirements are required for each utilization. The variety of applications, however, leads to various possibilities and opportunities according to differences in countries' national legislation and tax systems, feedstocks and spaces available, transportation possibilities, and so on [44], [53].

The CO_2 removal is unnecessary for many CHP and simpler combustion biogas applications. For more demanding scopes, like advanced engines, the heating value of the value has to be increased by reducing the carbon dioxide content. The most widespread method involves physical and chemical absorption by exploiting the solubility of CO_2 in water or other organic solvents. When a high purity is required, as is the case for the upgrading to biomethane, often the traditional methods are combined to maximize their outcome. Moreover, it is possible to add membrane separation systems to remove small impurities

and achieve methane content higher than 99%. Often in these last cases, a pure stream of carbon dioxide is also recovered and sent to higher-value-added applications.

T he biogas leaving the digester is saturated with water, which amount depends on temperature. At 35° C, its content is around 5%. For most of the applications, especially for those where high purity is required, a drying phase is necessary. The main effects of water traces rely on lowering the overall heating value and, in some cases, being of considerable importance, reactions with hydrogen sulfides to form aggressive ionic compounds. The removal of water content is probably the easiest among all the trace elements contained in biogas and can be achieved physically by condensation or chemically by adsorption in glycols or silica-based gels [44].

2.2.1. Hydrogen Sulfide Removal

Hydrogen sulfide H_2S is a poisonous and odorous molecule commonly present in biogas in concentrations up to 4000 ppm depending on the feedstocks, and eventually higher when digested by some particularly protein-rich substrates [54]. The main effects of its presence in the biogas produced stand on the damages it may cause to concrete and metallic equipment, facilitating their corrosion. Moreover, toxic compounds such as sulfur dioxides are produced when sulfides are burnt in the engines along with biogas. Consequently, H_2S concentration in biogas for combustion should not exceed 100 ppm, while for biomethane upgrading, a small concentration, lower than five ppm, is required [55]. This compound has to be removed as early as possible in the upgrading process, preferentially already in the digester.

Employed methods for H_2S removal use physical or chemical techniques to separate it from the biogas stream. Absorption in liquids exploits the affinity of hydrogen sulfide with water or organic compounds, such as ethers or glycols. This method can be coupled with the CO_2 removal to reduce the total costs associated with the process. Chemical methods rely on the possibility of making reactions with H_2S to form either more soluble salts, which can be precipitated, or insoluble compounds, which can be directly removed, usually by also forming elemental sulfur S_x. Among the most widespread reactants are those where Fe^{3+} can act as a chelating agent, forming elemental sulfur when reduced to Fe^{2+} or partial oxygenation with small oxygen dosing. Adsorption on activated carbons is also an applied technology. Carbons can be virgin or impregnated by oxides or alkaline solutions, such as sodium carbonate (Na_2CO_3), potassium iodide (KI), sodium hydroxide (NaOH) and potassium permanganate ($KMnO_4$). The operation is usually under pressure (6-8 bar), with swings when the sieve is fully loaded and needs replacement. Indeed, the

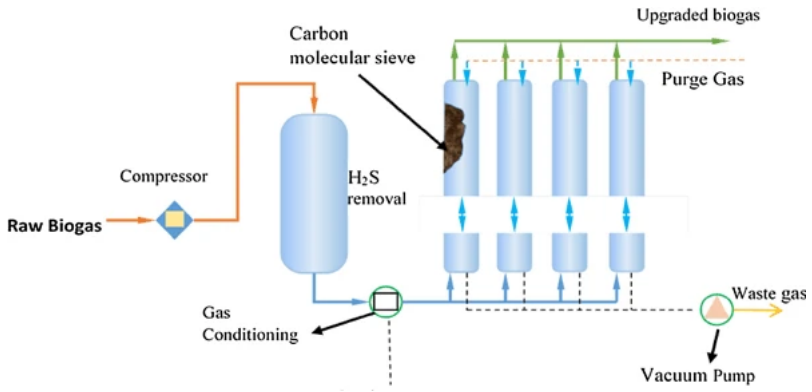

Figure 2.5: Example of H_2S removal by adsorption on activated carbon [44]

regeneration of the sorbent is the most significant drawback of this technology, which to operate continuously needs at least two scrubbing columns to allow regeneration, as shown in Figure 2.5. More recently, membrane technology is starting to be also applied in this field, potentially easing the removal of the smaller pollutants residues [44], [56].

Biodesulfurization, the biological-mediated technique to remove sulfur compounds from biogas, is a well-known and relatively cheap purification method. However, their application is flexible, primarily due to a need for more knowledge in the fields. It is possible to perform efficient purification (more than 95% of H_2S removed) with bio trickling filters: systems consisting of biomass adhered to packing materials, such as polymeric foams or rings. Their development, related to microorganisms' activity, strictly depends on operational parameters such as temperature and pH. Consequently, a full-scale application is only sometimes viable and requires constant control to guarantee adequate performance. In the family of biological methods for sulfide removal is also classified the oxidation by sulfur-oxidizing bacteria (SOB) [55], [56]. Since this technology is strictly connected with oxygenation, it will be discussed more in-depth in section 2.3.

2.3. Microaeration in Anaerobic Digestion

Microaeration, namely the injection of small amounts of air (oxygen) into an anaerobic digester, is considered a highly efficient, simple, and cost-effective technique for removing hydrogen sulfide from biogas. Due to a lack of standardization of the oxygen injection methodologies and definitions, the terminology is different among different literature sources: micro-oxygenation, limited aeration, micro-aeration, and other synonyms commonly refer to the same concept. These differences in the nomenclature also lead to a vague engineering definition of the process: the addition of oxygen can be one time for a digester, intermittent, continuous, and eventually with differences in the dosage point.

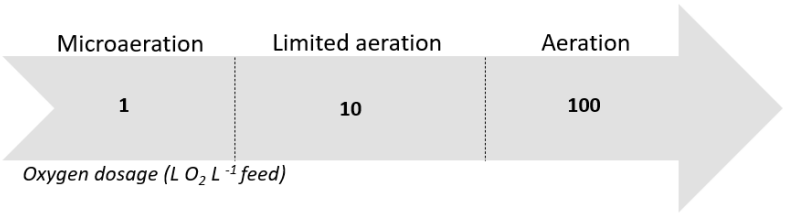

Figure 2.6: Different levels of oxygen injection define different aeration levels. Elaboration from [54]

Some scientific reviews have tried to generalize the idea by giving a quantitative definition of what should be identified as microaeration.

The most useful and practical approaches define it according to the proportion of oxygen with some process parameters or to reactor oxidation-reduction potential (ORP) [54], [57]. While the concept of the first definition is relatively simple, the more oxygen is added, the more aerobic effects there will be; the definition of ORP needs a more detailed discussion. Indeed, a ratio based on the flowrates is practicable only for continuous or semi-continuous injection, considering conditions for microaeration when the amount of oxygen added is lower than 1-1.5 L_{O_2} L_{feed}^{-1}. Figure 2.6 provides a semiquantitative assessment of different possible aeration levels based on this parameter [54]. Even more general can be the case of considering the oxygen added by comparing it to the reactor volume. In this case, microaeration usually defines the addition of oxygen ranging from 0.005 to 5L $O_2/L_{reactor}$/day).

A more standardized method could be related to the measurements of oxidation-reduction potential. Indeed, ORP measures the propensity of an aqueous solution to accept or donate electrons and therefore is frequently used to assess whether the environment in the aqueous phase is oxidative (more positive values) or reductive (more negative values) with respect to the standard hydrogen electrode (SHE). This method can thus be employed to detect small changes in dissolved oxygen concentrations, which is critical to measure with traditional methods due to shallow values. It is also possible to quantitatively describe changes in the amount of oxygen present, thanks to the fact that ORP varies linearly with the logarithmic of O_2 concentration. In fact, during microaeration conditions, the dissolved oxygen does not exceed the value of 0.1 mg/L.

To compare with the amount of dissolved oxygen (DO), it is possible to consider that the ORP value of -50 mV corresponds to the detection limit of the DO probe at 0.1 mg/L, and ORP values become more negative as DO reduces further. Consequently, *microaerobic conditions* may be defined as an aqueous media with ORP value in the range of 0 to

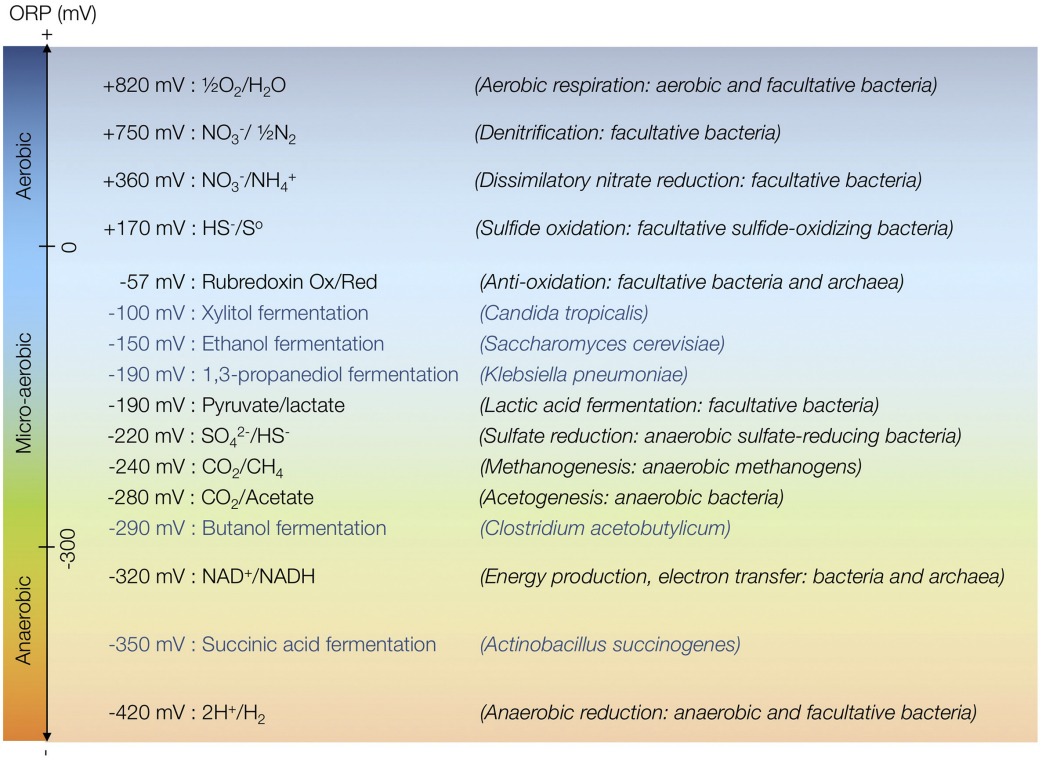

Figure 2.7: ORP (mV with SHE) of redox couples and various microorganisms participating in AD [57]

-300 mV with reference to SHE. As it is possible to see from Figure 2.7, every phase of AD leads to a specific ORP value, allowing for easy monitoring of the process with a simple measurement probe. Dosing air or oxygen to an anaerobic process elevates the ORP to a more positive value, slowly decreasing with the consumption of injected O_2 by facultative bacteria. Globally, a wide range of values has been reported as microaeration, probably since oxygen addition has not always been performed at the same process phase. A good compromise for microaeration to optimize anaerobic digestion has been found in the 230-260 mV SHE range.

2.3.1. Effects in the Anaerobic Digestion Process

As it is possible to imagine, adding oxygen to an anaerobic system can impact the overall process, even in small quantities. A schematic view of those is presented in Figure 2.8 The presence of small amounts of DO can allow the co-existence of facultative and anaerobic bacteria, which will thus not be exposed to oxygen. Indeed, oxygen is helpful in the hydrolysis phase by allowing the establishment of a more diverse microbial community. Diverse microorganisms lead to an increase in the direct activity and the secretion of more extracellular hydrolytic enzymes, eventually improving the hydrolysis of more

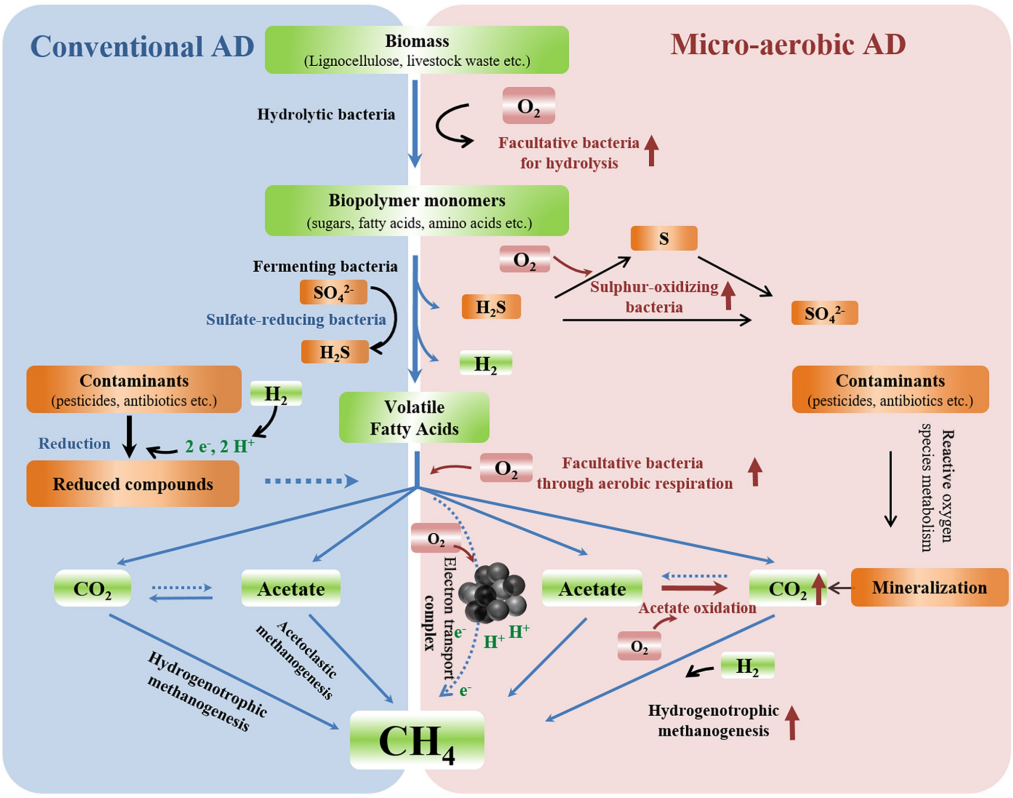

Figure 2.8: Overview of the effects of oxygen in the AD process [58]

complex biomasses without an expensive pretreatment. The co-existence of obligate and facultative anaerobes has beneficial effects throughout the process. Indeed, microaeration has been shown to maintain constant pH via partial oxidation of VFAs by aerobic respiration or selective oxidation of acetate via acetate-oxidizing bacteria syntrophic interaction between facultative bacteria and hydrogenotrophic methanogens. In general, microaeration helps stabilize the AD process, avoiding some of the shocks that may decrease microbial functions. It also may improve the removal of some of the most recalcitrant pollutants and substrates which would not be completely digested in complete anaerobic conditions [57], [58]. Finally, it is essential to remark that air containing oxygen can form flammable mixtures with biogas containing methane. However, when microaeration is considered, the low oxygen concentration resulting does not fall inside the flammability region, defined between the range of 5-15 % of methane in air [59].

Microaeration for sulfides removal

When sulfur compounds are present in the substrate, sulfate-reducing bacteria (SRB) convert it to the toxic and corrosive hydrogen sulfide H_2S, present also in the aqueous phase in the dissolved form H_2S/HS^-. The end-product of their metabolism is one of many

problems related to these families of microorganisms since they compete with methanogens for the substrate. They usually grow on acetate and hydrogen and have kinetic rates similar to or eventually faster than those of methanogens, thus reducing the overall biogas yield.

Sulfides can then be treated with some of the methods present in section 2.2.1 or converted to other compounds in the presence of oxygen. The most relevant sulfide removal bioconversion is represented in reactions R4, R5, R6, respectively yielding to elemental sulfur, sulfate, and thiosulfate. Under microaerobic conditions, the primary product is elemental sulfur, while thiosulfate is more favored when chemical oxidation is favored with respect to the biological pathway [54]. The formation of sulfur and sulfate can be controlled by the amount of oxygen supplied. Theoretically, 0.5 mol O2/mol S2- is necessary for the oxidation of sulfide to elemental sulfur (R4) [60]. These biological reactions are carried out by the bacteria family of sulfur-oxidizing bacteria (SOB), belong to phylum *Proteobacteria* with *Thiobacillus*, Halothiobacillus, Sulfuricurvum, and Acinetobacter as the main genus. SOBs are chemolitrophs, using oxygen as the final electron acceptor and sulfides as electron donors. Consequently, the addition of oxygen-enhanced SOB activity leads to significant removal of H_2S [54].

$$2\,HS^- + O_2 \longrightarrow 2\,S^0 + 2\,OH^- \tag{R4}$$

$$2\,HS^- + 4\,O_2 \longrightarrow 2\,SO_4^{2-} + 2\,H^+ \tag{R5}$$

$$2\,HS^- + 2\,O_2 \longrightarrow S_2O_3^{2-} + H_2O \tag{R6}$$

The whole set of sulfur reactions is strictly dependent on one from the other, as seen from figure 2.9. SOBs are generally attached to the reactor headspace walls or at the gas-liquid interphase, thus preventing most oxygen from reaching the liquid phase. The fact that most of the oxidative bacteria operate there is the reason why, in most cases, oxygen is injected directly into the headspace, making the residence time in this region the dominant criterion for H_2S removal efficiency. Sometimes the liquid phase has also been reported as an oxygen dosage point. However, hydrogen sulfide removal efficiency from the gas was reduced in these cases. Indeed, a solution of this kind will be more helpful when the main scope of microaeration is to stabilize the reactor or activate some facultative microorganisms. When the purpose is sulfide removal, oxygen control may also be referred to H_2S concentration, and biogas flow [61]. In this case, a proportional-integral-derivative (PID) controller may be applied, where the oxygen supply varies according to the difference between measured H_2S concentration and the fixed target. It is proved that such an approach and its relations with biogas production can be a simple but effective

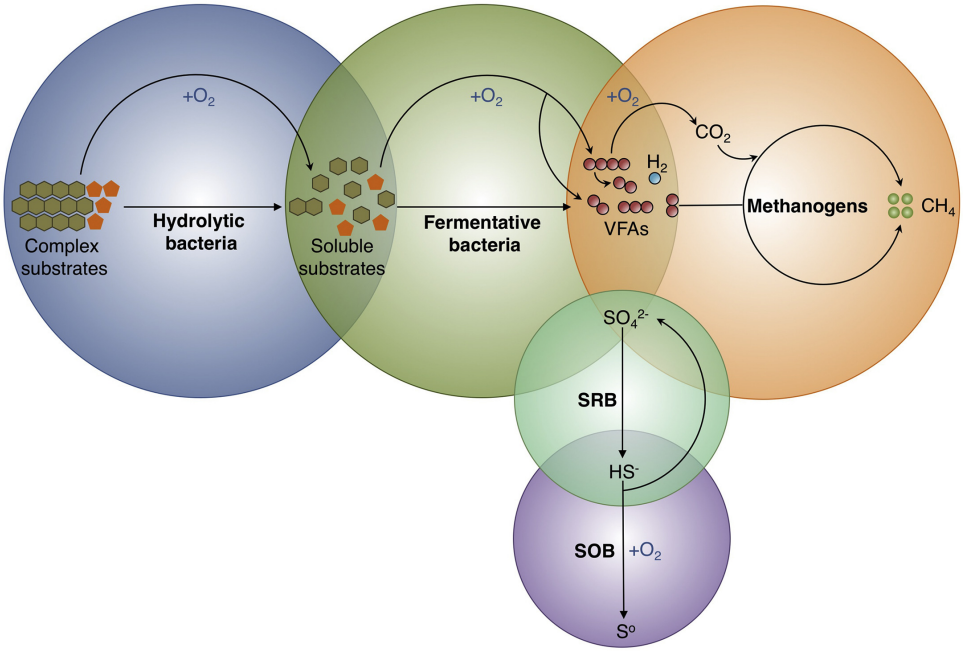

Figure 2.9: Relationships between microbial communities in microaerobic conditions [57].

method for microaeration control when sulfide removal is the primary purpose. Reference values are between 3.5 and 5 $L\,O_2$ per m^3 of biogas.

2.3.2. Current Limitations

A more detailed study of microaeration will be fundamental for its proper application at a significant industrial level. Current limits involve a not fully exploited knowledge of the microbiological reactions occurring and the influence oxygen presence can have on the metabolic pathways of sulfide oxidation.

From a more process-oriented perspective, it is clear that a lack of mathematical models representing such a process is undermining its applicability in many cases. This does not allow for monitoring and controlling the process of microaeration, which is almost always done following *rule-of-thumb* considerations. Indeed, while a few studies have been conducted to consider the sulfur reactions inside the AD environment, more needs to be done to consider the effects of small concentrations of oxygen, in particular related to sulfide removal.

3 | Anaerobic Digestion Modelling

Process modeling is a fundamental chemical engineering branch that evolved alongside computer capabilities advances. Modeling is the mathematical representation of real-world problems and industrial processes. This method enables the development and simulation of complex systems without actual experiments. The implications in the industry have been enormous, allowing process operations to be performed and established in such a way as to optimize their economic or technical output.

Anaerobic digestion systems are not an exception: the possibility of representing and simulating their processes can allow better and optimized operations, fully exploiting biomass potential. However, developing models for an adequate representation of AD has always been, and in most cases remains, loaded with difficulties and complexities. Such difficulty is mainly because AD systems are usually different from each other, both in terms of operating conditions and, more importantly, in terms of substrates and microorganisms. Different substrates lead to different kinetics, yields, and ways of growth or inhibitions for organisms that work with them. Moreover, similar feedstocks may behave differently if they are in different proportions or are treated in slightly different conditions.

Various approaches can be considered to produce models of AD processes. The most traditional is the one that aims to accurately represent all reactions occurring in the digester, depicting the reactor as a white box (this definition follows the idea that the knowledge of the process goes decreases on a black-white scale, where black-box defines pure data-driven models and white box fully mechanistically ones, with grey models those in between). Over time, it has become increasingly clear that a model capable of accurately representing AD processes would have been highly complex, requiring many parameters, equations, and computing power. Indeed, an adequate representation of each microbial family participating in the digesting activity could be performed by considering an increasing number of stages of the process and, consequently, more biochemical reactions.

Many models of this kind have been presented in the last years of the XX century. Most of them are highly specific to the substrate on which they developed. As a result, the need for general optimization and process development models emerged as a significant

driver in AD engineering research. Among them, a general approach for the most common AD substrate, activated sludge, has been developed in the last years of the previous century, resulting in Activated Sludge Models ASM1, ASM2, and ASM3. By considering the substrate on a COD basis, these models laid the groundwork for the development of the most advanced and, to the best of the author's knowledge, most current AD model: the Anaerobic Digestion Model No. 1. (ADM1) [62]. This model, provided in section 3.1.1, is regarded as the state-of-the-art in anaerobic digestion process modeling, describing a large set of reactions and currently, even though developed originally for wastewater treatment, applicable to a wide range of substrates.[63]. ADM1 uses numerous parameters to generate a system representation that is as close to reality as feasible. Indeed, its primary applications are in plant-wide simulations for design or optimization rather than in control systems. For this, plant-wide simulations and particular and dedicated improvements have been assessed over the years.

For the development of monitoring and control algorithms, there is a need to develop models independent of the system's phenomenological behavior. Ideally, such models should not depend mainly on their parameters and should be able to describe any change relevant to the dedicated control system in different situations [64], [65]. This outcome can be achieved by grouping several parameters and different reactions into more general families and working on global mass balances and model reactions. Such a procedure results in the construction of hybrid and semi-mechanistic models capable of bridging the gap between accuracy, complexity, stability, and adaptability. This approach aims to represent the process satisfactorily, without detailed knowledge of the influent characteristics and thus with a reduced number of experimental data required [66], [67].

A third family of models has been developed in recent years thanks to the advancement in machine learning and the data science field, the so-called data-driven models [66]. These models are based on the assumption that no knowledge of the process is needed if there are enough data to train artificial intelligence to interpret them correctly. A few applications of this artificial neural network modeling AD process are present in the literature [68]. However, their discussion will not be carried on further in the present work, representing an approach more applicable to energy system modeling [67].

3.1. Detailed Models

This section covers all of these models, aiming to describe all AD processes accurately without aiming at the use of a reduced set of variables. Consequently, the number of parameters and equations considered can be very high, according to the number of differ-

ent carbohydrates, proteins, lipids, fatty acids, alcohols, and other compounds. In many cases, complete parameter estimation and validation can be almost impractical. These white-box models are the ones on which the researchers focus their attention first. Dynamical models of AD have been developed since the late 1960s and early 1970s with the works of John F. Andrews, who also included the modeling end-product inhibition to improve control of digester stability [69]–[71]. The first models tried to represent the basic steps of anaerobic digestion, following the actual knowledge of microbial kinetics. First attempts provided a prediction of biogas production following the rate-limiting reaction, namely the methanogenesis [70]. Subsequently, such models have been developed by adding the second primary reaction, which has to be considered: the production of acetate from other VFAs with the *acidogenesis* reaction. These reactions have been traditionally modeled following the *Monod-type* equation, which considers a growth limited by one single substrate [72]. This empirical equation (Eqn. 3.1 represents the actual growth rate of a microorganism $\mu\,[d^{-1}]$ according to its maximum growth rate ($\mu_{max}\,[d^{-1}]$, the actual concentration of limiting substrate $[S]\,([g\,L^{-1}]$ and a parameter named half-velocity constant $[K_S]\,[g\,L^{-1}]$. The latter indicates the value of the substrate for which the actual growth is half the maximum.

$$\mu = \mu_{max}\frac{[S]}{[S] + K_S} \tag{3.1}$$

This reaction gave positive results, but it has been noted that methanogenesis also showed inhibition from VFA concentration, thus leading to the necessity of a new definition for this reaction step. This has been done following the Haldane reaction mechanism (Eqn. 3.2), where $[VFA]\,[g\,L^{-1}]$ is the concentration of VFA and $[KI]\,[g\,L^{-1}]$ its inhibitory constant [70].

$$\mu = \mu_{max}\frac{[S]}{1 + \frac{K_S}{[S]} + \frac{[VFA]}{KI}} \tag{3.2}$$

More reactions and dependencies were incorporated during the next two decades to construct sophisticated anaerobic digestion models. Those trying to add the phase of organics solubilization to the ones of acidogenesis and methanogenesis have the largest effect. Indeed, to improve model prediction, it has been necessary to act in two ways. To begin, improve the modeling of soluble organics digestion by adding the kinetics of more acidogenic and methanogenic reactions and enhancing the existing ones [73]. On the other hand, a significant advancement is considering how soluble molecules are formed from solid substrates, resulting in good modeling of the hydrolytic reactions. These reactions are influenced by both the concentration of substrate and the concentration of acidogenic bacteria, which secrete the necessary hydrolytic enzymes. A detailed representation will thus require an advanced kinetic mechanism, which should also consider the different

natures of the substances to be hydrolyzed. The first and easiest approach is to use a first-order kinetic equation (Eqn. 3.3. There, ρ_{hyd} $[g\,L^{-1}\,d^{-1}]$ is the hydrolysis rate; k_{hyd} $[d^{-1}]$ the kinetic constant; $[S_P]$ $[g\,L^{-1}]$ the concentration of solid particulate), which is, however, an apparent description of many more different sub-reactions. Indeed, it has been demonstrated that its kinetic hydrolyzed k_{hyd} largely varies by considering different substrates [74]. As a result, this reaction has applicability in lumped models, while various approaches have been investigated for mechanistic models. The most relevant are surface-based kinetics, which can consider enzyme attachment to solids and, eventually, shape-related interactions, or multiple-step reactions, primarily following a dual-step approach.[75], [76].

$$\rho_{hyd} = k_{hyd} \cdot [S_P] \tag{3.3}$$

Further relevant additions in developing detailed models include pH definitions and their relationships, as well as the effects due to the presence of minor compounds inside the fermentation environment. Indeed, certain substances can cause substantial inhibitions and limitations in the AD process. These can include molecules naturally present in feedstocks, such as ammonia, nitrates, and sulfur-derived compounds, as well as some non-indigenous molecules that can be considered contaminants in a stricter sense, such as metals or toxic organic compounds. Consequently, more models look into how to adequately describe the reciprocal interaction between all the substrates of AD, in particular by having a deeper looking into inhibition effects [77]–[79].

By the late 1990s, a consistent body of literature was dedicated to AD models due to all of the investigations. Still, there needed to be more generality and rigorous substrate-specificity, resulting in a lack of plant and industrial application. As previously anticipated, a group of researchers working as a task group sponsored by the International Wastewater Association (IWA) began designing a general anaerobic digestion model, giving rise to the ADM1.

3.1.1. ADM1

During the 8th World Congress on Anaerobic Digestion in 1997, the International Wastewater Association (IWA) defined the need to develop and deepen the construction of mathematical representations of AD, proposing a generalized model. Consequently, it proposed a dedicated board to tackle that challenge: the IWA Task Group for Mathematical modeling of Anaerobic Digestion Processes. The outcome of this challenge was visible in 2002 when the Anaerobic Digestion Model No. 1 (ADM1) was published [62].

Variable	*Unit of measure*	*Description*
X_C	$kgCOD\,m^{-3}$	Composites
X_{pr}	$kgCOD\,m^{-3}$	Proteins
X_{ch}	$kgCOD\,m^{-3}$	Carbohydrates
X_{li}	$kgCOD\,m^{-3}$	Lipids
X_I	$kgCOD\,m^{-3}$	Particulate Inerts
S_I	$kgCOD\,m^{-3}$	Soluble Inerts
S_{su}	$kgCOD\,m^{-3}$	Monosaccharides
S_{aa}	$kgCOD\,m^{-3}$	Amino acids
S_{fa}	$kgCOD\,m^{-3}$	Total LCFA
S_{va}	$kgCOD\,m^{-3}$	Valerate
S_{bu}	$kgCOD\,m^{-3}$	Butyrate
S_{pro}	$kgCOD\,m^{-3}$	Propionate
S_{ac}	$kgCOD\,m^{-3}$	Acetate
S_{h2}	$kgCOD\,m^{-3}$	Hydrogen
S_{ch4}	$kgCOD\,m^{-3}$	Methane
S_{IC}	$mol\,m^{-3}$	Inorganic Carbon
S_{IN}	$mol\,m^{-3}$	Inorganic Nitrogen
X_{su}	$kgCOD\,m^{-3}$	Sugar degraders
X_{aa}	$kgCOD\,m^{-3}$	Amino acids degraders
X_{fa}	$kgCOD\,m^{-3}$	LCFA degraders
X_{c4}	$kgCOD\,m^{-3}$	Valerate and butyrate degraders
X_{pro}	$kgCOD\,m^{-3}$	Propionate degraders
X_{ac}	$kgCOD\,m^{-3}$	Acetate degraders
X_{h2}	$kgCOD\,m^{-3}$	Hydrogen degraders
S_{cat}	$mol\,m^{-3}$	Cations
S_{an}	$mol\,m^{-3}$	Anions

Table 3.1: ADM1 state variable and their characteristics

The primary goal of this model was to provide a usable foundation for practical and industrial applications, thereby overcoming the existence of primarily substrate-specific

formulations. In fact, by starting with an approach inspired by the wastewater ASM, the ADM1 is intended as a valuable starting point for many improvements and different substrates. The model structure comprises biological and physicochemical conversion processes and could be implemented as a differential algebraic equations (DAEs) system or as a system of differential equations (DE). According to the execution method selected, it consists of 26 dynamic state variables and eight implicit algebraic variables, which, in the case of the DE implementation, can be calculated together with the other dynamic ones. An overview of the 26 relevant process variables of ADM1 is presented in Table 3.1 [62].

ADM1 model was developed on a shared COD basis for feedstock and biomass. Moreover, the influent substrate consists of a portion of inert and a portion of the degradable substance. This method maximizes the range of applicability while preserving standard reaction parameters and identifying the distinct steps of the process based on the COD flux along them. Indeed, while considering the total influent COD, it is vital to remember that not all of it can participate in AD and produce valuable products, with a portion, in some cases significant, serving as an inert and so being excluded. Figure 3.1 provides an overview, partially simplified, of the different steps considered and the possible reactive pathways that the COD flux can follow in ADM1. Many intermediate products are formed

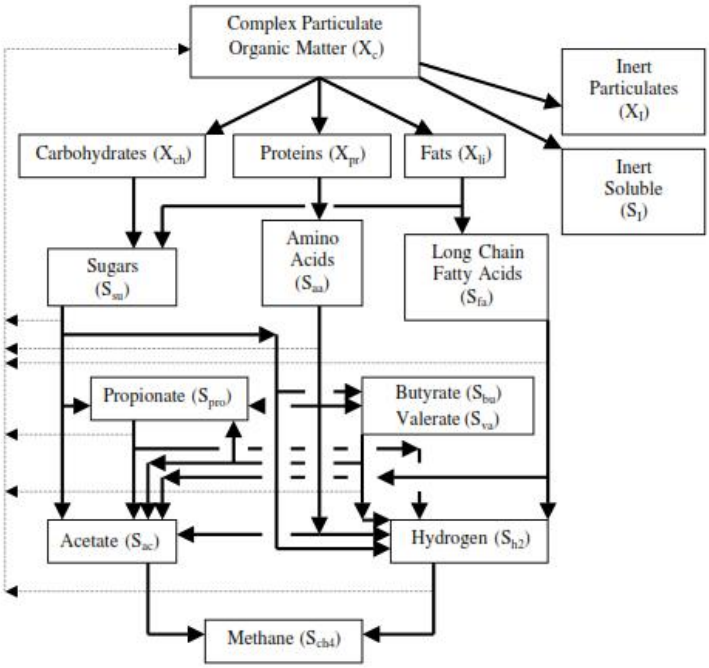

Figure 3.1: Scheme of COD flux and reactions represented by ADM1 model [80].

in the model's biochemical stages, produced in five major phases that run in succession and, in peculiar cases, with parallel reactions. Microorganisms only control the three

strictly biological steps, namely acidogenesis, acetogenesis, and methanogenesis. On the other hand, Extracellular stages are represented by two partially non-biologically regulated substrate solubilization reactions: disintegration and extracellular hydrolysis. This division comes from the description of influent composite as a homogeneous substrate, which can produce the three main biochemical polymers (i.e., carbohydrates, proteins, and lipids) with disintegration-hydrolysis sequential steps. Following the previously described approach, in this case, the representation of this step has been assumed to follow a first-order kinetic [81], [82]. The subsequent phases resemble all the microbial-assessed phases, lumping similar substrates (such as sugar, represented as glucose only) to provide a model with a reasonable number of parameters. However, the number of reactions considered is still relevant, allowing us to define ADM1 as a detailed model. A detailed description of all the assumptions, the reaction considered, and the reasons for those choices can be found in the book report dispensed to present the ADM1 [83]. Some general concerns that are pertinent to the current work are listed below. Monod-type kinetics account for substrate uptakes in intracellular biochemical processes. As illustrated in equation 3.4, limiting effects are introduced for each inhibitory factor with appropriate functions. There, the first part resembles the inhibited Monod equation for the rate of a $-j$ reaction, in terms of Monod constant (k_M $[g\,L^{-1}\,d^{-1}]$. The inhibitory terms are represented by the $I_{1...n}$ terms, each representing an effect on the kinetics of that reaction and consequently appropriately defined for each compound.

$$\rho_j = k_m \cdot \frac{S_j}{K_{S,j} + S_j} X_j \cdot I_1 \cdot I_2 \ldots I_n \tag{3.4}$$

Each microbiological group for which the response rate is computed has its inhibition function. For example, pH inhibition affects all groups, whereas hydrogen affects acidogens. Most functions are derived from empirical or semi-empirical laws, with parameters estimated from literature and experimental studies.

Along with the biochemical processes, major physicochemical ones are also represented simultaneously due to their impact on the system. These processes include interphase or intraphase interactions, such as liquid/gas transport, ionic dissociations, and acid-base equations. These transformations are essential for system design because, as expected, they directly impact critical process variables across all gas flows and transfer rates. Furthermore, as illustrated in figure 3.2, most biochemical conversions have direct interaction and link with physicochemical conversions. Notably, these later reactions are modeled as reversible and dependent on equilibrium constants, whereas *biochemical reactions* are defined as mono-directional.

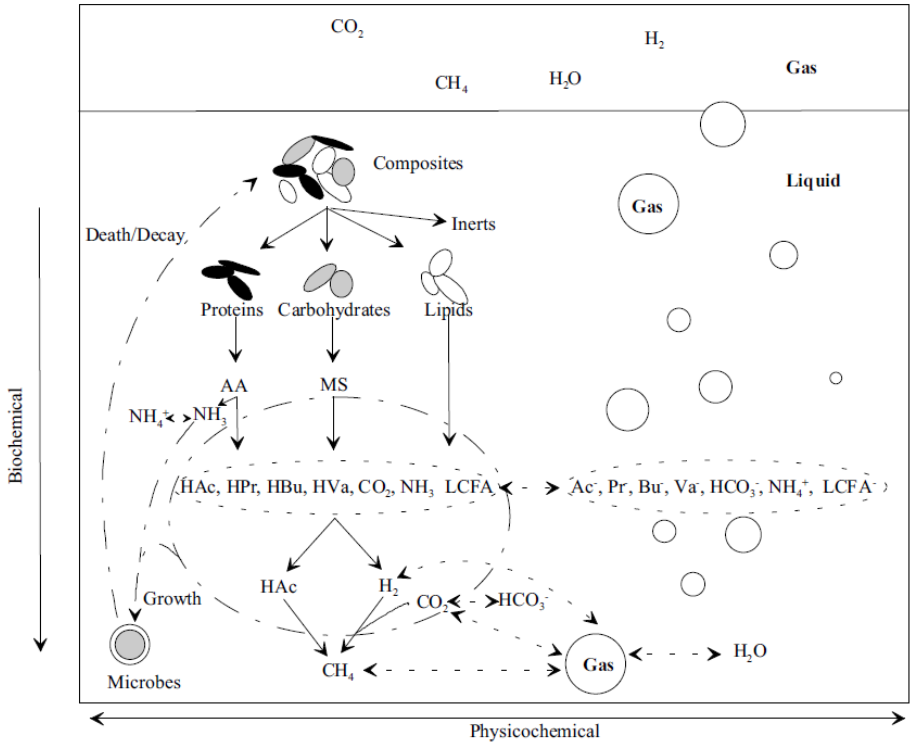

Figure 3.2: Representation of biochemical (vertical axis) and physicochemical (horizontal axis) steps of ADM1 [83].

Since its first release, ADM1 has been used and thoroughly tested in various applications and simulations. Its validity has been demonstrated in a wide range of domains, from the ones for which it was created to more complex ones, such as agro-derived waste digestion and co-digestion scenarios [84], [85]. In rare cases, especially when working with full-scale applications, ADM1 may need to obtain the actual values of the process variable. However, broad trends have always been correctly anticipated, even in these scenarios. As anticipated by the authors, the main critique was the lack of precise characterization of the influent COD and the validity of kinetic parameters. This feature is an inherent characteristic of the detailed models, of which ADM1 is the state-of-the-art representation in the AD field [86], [87]. Furthermore, the stoichiometry of the processes chosen to identify ADM1 and its COD link is solely based on catabolic metabolism. However, anabolic responses may substantially influence under substrate-limiting conditions, opening the view to criticalities in these circumstances [88].

In conclusion, IWA, successfully with ADM1, reached its scope of providing an adequate general AD model for potential use in industrial design and optimization applications. Moreover, the ADM1 structure provides a solid basis for many further developments and improvements, thus defining, after some decades of lack of standards, a common

framework for AD modeling [87].

3.1.2. ADM1-based Models

ADM1 was designed to serve as a standard structure for AD modeling at the industrial level. As a result, it did not aim to be a perfect model capable of accurately describing each of the innumerable possibilities that can be encountered when analyzing AD systems worldwide. The main goal of the IWA task group was to establish and define a common working ground, which could have aided researchers in defining more accurate case-by-case models by referring to the most general but accurate one. In this regard, ADM1 has pioneered numerous developments and enhancements over the years. Below is a description of those deemed most relevant for the current work.

Plant-wide simulations

Due to its inherent origin from aspects mainly regarding wastewater digestion modeling, ADM1 has been first applied to such systems. Indeed, its applicability in plant-wide simulations could have broadened its utilization at the industrial level. Consequently, it has been tested for such a system since its release. In practice, wastewater treatment plants (WWTP) and all biogas-producing facilities are made up of numerous interconnected units, of which the AD reactor is just a relevant one. The COST/IWA BSM1 model (Benchmark Simulation Model No. 1) was made available in 2001 by IWA and the European Cooperation for Science and Technology association [89]. Its goal has been to develop a platform for benchmarking control strategies for activated sludge systems on a plant-wide basis. Indeed, a broad monitoring control of all the units included in a plant is fundamental and much more effective than one based on individual processes. An extension of the previous benchmark has also been made available to improve the challenges of these topics, including a larger plant layout and more rigorous evaluation criteria, and the possibility to assess dynamic inputs. This extension allows a new stable and rigorous benchmark model for plant-wide simulations of WWTP, presented as the Benchmark Simulation Model No. 2 (BSM2) [90]. Within BSM2, ADM1 took place as the reference model for anaerobic digestion, and aspects of its implementation to facilitate stability and reduce its stiffness have been extensively analyzed [91].

Oxygen Influence

Typically, AD models do not investigate oxygen effects in depth. The conventional view that oxygen is toxic for AD processes is not entirely correct; in some cases, a proper

dosage of this compound can also result in beneficial results [57], [92]. Up to now, the most developed model able to represent oxygen effects in the AD environment is represented by the ADM1-Ox model [93], [94]. This model completely follows the logic behind the ADM1 in terms of COD flow, kinetic expressions, and other assumptions but adds one extra variable standing for dissolved oxygen. Moreover, it adds three new processes to account for aerobic uptakes by the three acidogenic groups. As said, the kinetic expressions recall the traditional ADM1, presenting a Monod saturation expression for the aerobic processes. An example is provided in equation 3.5, where the terms are those already described for ADM1, declined for the aerobic reaction. A further term is added to the factorial of inhibition functions to produce the I_j inhibitory term for all the reactions, according to equation 3.6 [93].

$$\rho_{j,aer} = k_{m,aer} \cdot \frac{S_{j,aer}}{K_{S,j,aer} + S_{j,aer}} \frac{S_{O_2}}{K_{S,O_2} + S_{O_2}} X_j \cdot I_j \tag{3.5}$$

$$I_{O_2} = \frac{K_{O_2}}{K_{O_2} + S_{O_2}} \tag{3.6}$$

New parameters, such as yield and saturation coefficients, must be adopted and estimated. The other significant addition concerns hydrolysis and is required due to oxygen's theoretical effect on that process. Indeed, increased rate constants could be used to simulate a faster hydrolysis process, but the authors chose a more mechanistic approach. By assuming that hydrolysis is catalyzed by extracellular enzymes secreted by the respective acidogenic biomass groups, the new reactions are modified to consider the concentration of these families.

This model successfully predicted the behavior of an aerated digester in the lab, but it has yet to be applied to larger plants [93]. It also included a quantitative description of the oxygenation effects, which may inspire future research. Indeed, it demonstrated that aeration, particularly if intermittent and limited in some cases, can benefit the global system by improving stability and, eventually, overall methane yield. [94].

Sulfur Influence

Sulfate reduction processes are an essential feature of anaerobic digestion systems. The original ADM1, however, did not consider any of those. This feature makes the model unsuitable for applications with relevant sulfur-based compounds, such as vinasses or cane-molasses [49]. In these cases, the influent sulfates undergo reduction processes to produce an excessive amount of sulfides in the gas and reduce methane yield in a un unpredicted way.

Consequently, sulfate reduction (SR) models have been developed over the years. Effective integration of the ADM1 model was done in 2003 with an extended version of ADM1 [95] by including some concepts and modeling assumptions previously assessed [79]. The major highlight of this model is that it models the sulfate reduction process by adding four new reactions, where the electron donor is represented by butyrate, propionate, acetate, and hydrogen, respectively. Consequently, as sulfate-reducing bacteria, four new groups of microorganisms must also be included. The kinetics of the process are represented by following the ADM1 principle, with two-substrates Monod-type kinetics (Equation 3.7. Also, in this case, an inhibitory function $I_{sulfide}$ is added to the global inhibitory function I_j to account for an excessive amount of sulfides which limit the microbe growths (Equation 3.8) [95].

$$\rho_j = k_m \cdot \frac{S_j}{K_S + S_j} \frac{S_{\mathrm{SO_4}}}{K_{S,\mathrm{SO_4}} + S_{\mathrm{SO_4}}} X_j \cdot I_j \tag{3.7}$$

$$I_{sulfide} = 1 - \frac{\mathrm{H_2S}}{KI_{sulfide}} \tag{3.8}$$

A similar model, but with different assumptions and applied in cases with industrially applicable conditions of sulfur loading, has also been developed by other researchers [96]. This latter model is built on the same basis as ADM1, thus being depicted as another extended version accounting for sulfate reduction. This version includes only three new SRB families, not considering the effects of sulfate reduction on butyrate as a substrate. Moreover, it includes acid-base equilibrium reactions and a more detailed parameters calibration and sensitivity analysis. As a result, it has been tested against industrial sulfate-rich wastewater. The model was able to predict a correct value for the most relevant process variable, including methane production decrease when sulfide content becomes significant. A relevant addition to this model is the inclusion of the gas phase transfer, allowing us to assess the concentration of contaminant H_2S in the biogas.

According to the literature available, these two examples are the most relevant ones in the field of modeling sulfate reduction in terms of the quality of their results. Other models have been designed to represent sulfur-derived compounds' impacts in AD correctly. In fact, by pairing different models' outcomes and experimental data, it has been proved that a balance between complexity and simplicity may be helpful when deriving models for sulfate processes [97]. Indeed, while detailed representations of SR processes for all microbial families can be helpful in some cases, such a complication is only sometimes required. Some conclusions can be drawn by considering the effect of each microbial activity separately. Accounting for hydrogen leads to poor performances when considering processes based on a single substrate, while acetate produces some errors. If the model is

built on pairs of substrates instead, it is possible to obtain good results even when only acetate and hydrogen are considered. As a result, employing more SRB families may only sometimes be necessary, potentially reducing the number of equations required to predict the phenomenon in an acceptable manner [97].

Sulfate Reduction and Oxidation Models

As introduced before, microaeration can effectively reduce the amount of hydrogen sulfide in produced biogas. However, there needs to be more approachability to such technology from an engineering perspective, particularly regarding its modeling and control [54], [55]. This gap in the literature is because, as previously stated, sulfur reduction and sulfide oxidation, or oxygen effects, have typically been treated as separate concepts. However, they are inextricably linked, and to produce effective models of microaeration and its effects, they must be modeled concurrently.

These considerations led to the development of a new ADM1-based model, accounting for both processes of reduction and oxidation of sulfur-derived components, named ADM1-S/O [98], [99]. This model stands on the basis defined by ADM1 and by the previous works on both sulfate reduction (SR) and sulfides oxidation (SO) kinetics [95], [100], but incorporating them in a singular model able to effectively represent the impacts of microaeration. One relevant model represented both SR and SO as dependent processes, with valid results for a lab-scale system [101]. However, it needed more connection with all the other process variables, and such a gap was still waiting to be filled. According to the published literature results, ADM1-S/O includes four reactions for sulfate reduction and one for sulfide oxidation, as well as the respective liquid-gas transfer rates and the correspondingly modified mass balances. The model is fully described in the dedicated report, where it has been tested and applied to a UASB reactor. The model has also been effectively used to validate assumptions about microaeration conditions quantitatively, and product distribution [98].

ADM1-S/O contains both equations, with a Monod-kinetic scheme for the biochemical and a power law relation for the oxidative chemical scheme. It demonstrated a relation between pure chemical (anoxic) and biochemical oxidation of sulfides and the latter's benefits. The model proved that in the presence of oxygen, sulfides are converted into their oxidative state by both pathways. The microbe-mediated one accounts for more than 60% of the total and can be up to 2.5 times faster (in the experimental conditions 29.5 $mg\,SL^{-1}d^{-1}$ for biochemical versus 12 $mg\,SL^{-1}d^{-1}$ for chemical oxidation) obtaining values similar to those already present in the literature. Accordingly, it also simulated that in microaeration conditions, elemental sulfur is the main product of oxidation, and

thiosulfate presence is almost always negligible, especially considering the biochemical reaction. [99], [102].

Another model in the literature with potential industrial applications is the Anaerobic Digestion Enhancement (ADE), which aims to be an upgraded version of ADM1 and a digital twin of an AD plant [103]. It uses generalized parameters to represent the kinetics of H_2S production and the effects of O_2 injection. This approach may enable the definition of optimal aeration conditions for AD, with flexibility for industrial conditions of co-digestion scenarios. This model may allow for the definition of optimal aeration conditions for AD, with flexibility for industrial co-digestion scenarios. Its stiffness and complexity, however, remain significant for its effective use in real-time control systems.

3.2. Lumped Models

Detailed models are a powerful tool in many situations, but due to their intrinsic complexity are only sometimes viable tools. Such mechanistically inspired models could indeed have many benefits and potentialities, but their requirements for parameter identification and lack of flexibility make them challenging to use for control purposes [65]. Consequently is helpful to reduce models' complexity by deriving more simple expressions and variables to facilitate practical applications. It has been proved that only some of the reactions and intermediates of AD have the same relative importance, and as a result, it is possible to remove or lump some of them [104]. Typically, these lumped variables (i.e., variables that represent a combination of different, eventually similar, components) are derived by working on global reactor mass balances and extrapolating the desired reaction from them.

In the literature, it is possible to find such lumped models, which are direct reductions of ADM1 [105] or others that are lumped by following the biochemical and mechanistic characteristics of the systems [65], [106]. This latter category has been chosen as the starting point of the present work. In particular, the choice has fallen on the AMOCO model[106]. This model founds extensive applicability in different conditions, especially for control-oriented simulations, and it is considered the most critical lumped model regarding AD developed so far [66], [67], [107], [108]. The following section will thus cover the AMOCO model's description and development, which, according to the authors' knowledge, is the most relevant.

3.2.1. AM2: AMOCO Model

In 2001, a model was developed within the AMOCO - FAIR European program's framework to be an easily identifiable model for control purposes in anaerobic digestion[106]. This model, lately named AMOCO or, in a few cases, AM2 (Anaerobic digestion Model No.2) [108], includes two bacterial populations, namely the acidogenic (X_1) and the methanogenic (X_2) microorganisms, and the two respective general reactions of acidogenesis from a solubilized substrate (R8) and of methanogenesis (R8), considering acetate as a reference species standing for all the VFAs.

$$k_1\,S_1 \longrightarrow X_1 + k_2\,S_2 + k_4\,O_2 \tag{R7}$$

$$k_3\,S_2 \longrightarrow X_2 + k_5\,CO_2 + k_6\,CH_4 \tag{R8}$$

For both reactions, the individual rate is given by a common kinetic relation, accounting for both a specific growth rate ($\mu_i\,[d^{-1}]$) and for the species concentration $X_i\,[g\,L^{-1}]$, as shown in equation 3.9, where the reaction rate is $r_i\,[g\,L^{-1}]$.

$$r_i = \mu_i X_i \tag{3.9}$$

The specific growth rates are obtained with Monod and Haldane expressions for acidogenic and methanogenic reactions, respectively, for the reasons explained in section 3.1. Bacterial biomass is measured in volatile solids (VS), which is the most commonly used organic matter content quantification in environmental engineering. For the same reasons why ADM1 developers made that choice defined by ADM1, COD (chemical oxygen demand) has been chosen as the unit of measure for the organic substrate because it reflects the chemical energy content that is made available for the growth of X_1 and X_2. As a result, S_1 is defined in terms of $[g\,COD\,L^{-1}]$; X_1 and X_2 as $[g\,VS\,L^{-1}]$; VFA, alkalinity (Z), inorganic carbon (C), bicarbonate(B), carbon dioxide in solution (CO_2) , and total alkalinity (Z) are described as molar concentrations in $[mmol\,L^{-1}]$.

The model results in a system of six differential equations derived from a mass-balance approach (Equations 3.10 - 3.15). The other variables, particularly the gas flows (q_C for

carbon dioxide; q_M for methane), are derived by simple algebraic equations.

$$\frac{dX_1}{dt} = (\mu_1 - \alpha D)X_1 \tag{3.10}$$
$$\frac{dX_2}{dt} = (\mu_2 - \alpha D)X_2 \tag{3.11}$$
$$\frac{dZ}{dt} = D(Z_{in} - Z) \tag{3.12}$$
$$\frac{dS_1}{dt} = D(S_{1,in} - S_1) - k_1\mu_1 X_1 \tag{3.13}$$
$$\frac{dS_2}{dt} = D(S_{2,in} - S_2) + k_2\mu_1 X_1 - k_3\mu_2 X_2 \tag{3.14}$$
$$\frac{dC}{dt} = D(C_{in} - C) - q_C + k_4\mu_1 X_1 + k_5\mu_2 X_2 \tag{3.15}$$

The gaseous flow rates are calculated assuming no methane is dissolved in the liquid phase. Consequently, the amount produced by the methanogenesis reaction entirely goes out from the digester (Equation 3.16). Conversely, for CO_2, its dissolved amount in the liquid must also be accounted for. Assuming that equilibrium is reached between liquid and gaseous phase, and it follows Henry's equation ($k_La[d^{-1}]$; $K_H = 16[mmol\,L^{-1}\,atm^{-1}]$, the outlet flowrate is computed accordingly (Equation 3.17).

$$q_M = k_6\mu_2 X_2 \tag{3.16}$$
$$q_C = k_La(CO_2 - K_H P_C) \tag{3.17}$$

In the dedicated reference, it is possible to find a complete description of the model variables, assumptions, and equations [106]. However, the appendix is provided with a brief recap of those.

The identifiability of a lumped model's parameters determines its reliability, robustness, and, thus, applicability. Indeed, the AMOCO model has its identification procedure based on linear regressions on steady-state data and influent characteristics of the process. This procedure allows the estimation of the kinetic parameters for the biomass, the gas-liquid transfer coefficient, and the six yield coefficients k_i. The lasts are obtained with a two-step approach, first obtaining four ratios and, subsequently, the single values. The reason for this approach is that usually, no data about biomass concentration are assumed to be available. Consequently, the second step uses the total suspended solids' data and a parameter accounting for the ratio of acidogens and total biomass. A more detailed description of the parameters identification is given in section 4.

The model validation by the authors showed a good representation of the steady state and

its dynamic predictions in various operating conditions. Some discrepancies are present in the pH, inorganic carbon, and alkalinity trends, most likely due to a need for more information about their influent value. [106]. Moreover, reports of its usage are present in the literature, both in terms of a dynamic simulation model and as control algorithms' starting point [109]–[111].

3.2.2. AM2HN

The primary limits of the original AM2 model lie in its assumption of starting from a fully hydrolyzed substrate, as well as a poor description of the variables related to inorganic carbon during the simulation. Consequently, two relevant improvements of the AMOCO structure are presented in this section, one accounting for the nitrogen effects (AM2N) and one for the hydrolysis stage (AM2HN). Since those two upgrades are one consequence of the other, it will just be described as the final result, named AM2HN [112], [113].

Biomass Decay Term

The first modification regards the mass balance equation of the two biomasses (3.10, 3.11), which, in the case of long-term simulations with high retention times, fail in predicting the values of the variables. This result is a consequence that in the original model, no terms describing the cells' death are present. A new version of these equations is proposed, stating that the decay terms account for a constant percentage of the maximum growth rate [112]. The resulting equations (3.18, 3.19) contain the new terms $k_i = 0.1 \cdot \mu_{i,max}[d^{-1}]$, stating that the decay term is given by the 10% of the individual μ_{max}

$$\frac{dX_1}{dt} = (\mu_1 - \alpha D - k_{d,1})X_1 \tag{3.18}$$

$$\frac{dX_2}{dt} = (\mu_2 - \alpha D - k_{d,2})X_2 \tag{3.19}$$

The addition of this term, which seems to be nothing else than a new addendum in the differential equations, has more relevant implications. This term modifies the steady-state expression for the two biomass terms, forcing a non-linear procedure for the kinetic parameters identification.

Nitrogen Role

AMOCO defines *alkalinity* as a non-reactive species, accounting for the sum of dissociated acids in the liquid phase. These are represented by VFAs and bicarbonate, while nitrogen contribution is neglected. However, this can lead to misleading results since free ammonia

strongly affects bicarbonate concentration. Moreover, ammonium ions are not constant throughout the process since they derive from biochemical reactions occurring in the system, above all, protein hydrolysis.

AM2 has consequently been modified to account for reactive nitrogen species N, accounting for its contents within substrate S_1, $N_{S,1}$, and for those contained in the biomass, N_bac. The first varies according to the substrate consumption, whereas the second term depends on the growth rate of the biomass. The new variable, dynamically described by its equation, be grouped to the original alkalinity (3.12 to have a new definition of Z given by equation 3.20.

$$\begin{aligned}\frac{dZ}{dt} = D(Z_{in} - Z) + (k_1 N_{S1} - N_{bac})\mu_1 X_1 - N_{bac}\mu_2 X_2 + \\ + k_{d,1} N_{bac}\mu_{1,max} X_1 + k_{d,2} N_{bac}\mu_{2,max} X_2\end{aligned} \tag{3.20}$$

This equation includes nitrogen dynamics and alkalinity by keeping the same number of state variables and differential equations. The results show that the precision regarding all the variables well estimated by the original AM2 is still the same. At the same time, relevant improvements are obtained in the dynamic description of the variable related to inorganic carbon. As a result, the model becomes more precise with the same level of complexity.

Hydrolysis Inclusion

To overcome the second major limitation of the AM2/AMOCO model lies in seeing the substrate as entirely soluble. This approach can be an applicable limit since it has been recognized that, in most cases, particulate hydrolysis is the rate-determining step of the whole process [76]. Including such a mechanism widens the model's range of applicability, allowing for a better description of the substrate conversion in many real scenarios.

The second improvement of AM2, derived from the AM2N, is the AM2HN, which includes the hydrolysis of particulate matter [113]. Indeed, this is done by adding a new state variable X_T $[gCOD\ L^{-1}]$, which states for all the hydrolyzable mixture which can be converted to soluble substances, according to the model reaction R9.

$$\mathrm{X_T} \longrightarrow \mathrm{S_1} \tag{R9}$$

To close the system, consequently, there is the need to add one differential equation describing the particulate substrate mass balance and to modify accordingly the one

describing S_1, which has to account for the product of the hydrolysis reaction (3.13). The results are given as follows (3.21,3.22) where, analogously as the ADM1, the reaction rate is expressed by a first-order kinetic of the type $r_{hyd} = k_{hyd}X_T$, also defining a new parameter to be identified.

$$\frac{dX_T}{dt} = D(X_{T,in} - X_T) - k_{hyd}X_T \tag{3.21}$$

$$\frac{dS_1}{dt} = D(S_{1,in} - S_1 - k_1\mu_1 X_1 + k_{hyd}X_T \tag{3.22}$$

The overall AM2HN model has been assessed in its dynamic comparisons against ADM1 results in terms of dimensionless variables $y*(t)$ (i.e., $y*(t) = y(t)/y^0$, as it was for AM2N) to represent its potentialities in control systems. The good results regarding inorganic carbon species already discussed in the previous section are still the same for the new variable. Additionally, there has been a remarkable improvement of the S_1 dynamic which now better represents the response at a step-wise input of a first-order system. Also, other simulations with reliable influent deviations and different feedstock characteristics almost perfectly reproduce the adimensional gas flows, making this model a promising tool for control systems in AD [108], [113].

4 | Improved Identification Procedure

The most crucial step in creating a mathematical model is parameter identification. Each model requires parameters, typically estimated from available experimental data, to represent them and ensure their applicability adequately. The model's realism and accuracy will be determined because any mathematical representation can be good if it relies on a good fit with experimental data. Indeed, the model must reflect reality, not the other way around.

4.1. AM2 and AM2HN Model Calibration

Robust parameter calibration is essential, particularly for these models, which are intended to be used in various industrial contexts. Since this is the ultimate purpose of lumped models, of which AM2/AMOCO and its derivatives are part, extensive attention has been paid to assessing the calibration's quality. This section will give an overview of how the parameters of the two models presented before are given. Please refer to the dedicated reference for a complete description of everything which may be omitted [106], [113].

4.1.1. AM2 Identification

This model has thirteen parameters to be identified from experimental data. These can be divided into three groups, including six kinetic parameters ($\mu_{1,max}, K_{S1}, mu_{2,max}, K_{S2}, K_{I2}$, α); one interphase transfer coefficient (k_La); and six yield coefficients (k_{1-6}). The description of all the mentioned parameters had already been given in the previous, except for the parameter α. Indeed, this specification refers to the fraction of the biomass in the liquid phase, and it is used to represent the reactor design mathematically simply: its values are between 0 and 1, where $\alpha = 0$ stands for an ideal fixed-bed reactor and $\alpha = 1$ for an ideal CSTR.

All the parameters are estimated according to steady-state and influent data at different dilution rates D, deriving the asymptotic expressions for the differential equations 3.10-3.15 and see how this fit with the data by linear regressions methods. Kinetic parameters are calculated from the equations regarding their growth rates and the substrates S_1 and S_2, which dynamics and equilibrium are, in fact, directly affected by the microbial kinetics. The liquid-gas transfer coefficient, calculated from the assumptions only for CO_2, its value is estimated from carbon dioxide outlet molar flow (3.17). The procedure is slightly more complex for the yield coefficients and is carried out following a two-step approach. The authors of the AM2/AMOCO model, assuming that measures of biomass quantities are commonly not easily obtained, derive a more simplistic approach to finalize the parameter identification. Firstly, four ratios of the six coefficients are estimated by manipulations of the gas flow equations (3.16, 3.17), and only afterward the single values are obtained. Indeed, it has been demonstrated that these values are only needed when assessing the biomasses' quantities. Consequently, measurements related to those are required to determine individual values. The frequently measured value of VSS is used to assess the total biomass quantity $(X_1 + X_2)$. The concentrations of the individual families are subsequently computed with the ratio ν between acidogenic and methanogenic bacteria, estimated from literature sources and exploited as shown in equation 4.1. This equation, further manipulated and adjusted to the available quantities, will provide the value of k_1 and, afterward, k_3. These two individual figures and the four ratios will provide all the six yield coefficients required.

$$\nu = X_1/(X_1 + X_2) \tag{4.1}$$

This procedure shows how it can be possible to identify practical values for the parameters of the developed model from industrially available measurements. However, some of these parameters show quite a high standard deviation, particularly those related to kinetic expressions, since deriving from rough approximations of the actual rates.

4.1.2. AM2HN Identification

This section covers the modified identification procedure described for AM2HN, which basis has been previously set by the AM2N. Since this is the model from which the present work started, much detail will be provided. Adding new terms leads to an increase in the number of parameters to be estimated. Moreover, AM2HN changes the source of its data to measurements based on the output of ADM1 simulations. This new approach has been made possible by the advancements in process modeling (in 2001, when the original

AM2 was released, the ADM1 was still in the embryonal phase) discussed, opening the possibility of direct comparisons between the variables. AM2HN also converts ADM1 and AM2 variables used in the present work.

The AM2HN model requires the evaluation of 15 parameters specific to the feedstock and reactor configuration. These are represented by: 6 yield coefficients (k_{1-6} $[-]$); the mass transfer coefficient (kLa $[d^{-1}]$); the hydrolysis kinetic coefficient (k_{hyd} $[d^{-1}]$); two biomass maximum growth rates ($\mu_{1-2,max}$ $[d^{-1}]$); the VFA inhibition coefficient for VFAs (K_{I2} $[kg\,m^{-3}]$); two semi-saturation constants ($K_{S,1-2}$ $[kg\,m^{-3}]$) and two biomass decay kinetic coefficients ($k_{d,1-2}$ $[d^{-1}]$). Immediately, by comparing these with the ones of AM2, it is possible to see that α is not identified anymore. This decision is taken to simplify the subsequent step by considering that this is an operational parameter and, thus, is commonly known or can be easily estimated by the reactor design and conditions. Following the approach of the AMOCO model also, in this case, the identification is carried out from the steady state conditions of the material balances at different dilution rates. The different conditions are obtained by varying this parameter in different ADM1 simulations instead of having different real scenarios. This solution can ease the way by which data are collected, providing quick access to a variety of different possible conditions. Such an approach relies on the fact that ADM1 simulations must be reliable, at least regarding their steady-state conditions.

Starting the discussion from the estimation of kinetic coefficients, adding the decay terms directly impacts the direct linearization of the expressions. Indeed, the mass balances used, related to S_1 (Equation 4.2) and S_2 (Equation 4.3) cannot be adequately solved, both being underspecified by one parameter. The index ss specifies that the actual variable value is at steady-state conditions.

$$S_{1,ss} = \frac{\mu_{1,max} - k_{d,1}}{\alpha D(1 + K_{S,1})} S_{1,ss} - K_{S,1} \cdot k_{d,1} \tag{4.2}$$

$$S_{2,ss} = K_{S,2} \frac{k_{d,2} + \alpha D}{\mu_{2,max} - \alpha D - k_{d,2}} + \frac{S_{2,ss}^2}{K_{I2}} \frac{k_{d,2} + \alpha D}{\mu_{2,max} - \alpha D - k_{d,2}} \tag{4.3}$$

To try to reduce the system and solve it, it is necessary to fix the value of one parameter or find a third equation. In AM2HN this has been accomplished by defining the value of $k_{d,1}$, fixed as the 10% of the respective $\mu_{i,max}$ ($0.1\mu_{i,max}$). The equations can so be rewritten as follows:

$$S_{1,ss} = \frac{1}{\mu_{1,max}} \frac{\alpha D S_{1,ss}}{0.9} + \frac{K_{S,1}}{\mu_{1,max}} \frac{\alpha D}{0.9} + 0.11 \cdot K_{S,1} \tag{4.4}$$

$$S_{2,ss} = \frac{1}{\mu_{2,max}} \frac{\alpha D S_{2,ss}}{0.9} + \frac{K_{S,2}}{\mu_{2,max}} \frac{\alpha D}{0.9} + \frac{1}{\mu_{2,max} K_{I2}} \frac{\alpha D S_{2,ss}^2}{0.9} + \frac{0.11}{K_{I2}} S_{2,ss}^2 + 0.11 \cdot K_{S,1} \tag{4.5}$$

In this way, equation 4.4 becomes now a multi-variable-linear expression, while the second (4.4) retains its nonlinearity and thus requires specific non-linear algorithms to regress the value of its parameters.

Expression 4.4 contains two angular coefficients to be determined. These are represented by the reciprocal of the maximum specific growth rate of the first biomass $\mu_{1,max}$ and the ratio between the former and the relative semi-saturation constant (K_{S1}). The intercept represents the semi-saturation constant itself. The independent variables are the dilution rate (D) and the concentration of substrate S1. The equation 4.5 has four angular coefficients. The first two are the correspondent of the previous equation for biomass two. The third is represented by the multiplication of the first by the reciprocal of the inhibition coefficient coming from Haldane kinetic expression – which reflects the methanogenesis biomass poisoning due to high VFA concentration. The fourth and last one is simply the reciprocal of the inhibition coefficient itself. Also, in this case, the intercept is represented by the semi-saturation constant relative to substrate S2. Both equations are so specified and solvable. However, introducing the fixed decay rate coefficient to relate the decay of the biomass to its maximum rate of production introduces an assumption that may not always be true, leading to instability in the solution and eventually to no precise results.

The coefficient of liquid-gas transport k_La is obtained accordingly to the expression obtained in AM2 from the values of the carbon molar outflow as represented in equation 4.6. Equation 4.7 is another representation of the same expression in which the value of the concentration of dissolved CO_2 is calculated by the inorganic carbon, pH, and dissociation constant for bicarbonate (pKb).

$$q_{C,ss} = k_L a \left(CO_{2,ss} - K_H P_c\right) \tag{4.6}$$

$$q_{C,ss} = k_L a \left(C_s s \frac{1}{1 + 10^{pH_{ss} - pKb}} CO_{2,ss} - K_H P_c\right) \tag{4.7}$$

In contrast to what has been done in AM2, estimating the yield coefficients k_{1-6}, k_{hyd} follows a one-by-one approach. Indeed, the advantage of using simulated values from ADM1 as steady-state data is that it also gives information about biomass. The lack of

such information was why a two-step approach was previously chosen. Linear regressions indeed obtain the single values on equations.

$$D(X_{T,in} - X_{T,ss}) = k_{hyd} X_{T,ss} \tag{4.8}$$

$$D\left(S_{1,in} - S_{1,ss}\right) + k_{hyd} X_{T,ss} = k_1 \alpha D X_{1,ss} \tag{4.9}$$

$$\left[D\left(S_{2,in} - S_{2,ss}\right)\right] = k_3\, \alpha D X_{2,ss} - k_2\ \alpha D X_{2,ss} \tag{4.10}$$

$$\left[(q_{C,ss} - D(C_{in} - C_{ss})\right] = k_5\, \alpha D X_{2,ss} - k_4\ \alpha D X_{1,ss} \tag{4.11}$$

$$\frac{q_{M,ss}}{X_{2,ss}} = k_6\, \alpha D \tag{4.12}$$

The regression of $k_h yd$ (equation 4.8) is straightforward and stable, while it is not the same for all the other stoichiometric coefficients. As said, the values of the parameters obtained from the regressions above may not always be reliable, retrieving negative or misleading values, which will be the cause for misleading results in the final simulation.

4.2. Improvement in Calibration

AM2HN presented excellent and remarkable results in dimensionless variables $y^*(t) = y(t)/y_0$, but no results were available regarding the absolute value of those variables. This decision is justified because it is a model devoted to controlling purposes. The main interest is consequently given more in the dynamics than in the variables' actual value. However, a robust and reliable model should also adequately represent the actual value of a process variable.

With the data available from the reports [112]–[114], the AM2HN model has been reproduced to validate the assumption of considering only the dimensionless quantities. The data are those of the implementation of ADM1 in the BSM2 benchmark [91]. At first, the same identified parameters have been applied to the same base-case scenario: assess the response of a system, originally in steady state conditions, at a 20% step increase of particulate influent ($X_{T,in}$) after 20 days and a step decrease back to original conditions at the 100th day. A summary of the input data used is given in A.2.

The results shown in figure 4.1 are identical to those given in AM2HN presentation [113], confirming that the model has been correctly reproduced. A deeper assessment has then been done by considering not only the dimensionless quantities and their actual value. This analysis shows that the parameters identified with the AM2HN approach give misleading results. Indeed, even though from a dimensionless perspective, everything seems to be coherent, this is not the case when the actual quantities are considered. It has been

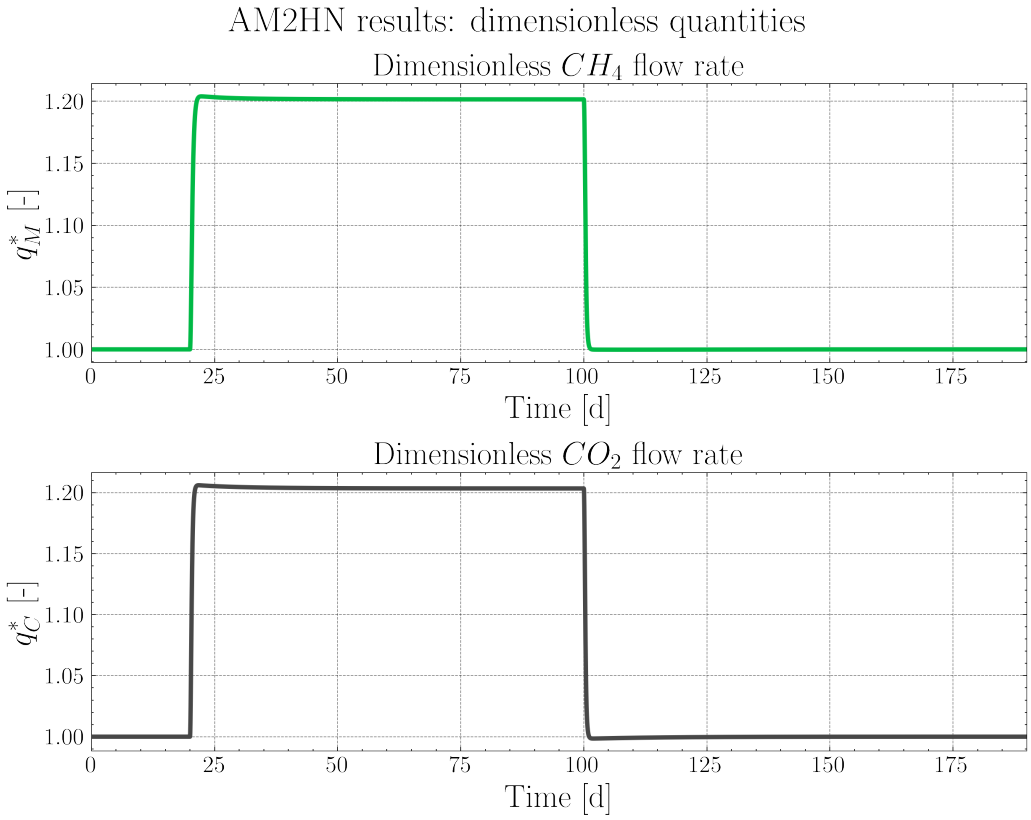

Figure 4.1: Gas flows dimensionless variables of AM2HN with original identification procedure.

chosen to show the results regarding the gaseous outflows for two main reasons. They are the most relevant regarding an industrial plant since they give the plant profits. Also, any error present before can be highlighted since those are the ultimate result of the model. As shown in figure 4.2, the resulting biogas from the simulation is primarily composed of CO_2, with a molar composition (directly comparable to the volumetric, under ideal gases assumption) of around 25% methane. This result does not seem realistic just by considering what biogas is, and it can be confirmed further by comparing this figure to those computed by ADM1 output. This value was available from the data and gave a methane fraction of around 64%. This low CH_4 concentration, resulting from the comparison between ADM1 and AM2HN results, is primarily due to a significant overestimation of the carbon dioxide gas, which, consequently, derives from the excessive estimation of the CO_2 produced by bacteria. As a result, while the AM2HN model has been demonstrated to describe AD variables effectively, further effort is required to estimate its parameters better. This improvement should allow the same dynamic trends and more realistic estimation of the process variables, particularly those related to inorganic carbon.

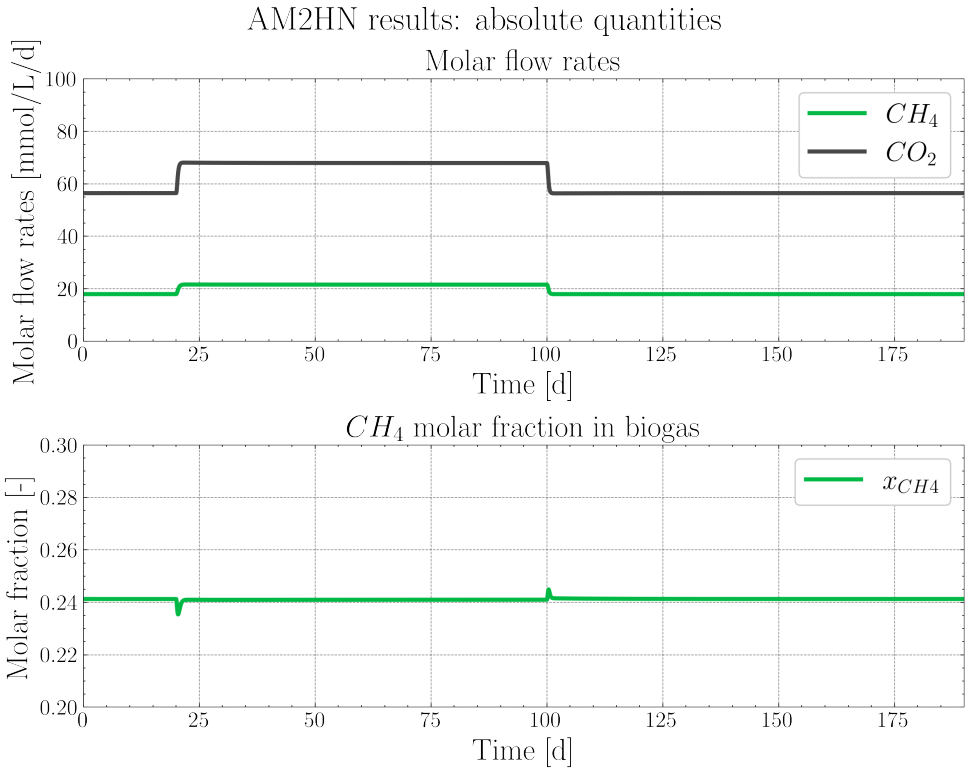

Figure 4.2: Absolute values of gaseous flows and methane molar fraction of AM2HN with original identification procedure.

4.2.1. Proposed *Hybrid* Identification

A new *hydbrid* identification approach has been developed, aiming at tackling the issue that arose. This modified calibration method aims to complement the data available from the ADM1 and used in AM2HN with the concepts presented in AM2. The experimental data and fitting results are compared in graphs for each dataset used. The final goal was to obtain a new set of parameters that, implemented in the AM2HN, give the same dynamic trend and a more realistic estimation of the absolute values of the variables.

Kinetic Parameters

Kinetic parameters for both microorganism families must be identified from experimental data. For methanogens, these are the maximum specific growth rate $\mu_{max,1-2}$, the half-saturation constant $K_{S,1-2}$, and the VFA inhibition constant $K_{I,2}$, as it was in the original procedure of AM2HN. As an additional improvement to the regression method, the estimation of the biomass decay constants $k_{d,1-2}$ is proposed. This decay term is calculated as a percentage of the maximum specific growth rate using a decay proportionality coefficient $C_{d,1-2}$ to keep the regression as stable as possible. This method is relatively stable

because it restricts its value between 0 and 1, avoiding unfounded results and producing reliable decay kinetics values. In AM2HN, a similar procedure was used, where the value was not calibrated but set to 0.1. The equation obtained is still derived from 4.2 and 4.3 to identify parameters for X_1 and X_2, respectively. In this case, also $C_d, 1-2$ are not defined and have to be estimated from the regressions on equations 4.13 and 4.14.

$$S_{1,ss} = \frac{\alpha}{(1-C_{d,1})\mu_{1,max}} DS_{1,ss} + \frac{\alpha K_{S,1}}{(1-C_{d,1})\mu_{1,max}} D + \frac{C_{d,1}}{1-C_{d,1}} K_{S,1} \tag{4.13}$$

$$\begin{aligned} S_{2,ss} = &\frac{\alpha}{(1-C_{d,2})\mu_{2,max}} DS_{2,ss} + \frac{\alpha K_{S,2}}{(1-C_{d,2})\mu_{2,max}} D + \\ &+ \frac{\alpha}{(1-C_{d,2})\mu_{2,max}K_{I,2}} DS_{2,ss}^2 + \frac{C_{d,2}}{(1-C_{d,2})K_{I2}} S_{2,ss}^2 + \frac{C_{d,2}}{(1-C_{d,2})} K_{S,1} \end{aligned} \tag{4.14}$$

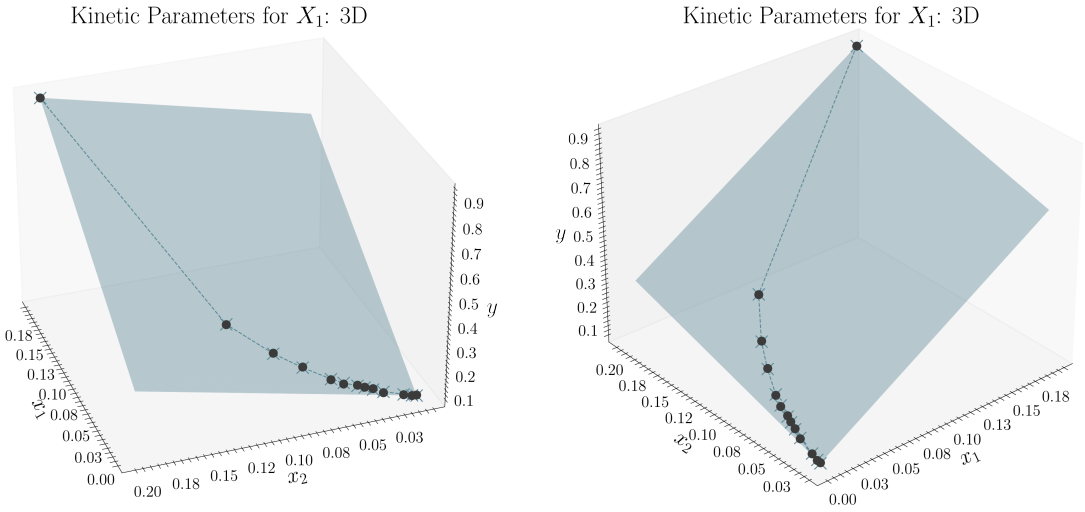

(a) Visualization from first perspective.

(b) Visualization from second perspective.

Figure 4.3: Tri-dimesional visualization of fitting for results of multi-variable regression on equation 4.13 for X_1 kinetic parameters.

As discussed before, the expression on S_1 can be regressed as a multi-variable linear regression of the form $y = \alpha_1 x_1 + \alpha_2 x_2 + \alpha_3$, where $x_1 = DS_{1,ss}$,$x_2 = D$, $y = S_{1,ss}$ and α_i are the parameters of the regression. On the contrary, the equation related to S_2 requires a non-linear analysis, with D and $S_{2,ss}$ as independent variables, and thus requires a non-linear regression algorithm to establish its parameters. Finally, the kinetic parameters can be then easily computed from the regressed coefficients. As it is possible to see from figure 4.3, the linearity of the multi-variable regression cannot be represented in a bi-dimensional environment. Aiming to provide a compelling visualization of the

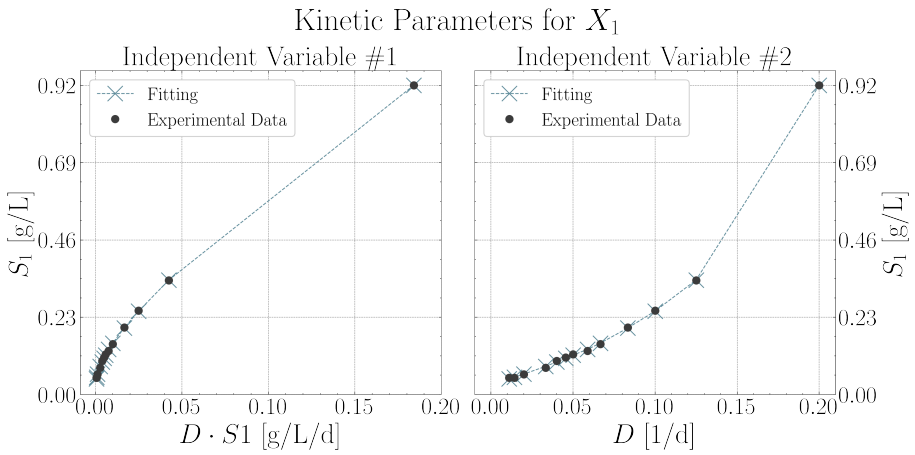

Figure 4.4: Results against each single independent variable.

fitting, the tri-dimensional representation and its projections on each plane are given by $x_{1,2}/y$, presented in figure 4.4 with the highlighted the fitting evaluation at coordinates corresponding to the data. Figure 4.5 shows the nonlinearity of the equations against the independent variable, which is associated with the parabolic shape, providing the algorithm's efficacy also in that case.

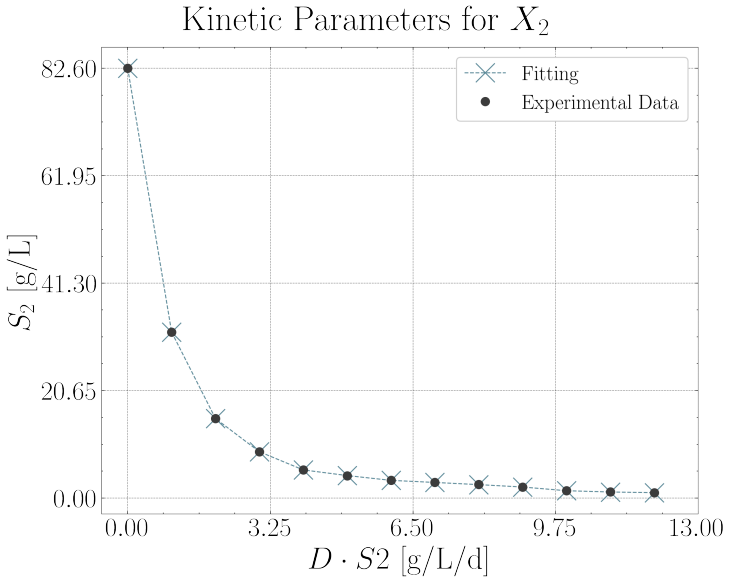

Figure 4.5: Results of regression on equation 4.14 for X_2 kinetic parameters.

Gas-Liquid Transport Coefficient

For the k_La, the same approach of AM2 first and AM2HN later has been chosen. This approach carries out a regression on the equation expressing the CO_2 gas flow (3.17), according to equation 4.6, which directly uses the carbon dioxide concentration in the

liquid phase, available from ADM1 simulations. Given the values CO_2 molar flow, $q_{C,ss}$, dissolved carbon dioxide concentration, CO_2, and partial pressure of it in the digester headspace, P_c, the regression are usually simple and stable, as shown by figure 4.6. That equation is also repeated below for the sake of simplicity.

$$q_{C,ss} = k_L a \left(CO_{2,ss} - K_H P_c\right) \tag{4.6}$$

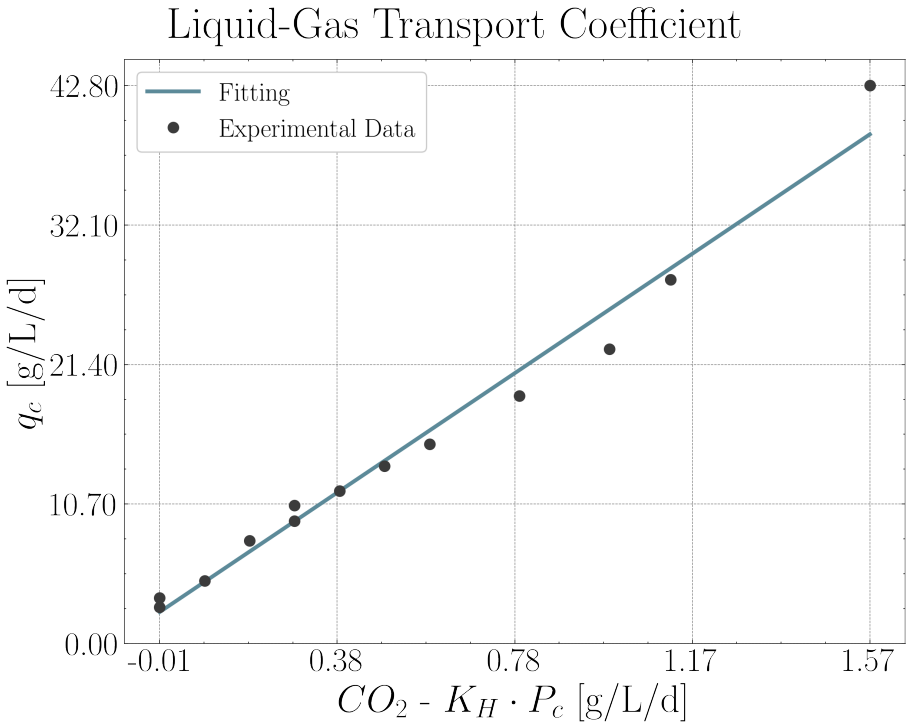

Figure 4.6: Results of regression on equations 4.6 for $k_L a$ mass transport coefficient.

In equation 4.6, another parameter given as input is a physical constant related to the system: Henry's constant K_H. This term is related to Henry's law of equilibrium and gives quantitative information regarding the solubility of a compound into another, in the present case of CO_2 in water [115]. In the previous works a value of $K_H = 16\,[mmol\,L^{-1}\,atm^{-1}]$ was given as a reference value. However, this value must be carefully evaluated in terms of measure unit and density dependency, directly affected by temperature. As a result, in the present work, the value of Henry's constant is calculated using an empirical expression that gives the solubility in water of a specific component in the gas phase.

Under the assumption that Henry's law is valid for dilute solutions up to 1 atm, it is

possible to calculate the respective constant obtained as the reciprocal of the compound solubility in water. In most cases, H_i is provided as the proportional constant for the species $-i$ of Henry's law $p = H_p x$, where p is the compound partial pressure $[atm]$ and x its mole fraction in the aqueous liquid phase $[atm]$. The immediate dimensional analysis leads to the unit of measure of H_p, which is in $[atm]$ as well and thus not adequate to be directly inserted in the model. The subscript $_p$ indicates that this is Henry's constant, referred to as pressure. To convert it for an appropriate unit of measure is possible to divide its value by the molar density of water $[mol\, m^{-3}]$, obtaining the constant for a relation accounting for molar concentration H_c [116]. The reciprocal of the latter is the required K_H for the AM2 model, in $[mmol\, L^{-1}\, atm^{-1}]$. All the calculations now described are reported in equations 4.15-4.17.

$$H_p = \frac{1}{\exp(A + B/T + C \cdot \ln(T) + D \cdot T)} \tag{4.15}$$

$$H_c = \frac{H_p}{\rho_{V,\mathrm{H_2O}}(T)} \tag{4.16}$$

$$K_H = \frac{1}{H_c} \tag{4.17}$$

The inputs are system temperature T $[K]$ and a set of experimental parameters, given for CO_2 in table 4.1. The density of water, which also depends on temperature, is assumed constant in the range of operating temperatures commonly utilized and equal to its value at 25 °C of 55 342 $[mol\, m^{-3}]$. This method allows obtaining the value of Henry's

Table 4.1: Parameter values for evaluation of solubility in aqueous solutions [116]

Species	***A***	***B***	***C***	***D***
CO_2	-159.854	8741.68	21.6694	-1.10261E-03

constant, in the correct unit of measure, for every temperature as long as the empirical parameters are valid. Figure 4.7 shows the results within the available temperature range. It is worth noting that the commonly used value, $KH = 16$ $[mmol\, L^{-1}\, atm^{-1}]$, is obtained at a temperature of 62° C, which is practically impossible to reach in a fermentative system. In most cases, anaerobic digestion occurs at temperatures ranging from 35 to 45° C, corresponding to the temperatures at which bacteria thrive in mesophilic and thermophilic environments. In this case, Henry's constant value varies between $KH = 26.5 - 21.5$ $[mmol\, L^{-1}\, atm^{-1}]$. As a result, this approach is used to upgrade the identification procedure properly.

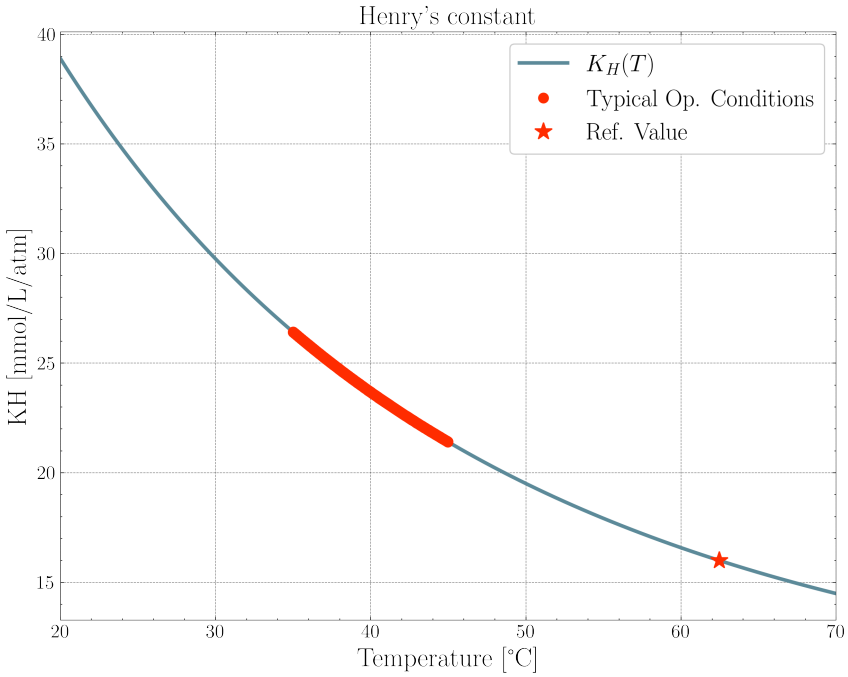

Figure 4.7: Trend of Henry's constant value for AM2/AM2HN model. Highlighted the ranges corresponding to typical operating conditions and the reference value from [106].

Yield Coefficients

In this case, the proposed procedure differs from the original identification of stoichiometric coefficients. This approach aims to simplify, speed up and improve the identification procedure's reliability and stability by adapting the dual-step approach initially proposed in AM2/AMOCO. Firstly, the rate constant k_hyd for hydrolysis is obtained in the same way proposed by the AM2HN identification method, from equation 4.8. The result of this first single variable linear regression is shown in figure 4.8. A two-step procedure inspired by AM2 calibration is then used for the six coefficients of biochemical reactions. At first, four are identified ratios, followed by two individual coefficients, which can close the system of unknowns. The two singular yield coefficients for substrate S_1 consumption (k_1) and methane production (k_6)are obtained from regressions on equations 4.9 and 4.12, indicating the steady state conditions for the respective process variable. Equations 4.9 to 4.12 are then reorganized to get two linear expressions explicit for CH_4 and CO_2 specific flow rate (equations 4.18 and 4.19). In this transformation, ratios between stoichiometric coefficients are performed and used as parameters for two multi-variable regressions according to AM2 approach [106]. In particular, the ratios $k6/k3$ and $k2/k1$ are from the methane flow rate, while $k4/k1$ with $k5/k6$ are in the carbon dioxide flow rate instead. In conclusion, the computation of each of the remaining individual coefficients (k_2, k_3, k_4, k_5) is performed by multiplication of the ratios for the respective single coefficient previously

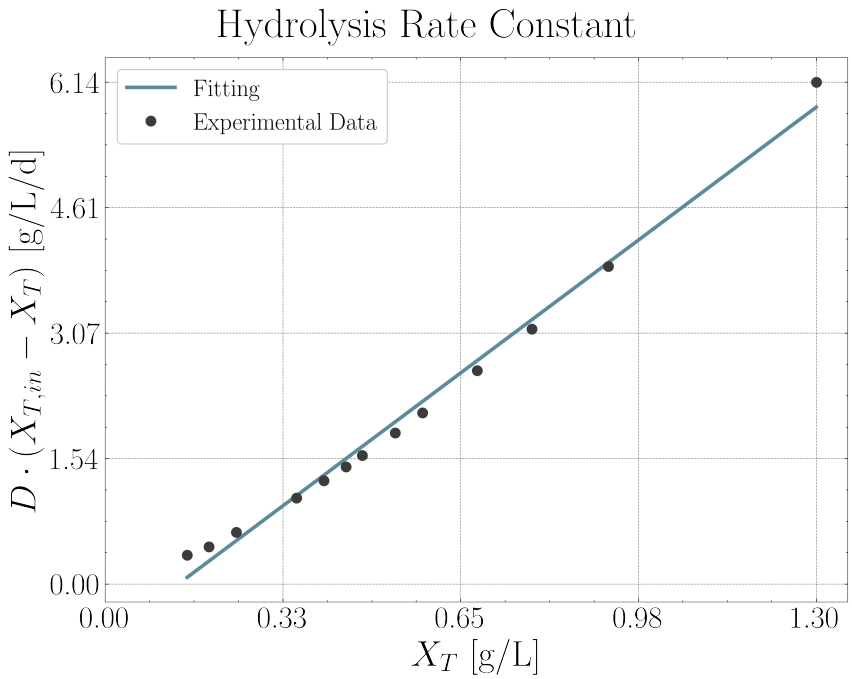

Figure 4.8: Results of regression on equations 4.8 for k_{hyd} hydrolysis rate constant.

obtained. The complete set of equations used in the regressions is reported below in the new order of utilization for completeness.

$$D(X_{T,in} - X_{T,ss}) = k_{hyd} X_{T,ss} \tag{4.8}$$

$$D\left(S_{1,in} - S_{1,ss}\right) + k_{hyd} X_{T,ss} = k_1 \alpha D X_{1,ss} \tag{4.9}$$

$$\frac{q_{M,ss}}{X_{2,ss}} = k_6\, \alpha D \tag{4.12}$$

$$q_M = \frac{k_6}{k_3}\, D\left(S_2^{in} - S_2\right) + \frac{k_6}{k_3}\frac{k_2}{k_1}\, \left[D\left(S_1^{in} - S_1\right) + k_{hyd} X_T\, \right] \tag{4.18}$$

$$q_C - D\left(C_{in} - C\right) = \frac{k_4}{k_1}\, \left[D\left(S_1^{in} - S_1\right) + k_{hyd} X_T\right] + \frac{k_5}{k_6}\, q_M \tag{4.19}$$

The results of these regressions are shown in the next figures. For the two single-variable regressions, only the bi-dimensional plane is shown (Figure 4.9) along with the fitting line. For multi-variable regressions giving the yield coefficient ratios are presented both the tri-dimensional (Figure 4.11) and their bi-dimensional representation (Figure 4.10), following the method mentioned above.

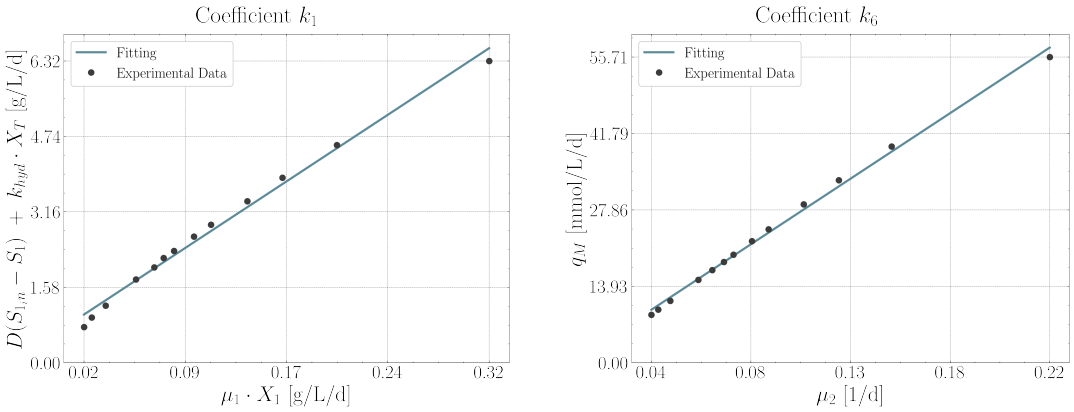

(a) Regression for k_1. (b) Regression for k_6.

Figure 4.9: Results of regression on equations 4.9 (Fig. 4.9a) and 4.12 (Fig. 4.9b) for singular yield coefficients.

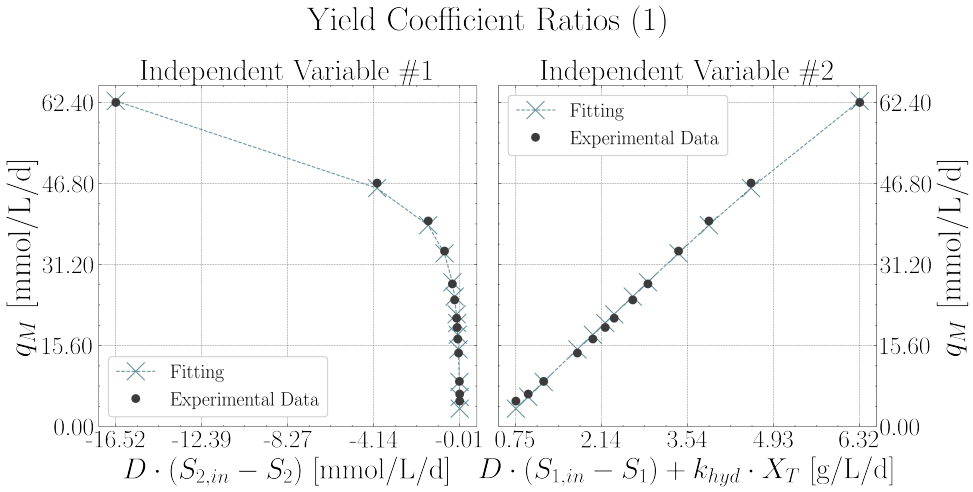

(a) Equation on methane molar flow.

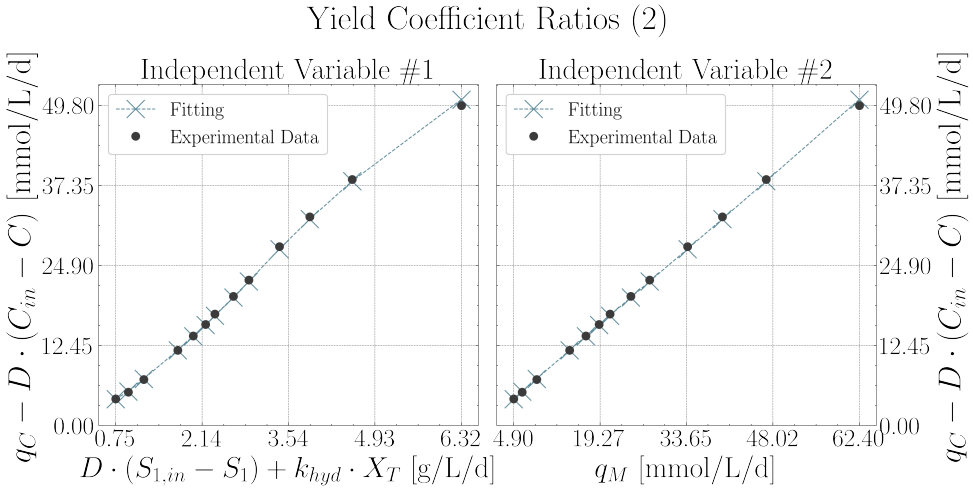

(b) Equation on carbon molar flow.

Figure 4.10: Bi-dimensional visualization for results on multi-variable regressions on equations 4.18 (Fig. 4.10a) and 4.19 (Fig. 4.10b).

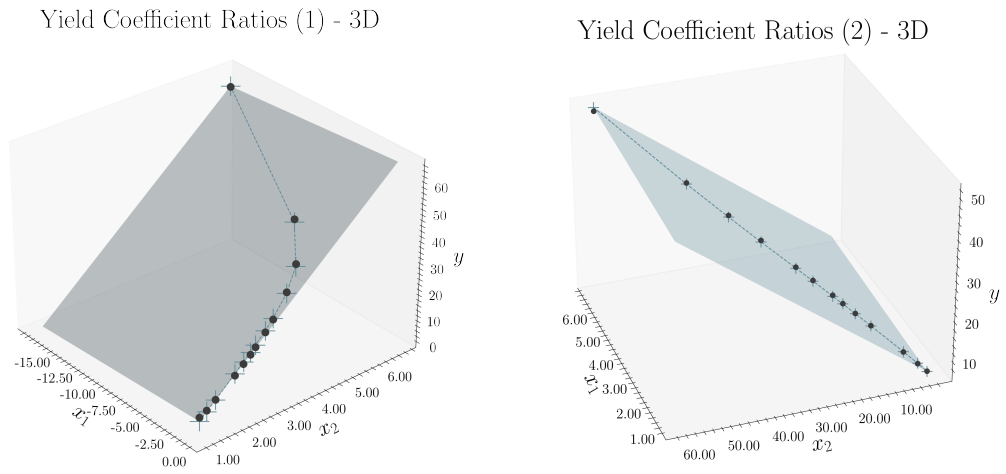

(a) Equation on methane molar flow.

(b) Equation on carbon molar flow.

Figure 4.11: Tri-dimensional visualization for results on multi-variable regressions on equations 4.18 (Fig. 4.11a) and 4.19 (Fig. 4.11b).

Parameters Results

The parameters under the label *AM2HN* are obtained following the regression approach used in the original report. These parameters are not calculated for dataset one since they are available from [113]. For dataset two, they are instead resulting from implementing that method. Finally, the results indicated as *New Approach* result from the new identification method described. A comparison of parameters obtained with the new approach and with the original one is given in this section.

Table 4.2 shows the results for those parameters for which identification is directly derived from AM2HN, namely those for bacteria kinetic equations and the mass transfer coefficient k_La. It is possible to not be similar among these numbers due to the same equations. However, the AM2HN approach gives a negative value with dataset two in one case, for K_{I2}, which was not given by the new procedure, which, conversely, gave a considerably large number. This result is probably due to the insensitivity of the non-linear regression performed on this parameter. Moreover, it is possible to see how the decay constants are now derived from experimental data and not assumed to be equal to 0.1. Results for yield coefficient estimation, the most innovative section of the new approach, are presented in table 4.3. As expected, no differences are shown for the hydrolysis rate constant, whereas a more considerable difference is shown for the other parameter in some cases. In particular, it is interesting to note that for dataset one, the original approach gives a value of k_5 remarkably larger than that of k_6. This conclusion is not realistic, if not impossible, since both are coefficients for the products of the methanogenesis reaction,

Table 4.2: Comparison of results obtained from calibration for kinetic parameters and mass transport coefficients.

		$mu_{1,max}$	K_{S1}	$mu_{2,max}$	K_{S2}	K_{I2}	$c_{d,1}$	$c_{d,2}$	k_La
DATASET 1	*AM2HN*	0.33	0.4	0.13	2.93	207	0.100	0.100	24
	New Approach	0.32	0.4	0.14	3.05	199	0.071	0.173	23
DATASET 2	*AM2HN*	0.30	0.3	0.34	0.07	-6	0.100	0.100	28
	New Approach	0.30	0.4	0.36	4.69	6.75E+08	0.074	0.089	122

and the first stands for the CO_2 produced, the latter for CH_4 produced. It follows that k_6 should be higher than k_5 to represent the reaction correctly.

Table 4.3: Comparison of results obtained from calibration for yield coefficients.

		k_{hyd}	k_1	k_2	k_3	k_4	k_5	k_6
DATASET 1	*AM2HN*	5.02	20	464	514	310	600	253
	New Approach	5.00	19	815	956	10	191	253
DATASET 2	*AM2HN*	0.30	10	-2	34	87	21	280
	New Approach	0.30	20	128	136	78	115	256

4.3. Model Results with Modified Approach

The new identification method leads to a new set to be applied in AM2HN and improve its results. The results are compared with an own simulation of ADM1, based on the same input data and influent deviations, in Python language based on PyADM1 [117]. The major drawback of the original AM2HN, namely the not realistic biogas composition with a CO_2 majority, is not present anymore. Indeed, as it is possible to see in figure 4.12, the absolute values of the outlet gaseous flows are better represented, even with the comparison with ADM1. However, a margin for improvement is still present, being the value of carbon molar flow under-estimated. Results available from the AM2HN in

dimensionless variables are also compared with those from the new identification method against ADM1 output. The results show a slightly larger error for dimensionless CO_2 flow rate with the new method when a system deviation is given. However, this deviation is because the absolute value of that variable is remarkably lower, and consequently, any deviation is amplified when a ratio is considered. The considerable improvement obtained

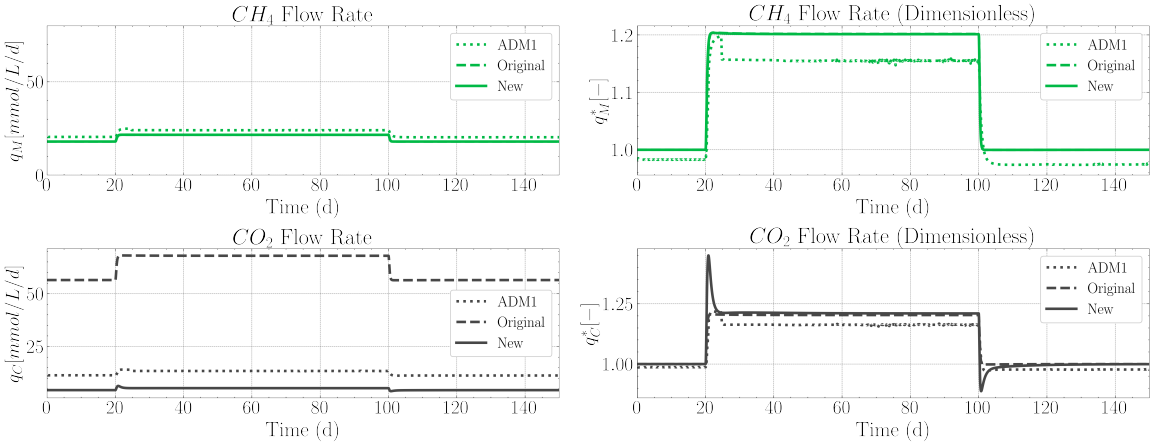

Figure 4.12: Comparison of results for gaseous outlet flow rates. *ADM1*: results PyADM1 simulation; *Original*: results AM2HN with parameters from [113]; *New*: results AM2HN with parameters from the new identification method.

with the new set of estimated parameters is seen clearly when the biogas composition is considered, as seen in figure 4.13. Reminding that according to the AM2 hypothesis, the resulting gaseous flow is composed of CH_4 and CO_2 only, it is possible to see that the new results are more realistic than the originals. The methane percentage is too high due to underestimating the carbon dioxide molar flow. This first conclusion can be misleading since the error has just been switched from one variable to another. However, the value of methane percentage now falls under a realistic range, even if in the upper percentile. Moreover, it has been noted that the regression which leads to the estimation of carbon dioxide production coefficient k_4 is almost insensitive to that parameter in a particular range. An improvement of the regression algorithm may thus lead to a higher value for this yield coefficient, which will raise the value q_C and, finally, a more precise value of x_{CH4}.

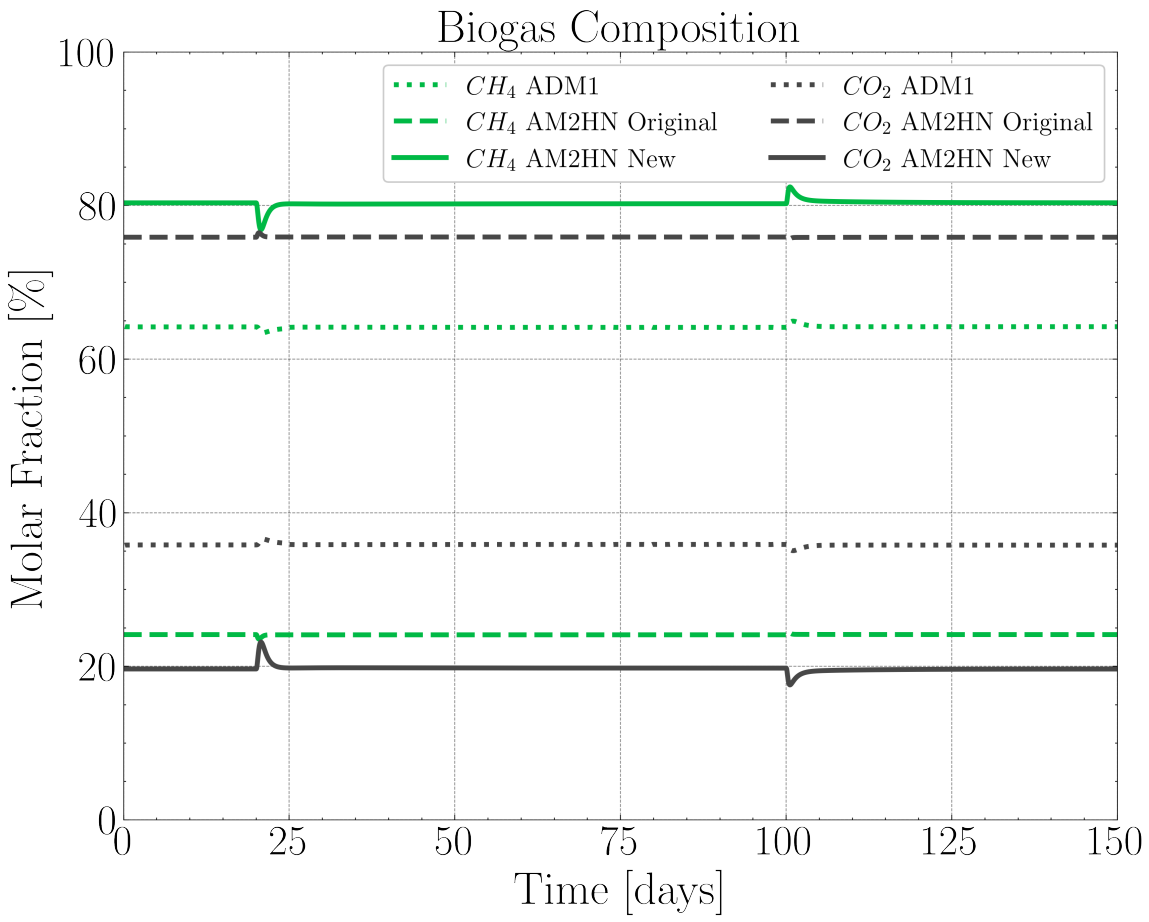

Figure 4.13: Comparison of results for gaseous outlet composition. *ADM1*: results PyADM1 simulation; *Original*: results AM2HN with parameters from [113]; *New*: results AM2HN with parameters from the new identification method.

Results for the other affected process variables lead to the same considerations for better quality for absolute results, and are presented in appendix B.2. In some cases, a slight overshoot is present due to a smaller absolute value of that variable, as already discussed for the CO_2 flow rate.

In general, the proposed identification method effectively improves the results of the AM2HN model, mainly when dealing with absolute values of the process variables.

4.3.1. Second Dataset Simulation

A test on the second dataset has been performed to prove the validity of the new procedure. The dataset represents another example of the application of the BSM2 framework for ADM1 [118]. Here the results are consequent to a deviation of +20% for the influent particulate X_T. In ADM1, this is equally divided between the variable related to the

influent particulate material: X_{pr}, X_{ch}, X_{li}. X_{xc} does not show deviations since its value is null from the start of the simulation according to the data provided. This approach assumes a substrate that can be a degraded influent to a WWTP. The most relevant fact on this simulation is that it is provided as an *intensive* treatment, with a very high flow rate. Indeed, the HRT is of only five days, compared to the 20 days of the previous dataset. Nevertheless, the estimation of the parameters took the same examples into account. In some cases, to obtain better results, it might be appropriate to proceed with an identification over a narrower range closer to the case under consideration. In

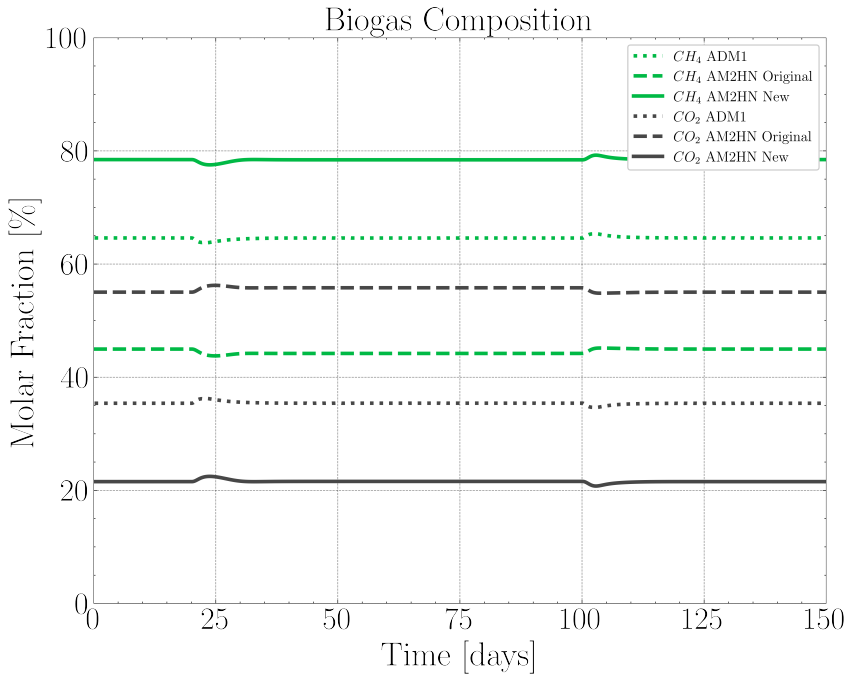

Figure 4.14: Comparison of results for gaseous outlet composition.*ADM1*: results PyADM1 simulation; *Original*: results AM2HN with parameters from [113]; *New*: results AM2HN with parameters from the new identification method.

this case, the results obtained for the gaseous rates and composition ((figure 4.14) with the parameters of the original procedure are more coherent with reality. Nevertheless, the new identification approach guarantees better accuracy for most variables in their dimensional and dimensionless representation. Moreover, the new parameters provide remarkable results and improvements in the accuracy of the total absolute flow rate, as shown in figure 4.15. This crucial process indicator is almost perfectly predicted by the model with the new identification method, even though the subdivision between the two gases does not reach this level of precision. Obtained results reinforce the idea that a better algorithm for parameter estimation may further improve these results.

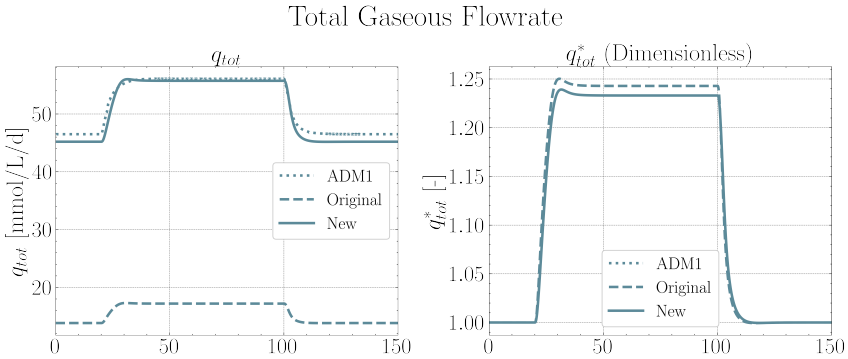

Figure 4.15: Comparison of results for total outlet gaseous flow rate.*ADM1*: results PyADM1 simulation; *Original*: results AM2HN with parameters from [113]; *New*: results AM2HN with parameters from the new identification method.

5 | ADOCS Model

Up to now, the models presented have represented anaerobic digestion with a focus on biogas and the biochemical reactions occurring prevalently in the liquid phase. When the model aims to assess the impact of microaeration for sulfide removal, it is also necessary to investigate what happens in the reactor headspace. There it is where SOBs are living and, consequently, where oxidation occurs. To realize that target the conceptualization of the digestion system requires further steps. ADM1 and AM2 models are interested in something other than the reactor's gaseous phase, which is considered an inert volume before the outlet.

The present study represents the sulfide removal happening in the headspace and thus requires a modelization of that reactor region. According to the typical AD modeling approach, the headspace is considered a continuous stirred tank reactor (CSTR) and modeled accordingly to provide a reasonably low complexity. The scheme proposed accounts for two different influent streams: one consisting of the gaseous products of anaerobic digestion and one for oxygen (or air, depending on the case) injected. The injection is assumed to be directly in the headspace since this is the most widespread solution nowadays and can also be readily applied as a retrofit to actual plants. In order to increase the model's reliability, a fictitious liquid gas equilibrium unit (*flash*) is inserted between the liquid phase and the gas phase. This addition should increase the model's reliability in describing the species distribution between the two phases considered and, according to the author's knowledge, is not present in any other model of this kind.

The liquid phase is modeled following the reaction of a lumped model, such it can be the AM2. Due to the improvements obtained by AM2HN, this latter version is used as starting point for current developments. All the newly added terms and equations will be described in the following sections but briefly summarized here. As a first addition, the water content in the influent stream is considered explicitly. The reason is that, in some cases, as in WWTP, water is a consistent amount of the influent and may significantly alter the vapor-liquid equilibrium. Moreover, it affects the reactor's liquid level, which is no longer assumed constant and is evaluated according to the influent deviations at

every step. A second significant addition is the presence of sulfur-reducing bacteria, which convert part of the substrate to sulfide during digestion, representing the sulfate reduction process. All these steps are grouped into the developed Anaerobic Digestion and Oxygen Control System (ADOCS) model presented in this section.

The overall scheme described is shown in figure 5.1 and can be summarized in a few key points:

- The liquid phase of the reactor, where biochemical reactions occur, is modeled as a CSTR according to the equations of the AM2HN model, accounting for sulfur reduction and water stream.
- The products of the CSTR enter a fictitious flash unit: the vapor outlet stream will enter the headspace, whereas the liquid represents the digestate.
- The vapor flow exiting the flash, raw biogas, enters the headspace, where oxygen is added. The sulfide oxidation is modeled by considering this region as a second CSTR.
- The outlet flow from this reactor is the global gaseous flow rate of the AD system after sulfide oxidation.

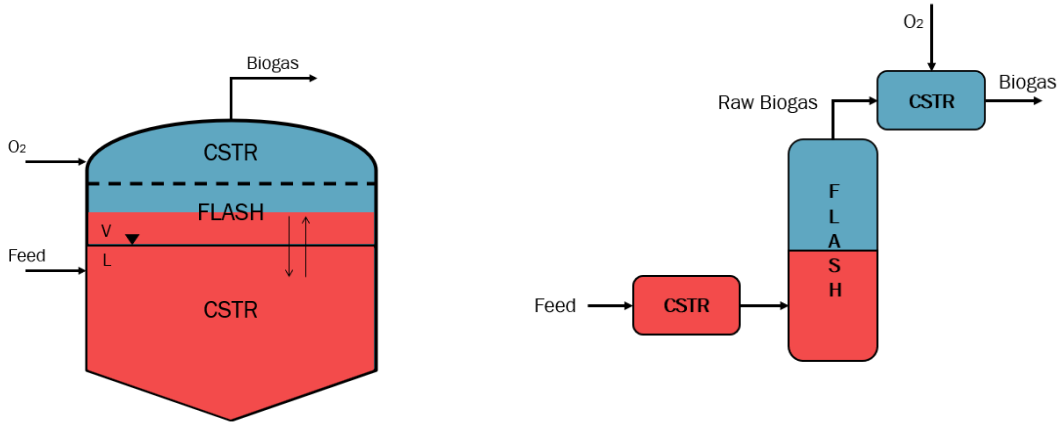

(a) Correspondence between digester areas and model blocks considered.

(b) Segregated blocks perspective.

Figure 5.1: Graphical representation of different blocks considered to model the anaerobic digestion system.

Table 5.1: Definition of deviations assigned to influent variables for the base-case scenario presented. Effects of each value A on each influent variable x_in as $x_{in}(t) = A \cdot x_{in}(t = 0)$.

time ***[days]***	$S_{1,in}$ ***[g/L]***	$S_{2,in}$ ***[mmol/L]***	C_{in} ***[mmol/L]***	N_{in} ***[mmol/L]***	$X_{T,in}$ ***[g/L]***	Q_{in} ***[m3/d]***
0	1	1	1	1	1	1
1	1	1	1	1	1	1.1
8	1	1	1	1	1.1	1.1
15	1	1	1	1	1	1.1
22	1	1	1	1	1	1

5.1. Methodological Note

All the simulations have been carried out by implementing the models in *Python* language. The choice is because it is a flexible, innovative, and relatively simple programming language. Moreover, its open-source nature allows for a large personalization and possibilities for industrial applications without great economical efforts. The two most utilized in the present work are the numerical library *numpy* and the optimization library *scipy*. For regressions, the algorithms of *sklearn* have been used, while for data visualizations, *matplotlib* and *scienceplots*.

5.1.1. Case Study Definition

In this chapter, all the results will be presented according to a base-case definition. This approach allows assessing the system response to specific deviations in the influent in organic concentration and total flow. The system's initial conditions are the steady-state values of the variables defined with the influent at the initial time. The case study is associated with the BSM2 implementation of ADM1 and has already been used in the AM2HN presentation. Its data for identification and influent condition are given in the appendix A.2 as *Dataset 1*. The simulation has been carried out for a 30 days time span. In tablen 5.1 are shown all the deviations assigned, where the value is the factor of multiplication assigned to the value of the influent at the initial time: $x_{in}(t) = A \cdot x^0_{in}$. A is a value in the table, x_{in} each of the influent variable. The four deviations are chosen to present, singularly, both the effect of a positive or negative deviation assigned to the organic concentration, X_T and the input flow rate, $dotQ_{in}$. Hours $[h]$ is the basic time unit in most simulations to allow a short computation period. In some cases, however, the results are presented for days $[d]$ for notational or practical reasons.

5.2. Liquid Phase

The AM2HN model, a modified version of the AM2/AMOCO model containing hydrolysis and nitrogen dynamics representation, is utilized as starting point for the representation of biochemical reactions in the liquid phase. In this section, a constant volume of the reactor is defined and assumed equal to a project parameter. Consequently, the dilution rate is computed as $D = \dot{Q}/V_{reactor}$ $[d^{-1}]$. The parameter identification is performed according to what is described in 4.3.1. The water content of the influent flow is added as an explicit term. However, it does not affect this section since all the variables are expressed in concentration, implicitly accounting for it. The AM2HN model is solved by numerical integration with the *odeint* solver, available from the *Scipy* library. All the equations are the same as the AM2HN model, except for S_2 balance. It includes an additional sulfate reduction term described in the next paragraphs.

5.2.1. Sulfate Reduction Modeling

Processes of sulfate reduction by sulfate-reducing bacteria (SRBs) have two impacts on the AD system, reducing the methane yield by consuming part of the VFAs and inhibiting the activity of the methanogens. The present model is intended to preserve the simplicity of AM2HN. Consequently, the explicit inclusion of all the sulfate reduction processes has been immediately excluded. According to the results that show that a good compromise between complexity and accuracy may be reached by including acetate and hydrogen only as a substrate for sulfate reductions [97], the approach followed that pathway. However, AM2HN does not include hydrogen but defines S_2 as the only substrate for methanogens. Consequently, the choice has been to consider SRB as a family of bacteria similar to the methanogens, which grows on the same substrate (S_2) but produces a different molecule. The biochemical equation represented as descriptive of sulfate reduction processes is thus the following:

$$CH_3COOH + H_2SO_4 \longrightarrow 2\,H_2O + 2\,CO_2 + H_2S \qquad \text{(R10)}$$

As a result, two state variables are added to the model: X_{srb} $[g\,L^{-1}]$, representing the microbial population of sulfate reducers; and S_s $[mmol\,L^{-1}]$, which defines the dissolved sulfide, lumped together. To avoid adding too many variables and ultimately being interested in the sulfide which will pollute the biogas, it has been decided not to include a detailed description of the species related to sulfur (i.e., sulfates, sulfide, thiosulfates) and of their interactions. Such an approach has certain limitations, as it does not allows for an estimation of the rate for reaction R10 on a biochemical basis. As a result, direct inclusion of the sulfate reduction process within the dynamic equations of AM2HN has not been

possible. The addition of that influence *a posteriori* has consequently been chosen, also allowing to minimize the computational complexity to be added.

Due to a lack of detailed biological knowledge of the system, the SR process has been modeled mathematically inspired. Such an approach intends to reduce the number of parameters to be estimated or defined as much as possible. The considerations taken into account are the following:

- The SRB bacteria population grows in a way *similar* to methanogens
- During their growth, SRBs consume a part of substrate S_2 and have sulfide production, S_s, as a result of their metabolism.
- Substrate consumption, sulfide production, and growth rate are related by a yield coefficient Y_{srb}.

Regarding the last point, the assumptions are those widely available in the literature for a Monod-type kinetic expression. Specifically, for sulfate reduction, the examples are those cited in the dedicated chapter [96], [98]. The result is that it could represent the SRB process occurring using an expression to describe the SRB population, a second one accounting for their growth rate and a yield coefficient. The inclusion in the AM2 reaction model can be described by a modification of reaction R8 as follows in reaction R11, where k_{srb} is ultimately represented from the yield coefficient, arising from a different mathematical description.

$$\mathrm{k_3\,S_2} \longrightarrow \mathrm{X_2 + X_{srb} + k_5\,CO_2 + k_6\,CH_4 + k_{srb}\,S_s} \tag{R11}$$

A mathematical recap based on the description above and the examples cited are given in 5.1. The definition of the function $f(t)$ describing the bacteria population will be discussed in the next paragraph; μ_{srb} $[g\,L^{-1}\,d^{-1}]$ is the microbial growth rate, which could be associated to dX_{srb}/dt. This can be obtained also from the substrate uptake rate $\rho_{uptake,srb}$ $[mmol\,L^{-1}\,d^{-1}]$, according to Monod description. The yield coefficient Y_{srb} $[g\,mmol^{-1}]$ has been obtained from the value presented by literature references [98] as the one referred to acetate ($0.0342\ g_{srb}\,g^{-1}_{COD,ac}$) and converted to the appropriate unit of measure, accounting also for the COD basis. The expression referred to S_2 indicates, with the subscript $-s$, that this is the influence of sulfate reduction, which has to be

added to the defined AM2 equation for that state variable (Equation 3.14).

$$\begin{cases} X_{srb} = f(t) \\ \frac{dS_s}{dt} = (1 - Y_{srb})\ \mu_{uptake,srb} = \frac{1-Y_{srb}}{Y_{srb}}\ \mu_{srb} \\ \frac{dS_{2,s}}{dt} = -\rho_{uptake,srb} = -\frac{1}{Y_{srb}}\ \mu_{srb} \end{cases} \tag{5.1}$$

The description of the microbial population is the most important and complex step. The present work aims at providing a modelization that could be accurate while not adding significant complexity to the calculations. So, the SRB population is not represented with a differential equation included in the system but explicitly with an equation of the Gompertz family. Gompertz equations are widely used to represent a population dynamic thanks to their sigmoidal shape and require a relatively low number of parameters. A modified version of the Gompertz equation, specific for applications in biological systems, is now a well-established mathematical approach to representing bacteria population. It allows for simple estimation of its parameters; it is flexible and can represent it accurately from a quantitative point of view in many cases [119]. The mathematical representation is given as follows:

$$X(t) = A\ \exp\left\{-exp\left[\frac{K_z\, e}{A}\,(T_{lag} - t) + 1\right]\right\} \tag{5.2}$$

$X(t)$ is the bacteria population in time t, the parameter K_z reflects a growth rate coefficient, and T_{lag} is the "lag time," the recovering period occurs when a population is transferred from a system to another. The parameter A reflects the upper asymptote of the curve [120].

The parameters of this equation have been compared to available variables and parameters to apply to the actual situation.In particular, the population X indicates the concentration of sulfate reducers X_{srb} $[g\,L^{-1}]$. The T_{lag} parameter is excluded or posed to zero since the environment does not change significantly in an AD system. Moreover, it has also been noted that it only partially impacts the final results. To define the upper asymptote A, it is of help to refer to the relationship between the biomass X_{srb} and its product S_s. In fact, by integrating the respective equation in 5.1, it is possible to explicitly see the relationship between the two variables, resulting in equation 5.3.

$$S_s(t) = \frac{1 - Y_{srb}}{Y_{srb}}\, X_{srb}(t) \tag{5.3}$$

$$S_s(t) = \frac{1 - Y_{srb}}{Y_{srb}}\, A\ \exp\left\{-\exp\left[\frac{K_z\, e}{A}\,(T_{lag} - t) + 1\right]\right\} \tag{5.4}$$

Equation 5.4 is obtained by inserting 5.2 into 5.3 and represents the trend of the dissolved sulfide concentration. It is not properly a Gompertz equation because the term outside the brackets is not the same as the one at the fraction's denominator inside. However, the upper asymptote is still represented by the first term, which can be named $S_{s,max}$ and gives equation 5.5. If this term is known, the upper asymptote for the bacteria population A, which can be now named $X_{s,max}$ (the name $X_{s,max}$ is used in this case instead of $X_{srb,max}$ to simplify the notation), can be calculated immediately with equation 5.6.

$$S_s(t) = S_{s,max} \exp\left\{ - \exp\left[\frac{K_z\, e}{\frac{Y_{srb}}{1-Y_{srb}}\, S_{s,max}} (T_{lag} - t) + 1 \right] \right\} \tag{5.5}$$

$$X_{s,max} = A = \frac{Y_{srb}}{1 - Y_{srb}}\, S_{s,max} \tag{5.6}$$

The problems are so reduced to the computation of $S_{s,max}$ $[mmol/L]$ following the subsequent approach to keep the model simple while providing an adequate system representation. That value, potentially different each time, represents a direct product of S_2 conversion. Thus such a dependence should be included. Moreover, it is derived only from that entering compounds containing sulfates, which quantity can be available or estimated in a simple term. Consequently, equation 5.7 defines the maximum value, at each time considered, for the sulfide concentration. It allows accounting for the substrate biochemical reaction dynamics up to S_2 and for a fraction defining the sulfur compounds present in the influent. An additional term is added to convert the sulfur fraction to a COD basis and to have the correct dimensions for the other equations. The parameter $\gamma_{S,in}$ $[-]$, defines the sulfate content which is present in the influent and can potentially be available to the SRB. It can be estimated on chemical measurements or as a percentage of the total protein content of the influent.

$$S_{s,max}(t) = \gamma_{S,in}(t)\, S_2(t)\, \frac{1000}{64} \tag{5.7}$$

Finally, for the only remaining term, K_z, of the modified-Gompertz equation, an approach based on similarities between the SRB and the methanogens has been perceived. Indeed, that term may be referred to as a tangent of the line described by the Gompertz equation. The present model should assess the fluctuation of bacteria state within the overall system more than bacterial population dynamics. Consequently, it has been chosen to provide the tangent value in such a way as to make the SRB population follow the trend described by methanogens dynamics, which in turn are determined from biochemical assumptions. The result is the following: the absolute value is added to guarantee a positive value,

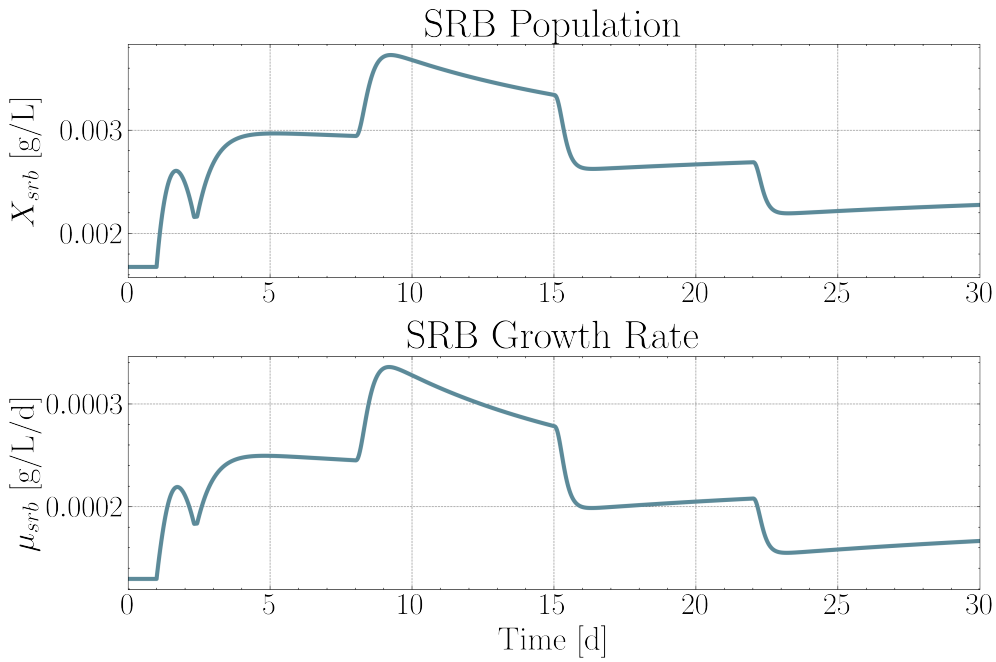

Figure 5.2: Kinetics of SRB bacterial growth. Total population and relative growth rate.

which is necessary for the Gompertz term. To improve the numerical stability of the solution, a minimum boundary can also be applied in specific cases. It should be defined accordingly to the value of the methanogens concentration.

$$K_{z,srb} = \left| \frac{X_2(t) - X_{2,0}}{t - t_0} \right| \tag{5.8}$$

As a result of the mentioned assumptions and parameters definition, equation 5.2 can be rewritten as:

$$X_{srb}(t) = X_{s,max} \exp \left\{ -exp \left[\frac{K_{z,srb}\, e}{X_{s,max}} (-t) + 1 \right] \right\} \tag{5.9}$$

Once the SRB population is known, it is possible to compute the associated dissolved sulfide S_s according to equation 5.5, with the appropriate value of $K_{z,srb}$. Figure 5.2 shows the value of the bacteria population during the case study, from 5.9, as well as their relative growth rate, defined in equation 5.16. The latter is not null even when the population is not increasing since it implicitly accounts for bacteria death and population. It is also possible to see that when a higher influent is fed to the system, the population increases accordingly.

Finally, from the amount of dissolved sulfide, the corresponding equilibrium concentration in the gaseous phase is calculated according to Henry's equation (5.10). The resulting specific H_2S gaseous flow rate (q_S $[mmol\, L^{-1}\, d^{-1}]$) is then computed from equation 5.13, where

$q_{tot} = q_M + q_C$ from AM2 variables. P_{dig} $[atm]$ is the digester headspace pressure, typically 1 atm or slightly larger. $K_{H,S}$ $[L\,atm\,mmol^{-1}]$ is the Henry's constant obtained in the form described in section 4.2.1. Its value has been computed as $K_{H,S} = H_{S,p}(T)/\rho_{water}$, with $H_{S,p}(T) = (0.13677 \cdot T + 2.0181) \cdot 100$ [116], where T $[K]$ is digester's absolute temperature.

$$y_S = \frac{K_{H,S}\, S_S}{P_{dig}} \tag{5.10}$$

The stoichiometry is then respected by a normalization of the obtained molar fraction equation 5.11 for each species $-i$. Consequently, the total specific outlet flow rate is recalculated to satisfy the mass balance 5.11 and from that, the actual value of the H_2S gaseous stream (5.13).

$$y_i^{norm} = \frac{y_i}{\sum_{i=1}^{3} y_i} \tag{5.11}$$

$$q_{tot} = \frac{q_M}{y_M} \tag{5.12}$$

$$q_S = y_S\, q_{tot} \tag{5.13}$$

This approach implies that the value total specific flow rate computed following AM2 equations is modified to include H_2S as well, and it is possible to the low value of that variable, typically present as an impurity. The results obtained with the new approach for flow rates and molar fraction are presented in figure 5.3 and compared with those of AM2HN. As it is possible to see, the effects of normalization can be considered acceptable and not affecting significantly the results. The principal reduction is observed in y_{CH_4}, which also considers the effects of inhibition described in the next paragraph. In fact, for CO_2, the difference is almost negligible, confirming the validity of the assumption. The concentration of H_2S is also in the range expected, being lower than 5%, with a value oscillating around 2%. It is also possible to see that the dynamics of the variables follow those defined by AM2HN and already validated. The methane flow rate presents the typical first-order response to deviations, increasing or decreasing. The new variable H_2S has the same methane trend due to the similarities assumed by the two microbial families producing these molecules. Conversely, for CO_2, the steady state is reached after the overshoot caused by the acidogenesis reaction. The impact of a 10% deviation in organics concentration is slightly more significant than the percentage applied to the total influent flow rate. The inhibition of hydrogen sulfide on methanogens is considered with a new term added in equation 3.16. The approach follows the one used to describe inhibitory terms in ADM1. A term I_S, comprised between 0 and 1, is added to the uninhibited expression of methane production. This solution is possible because, in AM2,

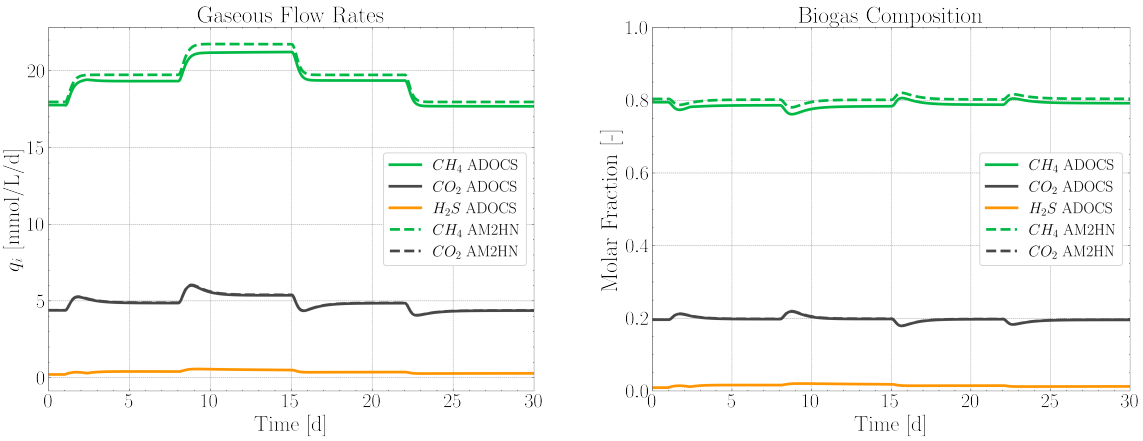

(a) Biogas flow rates resulting from the model. (b) Biogas composition resulting from the model.

Figure 5.3: Comparison of variables related to gaseous stream obtained with AM2HN (dashed lines) and with ADOCS (full lines) models.

this expression is also evaluated outside the differential equation system. Thus no significant modifications are required. The shape of the inhibition function, linear, and the $KI_S = 0.014272$ $[mmol\,L^{-1}]$ term have been chosen and calibrated according to a set of experimental values available in the literature [121].

$$I_S = (1 - KI_S) \cdot S_S \tag{5.14}$$

$$q_M = k_6\,\mu_2\,X_2\,I_S \tag{5.15}$$

Results of the inhibition term on the system are shown in figure 5.4b, where the reduction of methane production is directly comparable with the inhibition function. The latter is, in turn, commensurate to sulfide concentration and the symmetrical shape as per the shape of the function used. Figure 5.4a shows how the inhibitory term behaves at increasing S_S concentration. It has a maximum value of 1, meaning that no inhibitory effects are present when sulfide concentration is null. Further discussion is required to detail the second limitation occurring due to sulfate reduction presence, namely the acetate depletion to grow the SRB. Also, in this case, the similarity with methanogens is used as a basis for the implementation. Indeed, since both families of bacteria grow on S_2, their relative growth rate can be considered as substrate-limited growth, according to a Haldane kinetic mechanism (equation 3.2). Consequently, the growth rate of the SRB population can be represented as follows:

$$\mu_{srb}(t) = \mu_2(t)\frac{X_{srb}(t)}{X_2(t)} \tag{5.16}$$

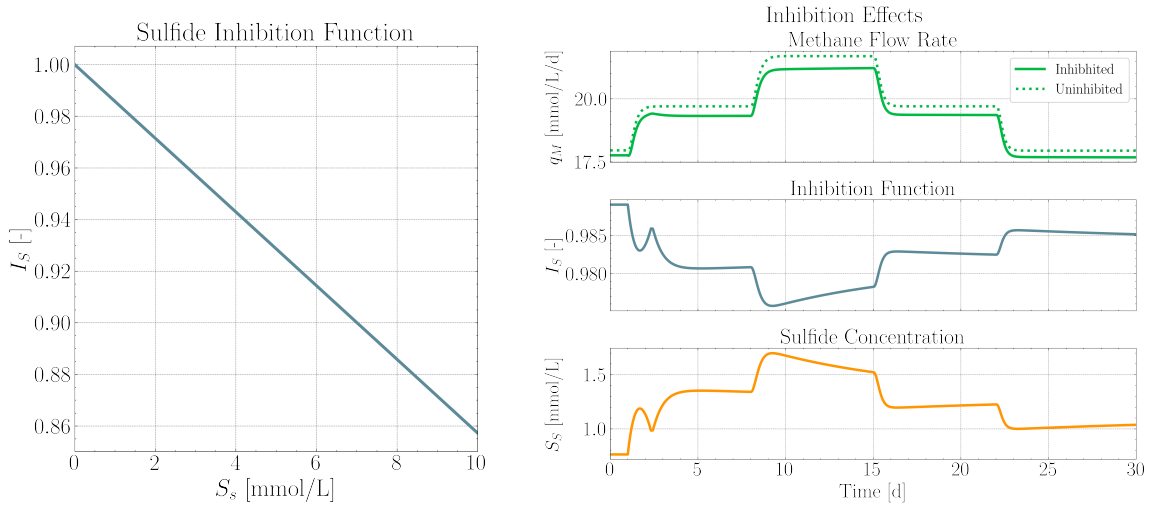

(a) Shape of I_S with respect to sulfide concentration.

(b) Effect on methane production with respect to sulfide concentration.

Figure 5.4: Sulfide inhibition function and its effect on the system.

The term μ_2 is represented as in AM2 by the Haldane equation and is the same as depicting the methanogens (X_2) growth. The ratio allows us to account for proportionality between the absolute growth rate of X_{srb} and X_2. This growth rate is distinct from the Gompertz derivative, as it can be the case in many other applications of such an approach.

As a result, in the dynamics of S_2 the SRB uptake term has to be added following equations 5.1. Consequently, equation 3.14 is transformed into equation 5.17.

$$\frac{dS_2}{dt} = D\left(S_{2,in} - S_2\right) + k_2\mu_1 X_1 - k_3\mu_2 X_2 - \frac{1}{Y_{srb}}\,\mu_{srb} \tag{5.17}$$

The effects of SRB population and SR processes on the two variables that are affected, S_2 and q_M, are described in figure 5.5. As it is possible to see, the most significant effect is the direct inhibition of methanogenesis, which, in the case conditions, is reduced by more than 2% in certain moments. The differences between the absolute values are more evident when the influent increases. At the same time, S_2 dynamics are eventually positively affected by the SRB population during the first days of a reduction in the feed.

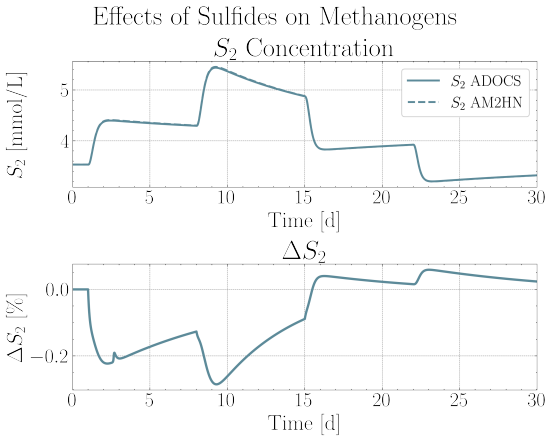

(a) Effects of sulfide inhibition on S_2..

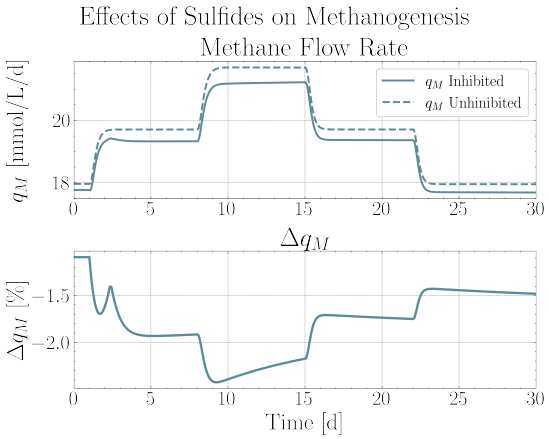

(b) Effects of sulfide inhibition on q_M.

Figure 5.5: Sulfide inhibition effects on the system with the relative difference with the uninhibited term.

Overall, this section adds a new gaseous stream which, in the AM2 approach, will leave the digester along with methane and carbon dioxide. In the system description chosen in the present work, that stream will instead enter into a fictitious ideal separation unit to more precisely describe the liquid-vapor interactions, accounting for water presence.

5.2.2. Liquid Level Dynamics

The global reactor mass balance is added to the model, externally from the aforementioned equations, to allow the computation of the liquid level inside the digester. This addition is done for two reasons:

- to express the gaseous flow rates as extensive variables, it is necessary to account for a volume.
- the ultimate purpose of the ADOCS model is to assess the headspace dynamics for which the gaseous volume is needed. The gaseous volume is not a fixed quantity but varies according to the liquid level, which has to be determined.

The modelization starts from the assumptions that dilution rate, influent flow rate, and liquid volume are related by the expression $D = \dot{Q}/V_{liq}$, as in the dynamic equations describing the microbial balances. In that case, a fixed term $V_{reactor}$ has been used to obtain different dilution rates for each influent deviation. That term is assumed to be the nominal specification of the liquid volume. Once the dynamic results are obtained, it is more accurate to define a fixed value of dilution rate D, which can be a design parameter

of the reactor, and from that, calculate the liquid volume V_{liq}. This approach is, of course, a simplification aimed at keeping the shape of the AM2HN model for ADOCS and avoids adding a further differential equation to be solved simultaneously. The correctness of the simplifaction is higher when influent differences are not large, and thus V_{liq} is almost equal to the nominal value $V_{reactor}$ for most of the time.

The mass balance is defined as follows (5.18- 5.20, where the variables with dot notation express fluxes and $h\,[m]$ are the liquid level.

$$\frac{dm_{liq}}{dt} = \dot{m}_{in} - \dot{m}_{out} \tag{5.18}$$

$$\rho_{liq}\,\frac{dV_{liq}}{dt} = \rho_{liq}\,\dot{Q}_{in} - \rho_{liq}\,\dot{Q}_{out} \tag{5.19}$$

$$\frac{\pi}{4}\,D_R^2\,\frac{dh}{dt} = \dot{Q_{in}} - D\,\frac{\pi}{4}\,D_R^2\,h \tag{5.20}$$

To get equation 5.19 from 5.18 is explicated the relationship between mass and volume through density ρ_{liq}. This density is assumed constant during digestion since the liquid phase is generally mostly composed of water, and the transformations occurring do not largely affect this term. Constant density allows to transform equation 5.19 into 5.20. The outlet flow rate is assumed to depend directly on the liquid level, as typically done for a cylindrical tank. A digester is typically compared to that shape, at least when the region where the liquid phase is considered. Consequently, $Q_{out} = D\,V_{liq} = D\,\frac{\pi}{4}\,D_R^2\,h$. The reactor diameter, an additional required input, is expressed as $D_R\ [m]$, and $D\ [d^{-1}]$ is the nominal operative dilution rate.

Equation 5.20 can be manipulated to give equation 5.21. The latter is a first-order differential equation of the form $\alpha y' + \beta y = \gamma$, which can be solved to give the level height profile in time as a function of the total influent flow rate 5.22. The term $S_R\ [m^2]$, standing for reactor surface, is the result of $S_R = \frac{\pi}{4}\,D_R^2$, and H_0 is the initial condition for the solution. Also in this case its value is defined as the variable value in steady-state conditions.

$$\frac{\pi}{4}\,D_R^2\,\frac{dh}{dt} + D\,\frac{\pi}{4}\,D_R^2\,h = \dot{Q}_{in(t)} \tag{5.21}$$

$$h(t) = \frac{\dot{Q}_i n(t)}{S_R\,D}\left(1 - e^{-Dt}\right) + H_0\,e^{-Dt} \tag{5.22}$$

The stream Q_{in} present in equation 5.22 is a *real* value, and thus a discontinuous step-increase for it does not correspond to what practically happens. When a step increase

is assigned to that variable, it represents the *set-point* value, which is reached with a particular dynamic according to the characteristics of the system employed. To adequately represent a step increase, as in the case study, it is thus necessary to model Q_{in} so that it does not have any not-realistic discontinuity. This modification can be done in two ways, whether information on the existing system is available. In the first case, the problem is simple: once the setpoint is defined, it provides information on the controlled variable according to the system and pipe design. If no specific knowledge is available, it is possible to tackle the problem with a general approach, which validity varies according to the specific case.

As a manipulated variable, it is assumed that the influent flow rate approaches the new steady-state according to a logistic shape after a step increase to its setpoint value. In particular, the upper branch of a logistic correctly represents the dynamics of a simple proportional controller for a first-order system. The logistic curve is obtained from a particular solution of Richard's differential equation [120] and defined for any time-dependent variable $Y(t)$ as:

$$Y(t) = \frac{A}{(1 + \beta e^{-k_d(t-t_0)})} \tag{5.23}$$

$$\text{with:} \quad \beta = 1 - \frac{A}{Y_0} \tag{5.24}$$

Equation 5.23 contains the parameter A, which is the upper asymptote, the initial condition $Y(t = t_0) = Y_0$, and the shape parameter k_d, which defines the slope of the function. For the actual purposes, it can be rewritten as:

$$Q_{in}(t) = \frac{Q_{in,SP}}{(1 + \beta e^{-k_d(t-t^*)})} \tag{5.25}$$

$$\text{with:} \quad \beta = 1 - \frac{Q_{in,SP}}{Q^*_{in}} \tag{5.26}$$

In this equation, the new value to be reached regarding the influent setpoint, occurring at time $t = t^*$, is defined as $Q_{in,SP}$. The *initial condition* is thus the value assumed by Q_{in} at the time of the change, namely $Q^*_{in} = Q_{in}(t = t^*)$. The shape parameter k_d is the only value to be provided by the user and can be related to the proportionality constant of a controller or defined according to experimental data. In the present study, its value has been posed equally to 1 from the analysis of the results.

The resulting flow Q_in is the one used throughout the whole simulation. The differences between a step increase and the proposed modification are shown in figure 5.6, where the results for the full-time span and detail for both the positive and the negative deviation are

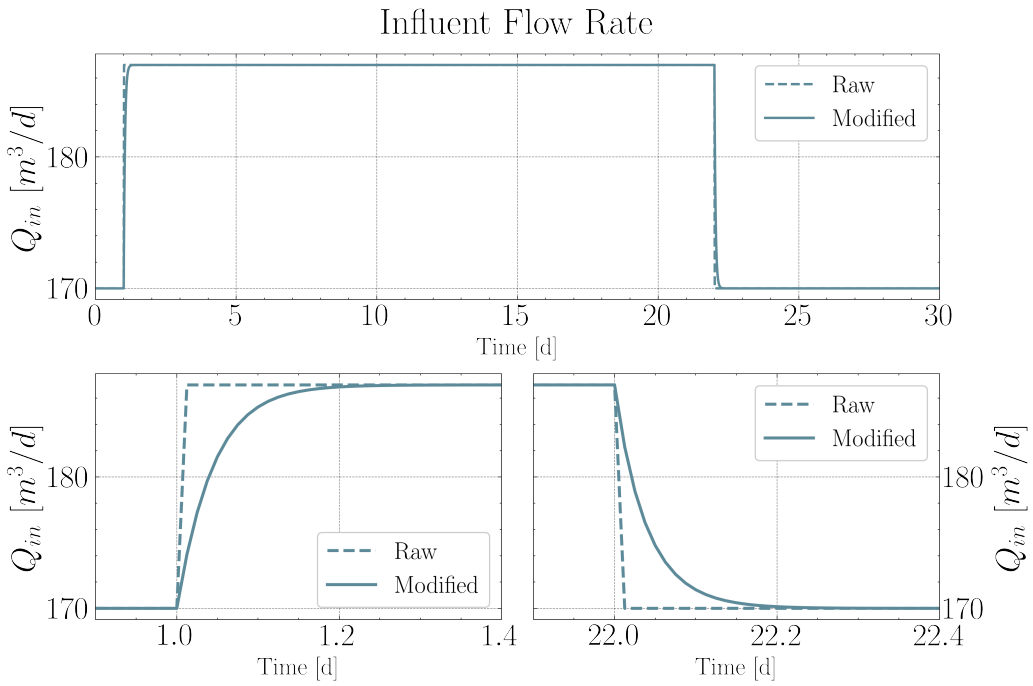

Figure 5.6: Differences between theoretical step increase (*Dashed Line*) and realistic value (*Full line*), with details of both deviations.

present. The dynamics are reasonably slow since the reactor diameter is high (20 meters in the case study, even more in some large-scale plants) and produces a slow response.

Consequently, the liquid level dynamics results are presented in figure 5.7. In figure 5.7a, the results regarding the liquid level h_{liq} are shown, and the plot of the influent flow rate is also repeated to simplify the comparison. Figure 5.7b shows the dynamics of the liquid volume V_{liq} $[m^3]$, calculated by assuming a cylindrical shape as in equation 5.27, which follows the shape defined by tank height. It also shows the results for the gaseous volume V_{gas} $[m^3]$, which is the one used as a volumetric variable in the CSTR equation for the headspace will be detailed later. This latter variable is computed by accounting for a design-defined $V_{headspace}$, which is never occupied by the liquid, and a variable part dependent on the liquid level. The result is shown in equation 5.28, where $V_{reactor}$ $[m^3]$ is the nominal liquid volume of the digester; $V_{headspace}$ $[m^3]$ the area over the maximum allowed liquid height; and V_{liq} is the liquid volume calculated previously. In the case study, the value of V_{gas} is always lower than $V_{headspace}$ since the liquid volume is always higher than its nominal value. That is a result of the deviations assigned to $\dot{Q_{in}}$, which

never decreases to a lower value concerning the beginning.

$$V_{liq} = \frac{\pi}{4} D_R^2 h \tag{5.27}$$

$$V_{gas} = V_{headspace} + (V_{reactor} - V_{liq}) \tag{5.28}$$

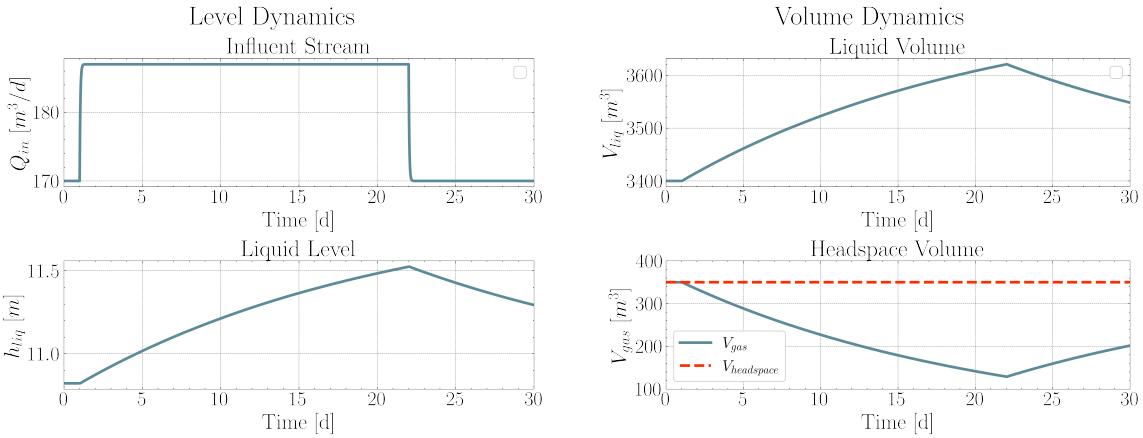

(a) Liquid volume dynamics and individual entering flow rate.

(b) Gaseous volume dynamics resulting from fixed term, $V_{headspace}$, and from a variable term related to liquid level.

Figure 5.7: Results of level dynamics for liquid and gaseous volume

A value for maximum and minimum height can also be provided to the model, which will output an error message and suggest reducing or increasing the entering if this limit is overcome.

5.3. Vapor-Liquid Equilibrium

The additional improvement to AM2HN results is the addition of the vapor-liquid equilibrium to assess the thermodynamic condition of the produced biogas. Up to the moment, it is assumed that what is not converted to biogas remains in the liquid phase. Consequently, no interactions with the rest of the system are considered. On the contrary, the present work aims at giving a preliminary evaluation of the thermodynamic conditions of the system.

It is assumed that the biogas produced accordingly to the equations already discussed enters, along with water, a vapor-liquid separation unit where it reaches the equilibrium. Water is the only element added to those constituting biogas because it is typically the

principal constituent of the liquid phase. Its effect on thermodynamic equilibrium is the most relevant. Consequently, the effects of the solids and the organic species are neglected.

At first, the specific flow rates given as output following the AM2 approach must be converted into the correspondent extensive variable. This derivation is done by multiplying the specific rate by the liquid volume V_{liq} obtained in 5.27. The resulting molar flow rates F_i $[mol\,h^{-1}]$ are obtained for species $i = \{CH_4, CO_2, H_2S\}$ from equation 5.29, whereas the one for is obtained accordingly to equation 5.30. The other terms are for the most conversion units, except from γ_w $[-]$, which defines the water fraction of the influent. This value is typically known and, in the present study, is set to 0.97. This large value is normal for WWTP, the type of plant considered in the present scenario. With all the flows available, it is then possible to compute the feed molar fractions z_i $[-]$ for all the four compounds considered: chCH4, CO_2, H_2S, and H_2O, with 5.31. NC stands for the number of components; thus, it is equal to four in the present case. As it is possible to see from figure 5.8, the flow is mostly composed of water (consider the different scales in 5.8a), which varies only according to deviation assigned to Q_{in}. This result is reasonable since water constitutes almost the entire digester influent stream and does not participate in biochemical reactions. Conversely, the other streams result from digestion processes and thus, as expected, vary when there is either a deviation in influent organic concentration (days 8 and 15) or the total influent flow (days 1 and 22).

$$F_i(t) = q_i(t)\,\frac{V_{liq}(t)}{24} \tag{5.29}$$

$$F_W(t) = \gamma_w \cdot \dot{Q}_{in}(t) \cdot \rho_{H2O}\,\frac{1000}{18 \cdot 24} \tag{5.30}$$

$$z_i = \frac{F_i}{\sum_{i=1}^{N} CF_i} \tag{5.31}$$

The resulting molar flows are those that enter the separation unit, which is modeled as an isothermal and isobaric flash separation, with one feed, F $[mol\,h^{-1}]$, and outlet streams, one for vapor, V $[mol\,h^{-1}]$, and one liquid L $[mol\,h^{-1}]$. For such a unit, it is possible to derive from mass balances and stoichiometric equation the so-called Rachford-Rice equation [122], which solution allows to determine the liquid-vapor equilibrium. This method is commonly used in chemical engineering to estimate how a stream can be divided between two phases accurately enough for many purposes.

$$f(\alpha) = \sum_{i=1}^{NC} \frac{z_i\,(K_i - 1)}{1 + \alpha\,(K_i(T) - 1)} = 0 \tag{5.32}$$

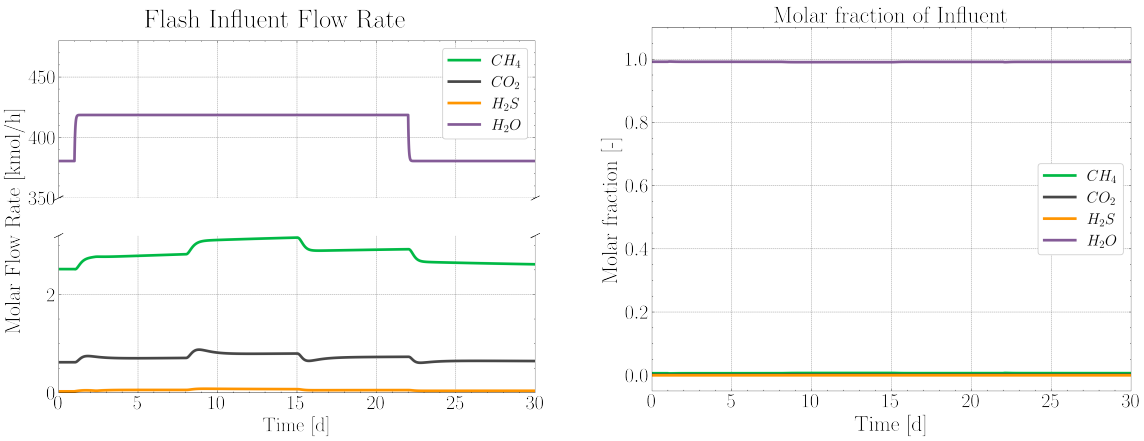

(a) Influent molar flow rate.

(b) Influent molar fraction.

Figure 5.8: Flash influent stream characteristics.

Rachford-Rice equation (5.32) has to be solved for the vaporization ratio $\alpha = \frac{V}{F}$, with $F = \sum_{i=1}^{NC} F_i]$ as the total feed flow rate, and $V = \sum_{i=1}^{NC} V_i$ as total outlet vapor flow rate. The equilibrium equations have the shape described by equation 5.33, where y_i and x_i are the molar fraction in the vapor and the liquid phase, respectively. The equilibrium coefficient K_i assumes a different form according to the hypothesis of an ideal or real gas mixture. For an ideal mix, it is given by $K_i = P_i^0(T)/P$, where $P_i^0(T)$ $[atm]$ is the compound vapor pressure at system conditions of T $[K]$ and P $[atm]$. For supercritical components, such as CH_4, CO_2 and according to system conditions eventually also H_2S, its value is given by $P_i^0(T) = H_i(T)$, following Henry's equation.

$$y_i = K_i(T)\, x_i \tag{5.33}$$

The parameter α is obtained with the solution of the Rachford-Rice equation, and with that value is possible to obtain the total liquid and vapor flow rates with 5.34 and 5.35. The α dynamic trend is shown in figure 5.9, which generally shows an extremely low value for that parameter, meaning that most of the influent flow is retained in the liquid phase. This result is correct since most of the feed is water, which is the less volatile compound. A consequence of the large quantity of water is the peaks corresponding to the deviations of Q_{in}. These peaks are not present when the deviation is assigned to $X_{T,in}$ because the overall volatility change is more controlled when the difference comes from one of the volatile species produced from organics degradation. Afterward, their composition can be immediately obtained with equation 5.36 and 5.37. Once these values are known, it is possible to compute also the value of the individual streams. The computation follows

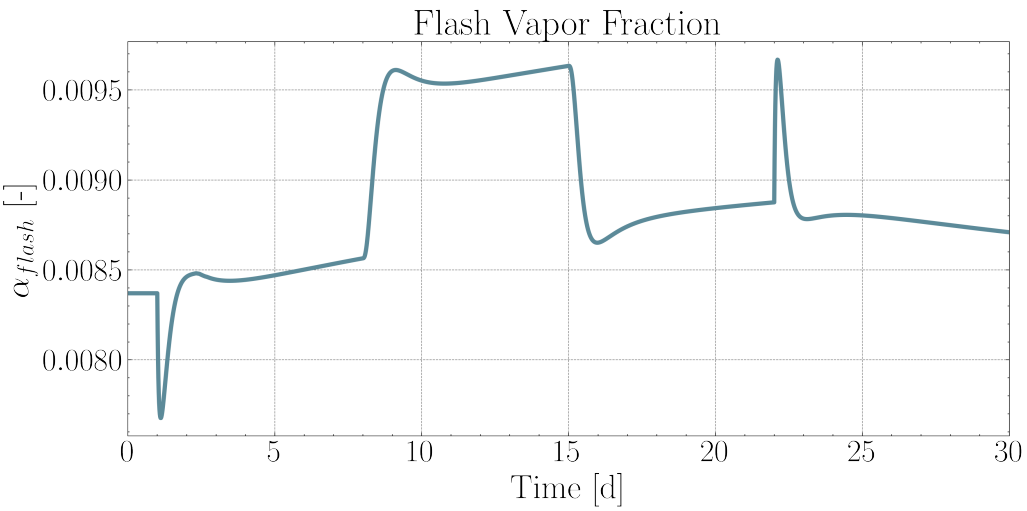

Figure 5.9: Flash vapor fraction from Rachford-Rice solution.

$V_i = y_i\, V$ for the vapor and $L_i = x_i\, L$.

$$V = \alpha\, F \tag{5.34}$$

$$L = F - V \tag{5.35}$$

$$x_i = \frac{z_i}{1 + \alpha\,(K_i - 1)} \tag{5.36}$$

$$y_i = K_i\, x_i = \frac{K_i\, z_i}{1 + \alpha\,(K_i - 1)} \tag{5.37}$$

The resulting streams are presented in figure 5.10 and 5.11 for vapor and liquid, respectively. As it is predictable, the liquid stream is almost entirely constituted by water, with a minor part of dissolved CO_2 and H_2S. Despite being more abundant than the other two compounds in the influent, methane is less retained in the liquid phase due to its extremely low solubility. For the gaseous stream, it is interesting to note that the water percentage is not null, and neglecting its presence could have caused misleading results in the definition of headspace reactions. Generally, the trends follow those defined by the influent and, even, may not be perceived from the representation; also, the H_2O and H_2S curves have a not constant trend. While the obtained liquid stream will define the digestate and is thus not investigated anymore, the vapor stream goes from the liquid to the headspace section of the digester. Consequently, this stream will constitute CSTR's feed according to the definition given at the beginning of this section.

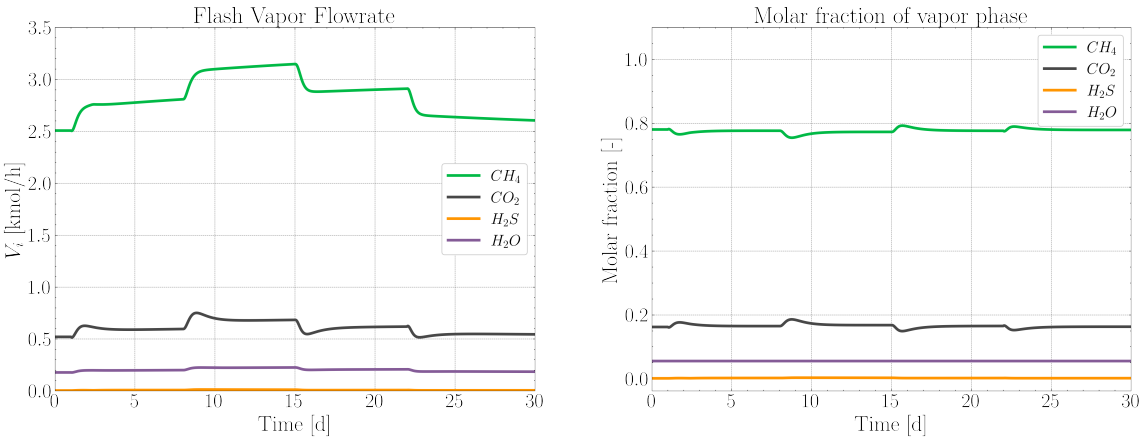

(a) Vapor stream molar flow rate. (b) Vapor stream molar fraction.

Figure 5.10: Flash outlet vapor stream characteristics.

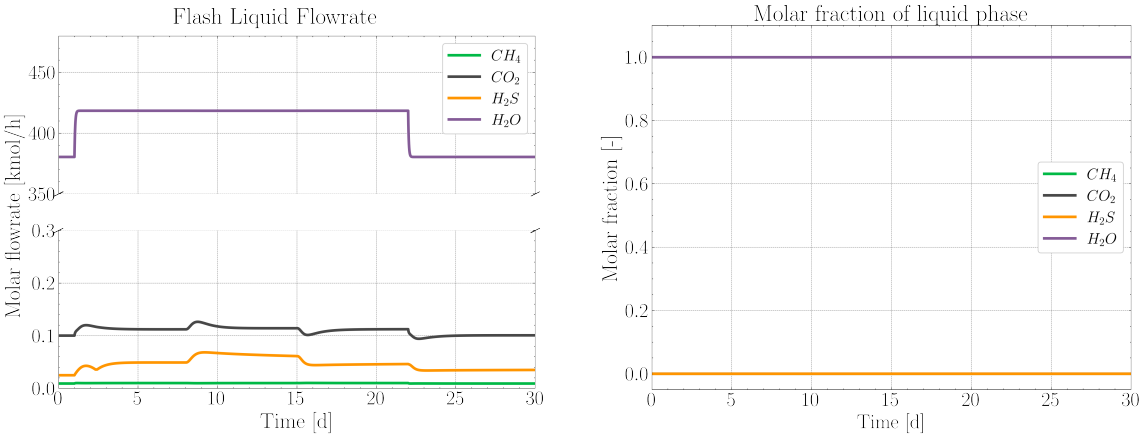

(a) Liquid stream molar flow rate. (b) Liquid stream molar fraction.

Figure 5.11: Flash outlet liquid stream characteristics.

5.4. Headspace Dynamics

This section covers the ultimate purpose of the ADOCS model: the oxygen effect for sulfide removal. Indeed, model additions made in the previous sections of the chapter are general considerations that can also be applied to models such as AM2HN. Here will instead describe the digester area where are not occurring the typical reactions of anaerobic digestion are not occurring: the headspace. In fact, following the digester description given in Chapter 2.3.2, this is the area where the microorganisms responsible for sulfide oxidation are present, the sulfide-oxidizing bacteria (SOB), and their metabolic reaction occurs.

5.4.1. Mass Balances

The modeling approach is relatively simple and considers the headspace behaves like a CSTR reactor, as shown in figure 5.1, as is commonly the case for anaerobic digestion processes. This reactor has two influent streams, represented by the products of anaerobic digestion and the oxygen injected to guarantee the microaerobic conditions for SOBs. Then, a single mixed stream will leave the digester after a specific residence time $\tau_{headspace}$ $[h]$. The equation representing such a system is derived from the classical CSTR balance in molar terms:

$$\frac{dn_i}{dt} = \dot{n}_{i,IN} - \dot{n}_{i,OUT} + r_i\, V_r \tag{5.38}$$

Equation 5.38 has to be written for every species present in the system so that $i = CH_4$, CO_2, H_2S, H_2O and O_2. A new species, S_x, is also added to represent the elemental sulfur produced by oxidation. It includes a term of accumulation $\frac{dn_i}{dt}$ $[mol\, h * -1]$; the influent and outlet molar flow $\dot{n}_{i,IN}$ $[mol\ h^{-1}]$ and $\dot{n}_{i,OUT}$ $[mol\, h^{-1}]$; the term accounting for generation or consumption due to reactions occurring r_i $[mol\, h{-}1\, m^{-3}]$ and the reactor volume V_r. The application of equation 5.38 to the headspace, as in the present case, results in equation 5.39. There, the influent flow is the flash outlet vapor flow V_i, to not confuse with a volume, and the reactor volume is V_{gas}, as defined in equation 5.28. The reactive term r_{SOB} is attributed only to SOB bacteria, assuming that that is the only reaction occurring. Note also that in equation 5.38, the stoichiometric coefficient is included in the reactive term, whereas it has been explicated in 5.39 as ν_i.

$$\frac{dn_i}{dt} = V_i - \dot{n}_{i,OUT} + \nu_i r_{SOB}\, V_{gas} \tag{5.39}$$

Following the description given in the dedicated chapter, the reaction chosen to represent the system describes the conversion of sulfide into elemental sulfur, neglecting those representing oxidation to other compounds. The model reaction is reported below:

$$2\,H_2S + O_2 \longrightarrow 2\,S_x + 2\,H_2O \tag{R12}$$

Consequently, according to reaction R12, two species, CH_4 and CO_2, are treated as inerts, and consequently, their outlet flow rate is equal to the rate entering the headspace. The other species, namely H_2S, H_2O, O_2, and S_x, are considered reactants or products and thus require a dynamic representation. In particular, H_2S, H_2O, O_2 are gaseous species, and the influent flows are defined as the gaseous stream exiting the flash for the first two and as an externally manipulated variable for oxygen. Conversely, S_x is a solid species

whose influent flow is null, whereas the outlet is neglected. It implies that all the sulfur produced will be retained inside the digester, as commonly occurs when microaeration is performed. The complete set of equations describing the headspace is given below:

$$\dot{n}_{M,OUT} = V_M \tag{5.40}$$

$$\dot{n}_{C,OUT} = V_C \tag{5.41}$$

$$\frac{dn_S}{dt} = V_S - \dot{n}_{S,OUT} - \nu_S r_{SOB} V_{gas} \tag{5.42}$$

$$\frac{dn_W}{dt} = V_W - \dot{n}_{W,OUT} + \nu_W r_{SOB} V_{gas} \tag{5.43}$$

$$\frac{dn_O}{dt} = \dot{n}_{O,IN} - \dot{n}_{O,OUT} - \nu_O r_{SOB} V_{gas} \tag{5.44}$$

$$\frac{dn_{Sx}}{dt} = \nu_{Sx} r_{SOB} V_{gas} \tag{5.45}$$

The influent flows are given by V_i $[mol/h]$ for all the species originating from the flash. The term for oxygen is instead given by $\dot{n}_{O,IN}$ $[mol/h]$ since it is determined externally. The stoichiometric coefficients are not defined explicitly from reaction R12 apart from their sign since their experimental value may slightly differ from the theoretical one, as will be discussed in the section dedicated to the kinetics considered. Equations 5.40 and 5.41 represent the two inert species for which no reactions occur. Equations 5.42 to 5.45 are those describing the SOB kinetics and are related by the reactive term r_{SOB}, which shape will now be discussed. Moreover, the direct dependence on the gaseous volume also considers the reactor's residence time, which is a significant parameter impacting microaeration effects [99]. The presence of the headspace, where the gas streams will be retained for a certain amount of time, inserts a *lag-time* to the system. In fact, a molecule entering the headspace at $t = t_0$ will exit it a $t_out = t_0 + tau_{headspace}(t = t_0)$. The terms $tau_{headspace}$ $[h]$ is the headspace residence time, defined as $tau_{headspace} = \frac{V_{gas}}{Q_{vap}}$, where Q_{vap} $[m^3\,h^{-1}]$ is the volumetric equivalent of the CSTR influent flowrate from the flash V. Consequently, when analyzing the results, it should be kept in mind that they need to be shifted to t_out, even though they will be presented according to the inlet time t to help the comparison. An idea of the difference between the two times is given in 5.12, where the headspace residence time is plotted against both the defined time vectors. Furthermore, it is relevant to highlight that the obtained residence times of 1 to 5 hours well match industrial values present in the literature [54]. It is also important to consider that oxygen is an inhibitory term for anaerobic bacteria, such as methanogens. The approach is already described and follows the ADM1 way of expressing inhibitions. The methane outlet molar flow rate $n_{M,OUT}$ is multiplied by an inhibition function for oxygen I_{O_2} (Equation 5.48), which value is in the range [0-1], where one represents a

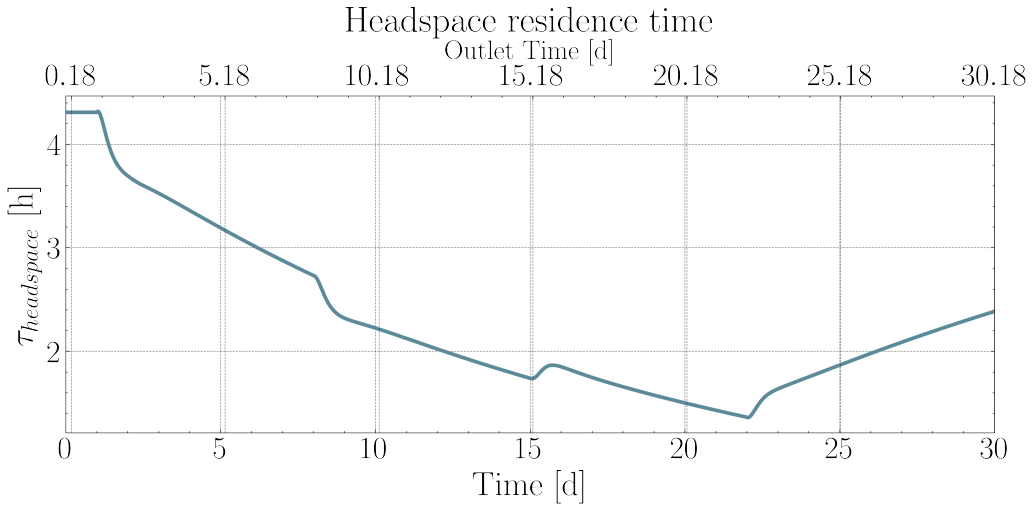

Figure 5.12: Headspace residence time on two axes. Lower axis refers to the absolute time t; upper axis refers to shifted time t_{out}.

null effect of inhibition. The effect is analogous to the inclusion of an additional term in the AM2 expression describing methanogenesis (Equation 3.16), which has been already modified to account for sulfide inhibition as given in 5.15. The full result of this approach could be seen as 5.47, which is, however, not implemented as it is directly comprised in equation 5.48. The effect of inhibition is consequently added *a posteriori* to the produced methane stream. It should require a re-estimation of the flash-CSTR system to bring the system to convergence. However, the modification added by this term is practically irrelevant; thus, that step can be avoided. The shape of the inhibition function and its constant $K_{I,O_2} = 3.293807642e-3$ $[kg\ m^{-3}]$ have been determined according to literature sources [98], [121]. The term S_O $[kg\ m^{-3}]$ refers to the oxygen concentration in the liquid medium, inhibiting the methanogens, and is calculated from the gaseous concentration with Henry's equation. It has been noted that its value is typically low, as it should also be by accounting for the oxygen solubility in water and the activity of the facultative microorganisms, and so almost null will also be the inhibition effect. This is shown in 5.13, where the value of I_{O_2} is presented according to the gaseous oxygen fraction (Figure 5.13a). The almost irrelevant effect on methanogenesis is also shown in figure 5.13b, where it is possible to observe that the reduction caused by oxygen is orders of magnitudes lower

than that caused by sulfide (note the y-axis scale).

$$I_O = \frac{1}{1 + \frac{K_{I,O_2}}{S_O}} \tag{5.46}$$

$$q_M = k_6 \, \mu_2 \, X_2 \, I_S \; I_O \tag{5.47}$$

$$\dot{n}^{inhib}_{M,OUT} = \dot{n}_{M,OUT} \cdot I_O \tag{5.48}$$

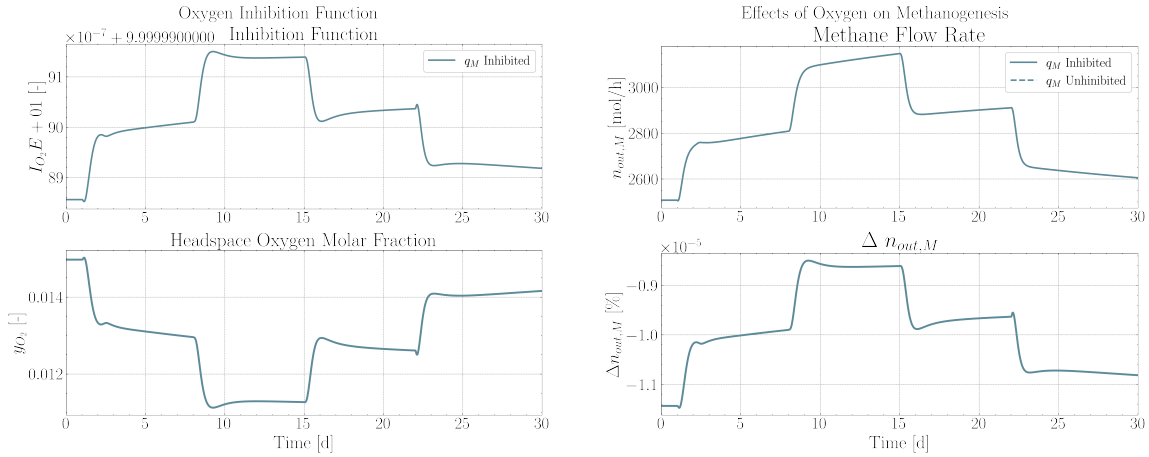

(a) Oxygen Inhibition function as a function of headspace oxygen molar fraction.

(b) Effects of oxygen inhibition on q_M.

Figure 5.13: Oxygen inhibition function and its effects on the system, with the relative difference with the uninhibited term.

5.4.2. SOB Kinetics

There are two possible approaches to describe the kinetics of sulfide oxidation. The first follows biochemical-inspired reasoning and includes the SOB population's representation, their sulfide uptake, and their sulfur production. This approach is used in ADM1-S/O [98] and requires at least three additional differential equations to be solved simultaneously. A second approach is more mechanistic and assumes that it is possible to fully describe the sulfide oxidation with a power law kinetic expression. That is of the type $r_{SOB} = k_{SOB}\ c_S^{\alpha}\ c_O^{\beta}$, where k_{SOB} is an experimental kinetic constant; c_S and c_O are reactants (H_2S and O_2) concentration, and α and β are experimental parameters. Such an approach is commonly used and has proved efficacy in describing chemical oxidation [55], [98]. In contrast, there are few references, but with positive feedback, for its applicability to biochemical oxidation [102].

During SOB activity, a combination of chemical and biochemical oxidation has been proved, with the latter being slightly more relevant and faster [99]. The fact that ADOCS is thought of as a lumped model which aims to describe the microaeration effect with a little computational effort and with a few numbers of parameters has guided the choice towards the description of sulfide conversion as a single process, including both biochemical and chemical oxidation under a common expression. Consequently, a power-law kinetic has been used to define the reaction rate occurring in the headspace.

To define the parameters to be used with a lack of experimental capacity, literature sources have been investigated [99], [102]. A large parameter variability is present due to different environments and estimation methods. However, a common basis is to have the kinetic parameters in terms of mass instead of moles, giving r_{SOB} $[g_S\, m^{-3}\, h^{-1}]$. The concentration is so defined as w_i $[g_i\, m^{-3}]$ to simplify the notation and limit the possibility of confusion, and can be directly derived from their molar equivalent with simple manipulations. Consequently, the kinetic constant assumes the unit of $\left[\left(g_S\, m^{-3}\right)^{1-\alpha}\left(g_{O_2}\, m^{-3}\right)^{1-\beta}\, h^{-1}\right]$. Despite the differences, some common considerations can be derived from those parameters available in the literature. It is important to remind that these values usually refer to or are calculated for chemical oxidation. In particular, there is usually a linear dependence from sulfide concentration, giving α close to 1 in most cases. Conversely, there is less consensus regarding the term for oxygen concentration, but most models agree in defining a low dependence from that variable, posing β between 0 and 1. Regarding the last parameter, k_{SOB}, there is a large variability in the results available, but in general, a value in the range $0.1 - 1.5$ seems to be accepted. In conclusion, the stoichiometric coefficients are often defined in terms of mass and equal to $R_b = 2\, g_S\, g_{O_2}^{-}1$ for pure biochemical oxidation, equal to the theoretical molar ratio. However, when chemical oxidation is also considered, it can be possible to reduce this value to 1.7 or 1.8. The major study that proposed and validated a power-law expression accounting also for biochemical oxidation has been used as the main reference for the present case [102].

Equations 5.42 to 5.45 can be finally completed to describe the headspace dynamics, providing the following set of equations, where the reactive term is divided by the molecular

weight of sulfur MW_S $[g_S\, mol^{-1}]$ to convert it to a molar basis.

$$\frac{dn_S}{dt} = V_S - \dot{n}_{S,OUT} - \frac{r_{SOB}\, V_{gas}}{MW_S} \tag{5.49}$$

$$\frac{dn_W}{dt} = V_W - \dot{n}_{W,OUT} + \frac{r_{SOB}\, V_{gas}}{MW_S} \tag{5.50}$$

$$\frac{dn_O}{dt} = \dot{n}_{O,IN} - \dot{n}_{O,OUT} - \frac{r_{SOB}\, V_{gas}}{MW_{O_2}\, R_b} \tag{5.51}$$

$$\frac{dn_{Sx}}{dt} = +\frac{r_{SOB}\, V_{gas}}{MW_S} \tag{5.52}$$

$$\text{with:} \quad r_{SOB} = k_{SOB}\; w_S^{\alpha}\; w_O^{\beta} \tag{5.53}$$

In the present simulation, an example influent flow rate for oxygen has been defined at each time step according to the individual biogas flow rate as $Q_{O,IN} = 0.015 \cdot Q_{biogas}$ $[m^3\, h^{-1}]$. Moreover, according to Euler's backward method, the differential equations are solved in their discretized form to increase the system's stability. To do this, the number of moles for each species is related to the respective flow rate by $n_i(t) = \dot{n}_{i,OUT}(t) \cdot \tau_{headspace}(t)$.

The results obtained for the CSTR modeling approach of the headspace are reported in the graphs 5.14 and 5.15. Figure 5.14 presents what occurs to the gaseous stream, with full

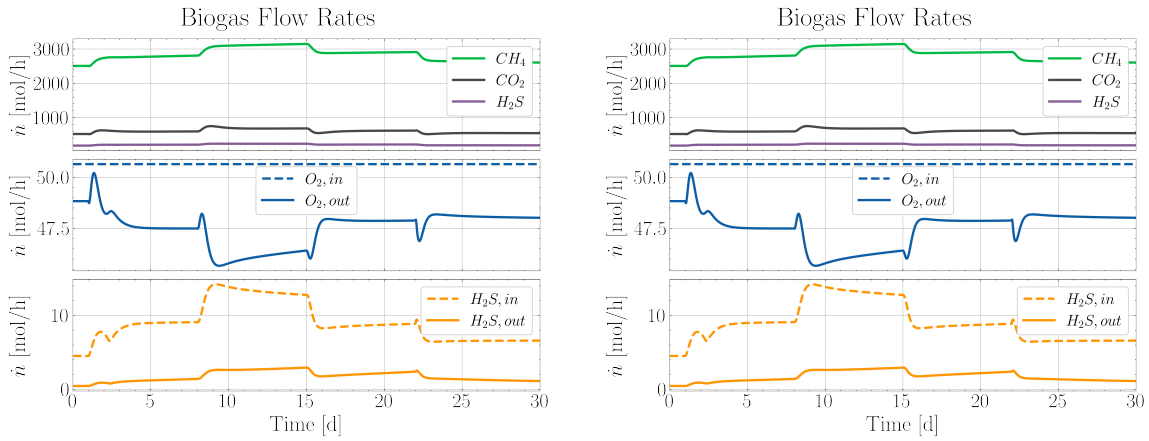

(a) Biogas molar flow rate.

(b) Biogas molar composition.

Figure 5.14: Headspace biogas stream characteristics. Full lines: digester outlet; dashed lines: headspace influent.

lines representing the variables of the outlet and dashed lines representing the respective headspace influent for variables where that presentation is relevant. It is possible to notice the large reduction in H_2S concentration (shown in [ppm], as it is commonly done) thanks to SOB activity. Being the influent oxygen defined as a constant flow, it is less abundant

in the outlet stream when a larger amount of sulfide is present in the influent. This result is because the more H_2S enters, the more will be present in the CSTR. This rise increases the reaction rate, leading to larger oxygen consumption. It is rarely the case since microaeration, by definition, leads to small oxygen concentrations. However, an alert message should be prompted if the oxygen reaches the flammability region for the mixture. Figure 5.15 shows two process parameters that are also useful to assess the quality of the

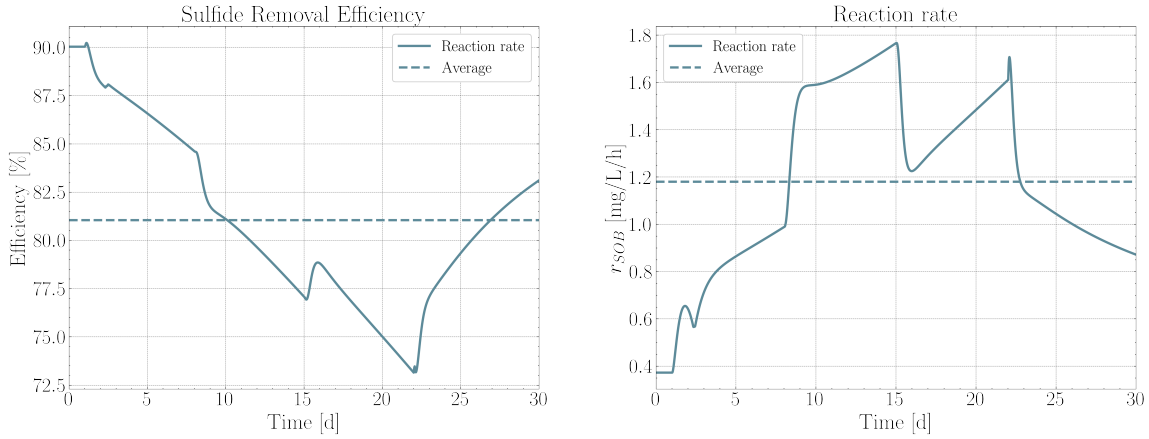

(a) Sulfide removal efficiency.

(b) SOB reaction rate.

Figure 5.15: Results of SOB activity in the headspace. Full lines: instantaneous value; dashed lines: averaged value.

model presented, despite the lack of experimental data. Indeed, it is possible to see that for both the removal efficiency, defined as $\eta_{removal} = \frac{n_{S,IN} - n_{S,OUT}}{n_{S,IN}}$, and the reaction rate r_{SOB} fall within ranges reported in the literature [54], [99]. In particular, the average value of the latter of 1.18 $mg\,L^{-1}\,h^{-1} = 28.32\ mg\,L^{-1}\,d^{-1}$ is in good agreement with average reference values ranging within $12 - 60\ mg\,L^{-1}\,d^{-1}$, considering those referred either to chemical or biochemical oxidation [99], [102]. Moreover, the model also represents the relationship between headspace residence time and removal efficiency, with the latter substantially reduced when $\tau_{headspace}$ decreases. As clear from the comparison emerging from this picture, the impact of reaction rate on the efficiency is not comparable with the one of the reactor headspace, which largely affects the results. This demonstrates how vital it is to model the digester's liquid level to obtain a dynamic headspace volume.

5.5. Industrial Case Study

In order to prove the model's validity in industrial scenarios, is performed a comparison with data provided by a company. The data refer to a plant owned by *Thöni GmbH*, referring to a medium-size digester that produces 1 MW of power. The data available

were not highly detailed, so several assumptions must be made in some cases.

The available data refer to an entire winter month, specifically January 2022. Their origin is from an unknown plant in the Trentino-Alto Adige region, where microaeration for sulfide abatement is carried out. The plant is constituted of one digester and one post-digester. Consequently, only the first is modeled, and the absolute values of the data are considered accordingly. Data available are the amount of influent and its origin, measured daily. From that, rough information about the organics' composition can be deduced and used in the model. Moreover, it is assumed that the influent is a constant flow since no field information is available. Moreover, data regarding the resulting gas composition are available before and after the microaerobic treatment.

The oxidative flow is constituted by air, and its flow is not subjected to a detailed measurement. Consequently, the possibility of having air instead of pure oxygen is added to the ADOCS model. As a rough indicator, a range of $8-10\ m^3\,h^{-1}$ is therefore considered, accordingly to the given information.

The identification is performed to obtain the model parameters as described in the current work. It must be highlighted that, due to a lack of detailed information, the ADM1 simulations may need to be more accurate. The information about the influent is converted into the respective concentrations of protein, carbohydrates, lipids, and inert fractions to have acceptable entering values for ADM1. For ADOCS, the given input is condensed into two variables: Q_{in} $[m^3\,d^{-1}]$ and $X_{T,in}$ $[kg_{COD}\,m^{-3}]$, standing for total influent flow rate and organics concentration, respectively. The data manipulated as ADOCS input for all the days available are shown in 5.16.

5.5.1. Results Comparison

The results are shown for two weeks, starting from January 14th. This period is chosen because the impact of the first influent data available is seen after some time due to the lag times typical of AD systems. After fourteen days, it is reasonable to assume that the outputs are affected only by the known data and not by whatever happened before the information became available.

Overall, the model predicted represents quite well the system behavior, even though, in some cases, the dynamics could be more perfectly reflected. Consequently, it is possible to conclude that the ADOCS model satisfactorily represents a complicate system with large fluctuations and instabilities. In particular, figure 5.17a shows how the model well-predicts the general absolute values for methane production and sulfate reduction processes. It is also interesting to highlight that ADOCS perfectly reflects the ADM1 results for the CH_4

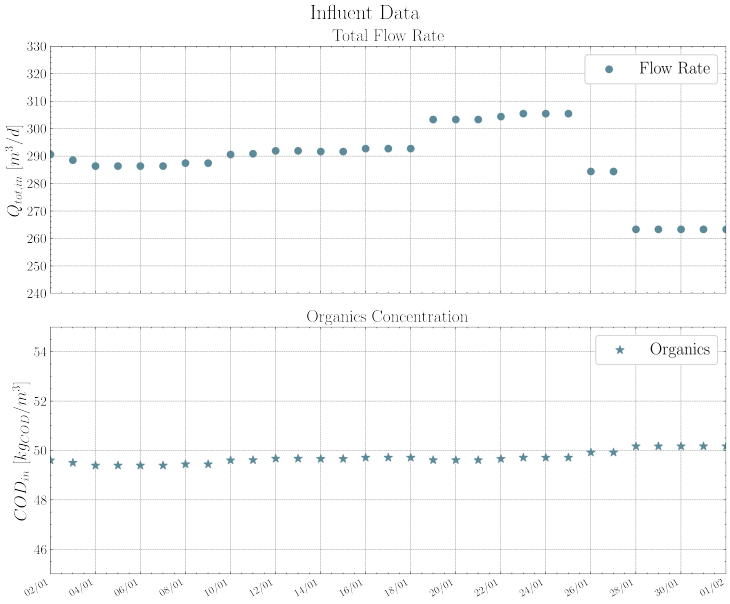

Figure 5.16: Given influent data expressed as ADOCS variables

fraction. ADM1 does not represent the minimal deviations present in the data, making it possible to conclude that the available input data are probably insufficient to reflect all the occurrences.

Figure 5.17b shows that, despite some incorrect trends, the general behavior is adequately predicted. The ultimate goal of ADOCS is to asses whether the injected oxygen is enough to reduce the sulfides to an acceptable value. This result can be assessed by looking at absolute results for concentration.

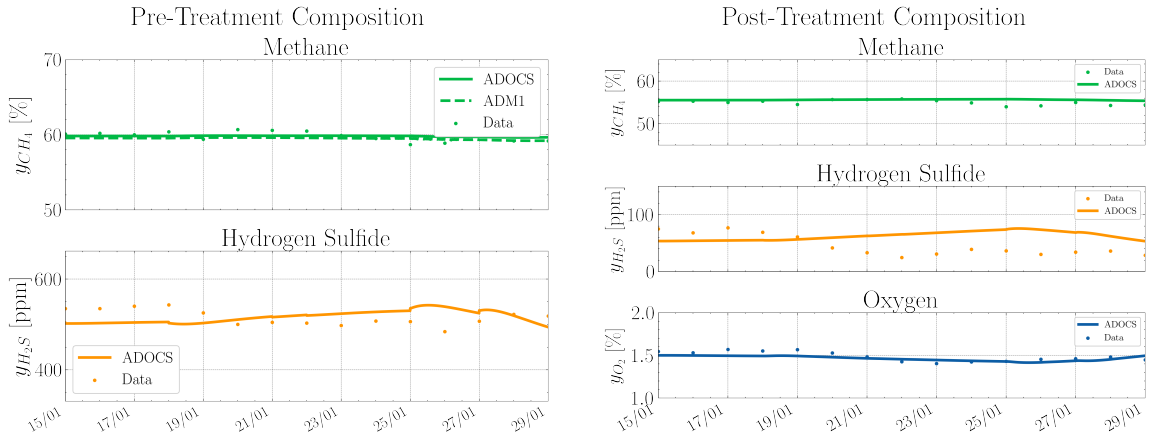

(a) Pre-microaerobic treatment results. (b) Post-microaerobic treatment results.

Figure 5.17: Comparison between industrial data and model predictions.

6 | Control Algorithm Definition

The ADOCS model is developed to provide a possible application within a real-time control system for sulfide reduction by microaeration. Such a technology can be obtained by implementing the sections described in the previous chapters. Indeed, while the base-case study has been described with predefined influent deviations, it is possible to use data obtained from an actual plant instead. The data required are, in fact, commonly available and frequently measured: total flow rate, organics, carbon and nitrogen concentration, and pH for the influent; design parameters such as diameter and volume of the reactor to provide the extensive variables.

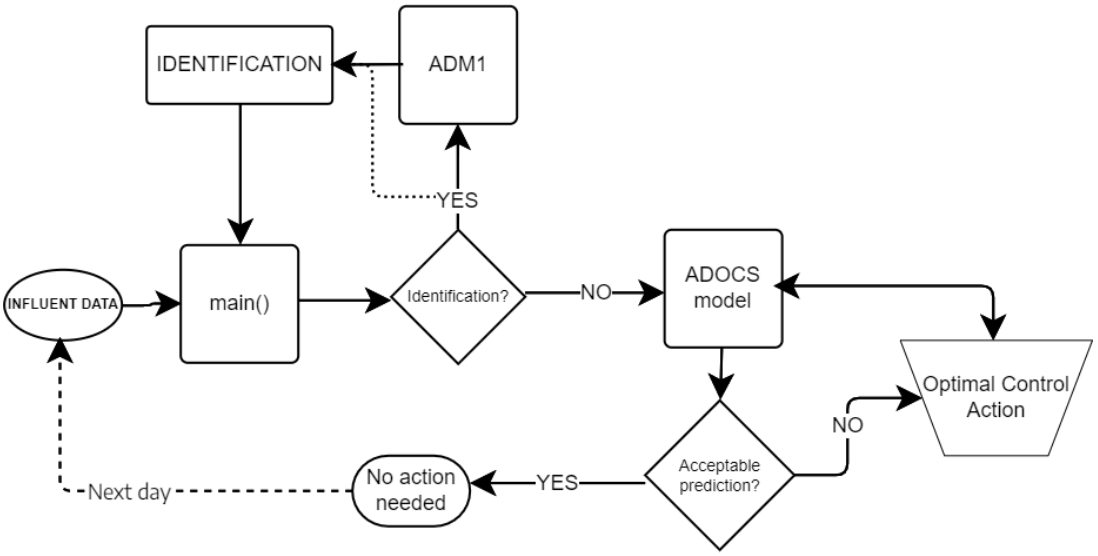

Figure 6.1: Proposed control algorithm for practical applications of ADOCS model.

The proposed control algorithm to be adopted is shown in figure 6.1. It is built on three macro-blocks: the ADOCS model, the identification procedure, and the control action. These are all called, directly or indirectly, from the main code, which retrieves the influent data at each period considered. The identification has to be performed in two cases, at the beginning and in case of large influent deviations. If it is the first time using the model in that plant and there are no parameters available, there are no other choices but to

estimate them. Consequently, steady-state data should be obtained for different retention times with ADM1 simulations, and then the identification can be performed as described in chapter 4.3.1. Eventually, it could also be possible to use the AM2 identification approach and thus use field measurements for this purpose. However, the validity of this hypothesis is not further investigated since the ADOCS model has been built with its identification procedure. In another case, identification may be required: when the influent variables are consistently different from the ones for which the estimation has been carried out. This situation does not frequently happen since, most of the time, anaerobic digesters are designed to operate within a well-defined and specific range of influent conditions. In fact, for deviations to values relatively close to the one assessed initially, a re-parametrization is not necessary, as the lumped approach suggests limiting the computational efforts needed. As a *rule-of-thumb*, it is possible to say that a new identification is required if the influent variable varies by more than the 70% of their original values for the most sensitive variables: influent total flow rate Q_in and influent organic concentration $X_{T,in}$. That value can be higher if a significant deviation is limited in time. Whenever proceeding with a new identification, a rough estimation can be done by changing the influent variables without changing the steady-state dataset, thus avoiding the ADM1 simulations. This approach, however, produces misleading results since it implies that different sets of influent data will produce the same steady-state process variables. As a result, proceeding to new ADM1 runs should be preferred whenever it is needed to re-parametrize the model.

When the parameters are obtained, it is possible to perform the simulation of anaerobic digestion according to the ADOCS model for the desired time horizon. If an oxygen injection is present, it will be considered to evaluate the SOB activity. At this point, the model will assess if the predicted H_2S concentration in the exiting biogas is lower or higher than the acceptable threshold, fixed by the operator according to the biogas usage. An acceptable concentration can result in adequate oxygenation or low production of sulfides by SRB. The latter situation can be the case, for example, when the digestion of sulfate-deficient substrates occurs.

If the prediction of sulfide content in biogas is not acceptable, namely because H_2S concentration is higher than the threshold value, the oxygen injection will be increased to reduce it. As can be seen in the diagram, the connector between the control action and the ADOCS model is bidirectional. This representation occurs because the control action is not defined by itself and is added to the model. In contrast, it is defined according to the effects it produces in the system as calculated by the ADOCS model. This approach allows the estimation of the correct timing and the magnitude of oxygen injection that

will keep the existing sulfide concentration within the acceptable range if the intrinsic characteristics of the system make it possible. The sulfur concentration can be so high, or the threshold so low, that microaeration cannot reduce enough sulfide content, for example, because it would require an amount of oxygen too large to be sustained.

More details on the procedure established to perform a first predictive optimization of the oxygen injection are provided in the next section.

6.1. Oxygen Injection Control

This section will present several examples to define and headline the importance of having a control system based on a predictive model. The established procedure to assess the oxygen dosage is thus described for two possible solutions: one where the oxygen injection is based on a non-predictive scenario and the second where a predictive approach is pursued. The latter's advantages are consequently highlighted, and such a procedure is applied to the base-case scenario.

The study examples are obtained with values for the variables obtained from partial simulations of the base-case scenario. However, they do not represent in any manner the case study. The first results are thus only used to describe the injection technique defined, which is applied to the base-case scenario in the last section of this chapter. The influent variables are those entering the headspace, namely the amount of biogas produced resulting from digestion (constituted by CH_4, CO_2, and H_2S) and of oxygen injected from the outside. The values of composition are reported following general industry standards. Consequently, H_2S fraction is referred to in terms of $[ppm]$ (parts per million), whereas the [%] (percentage) is used for all the other species considered. In all the examples proposed, the headspace residence time is constant, so the effects of sulfide removal are only dependent on the concentration of the reactants according to the power law kinetic equation applied. In addition, a maximum value of O_2 flow rate is also assigned to provide more realistic results. This constraint can be reasonably defined according to the available system, for example, the pipes of the injection system in real applications; or as a certain percentage of the biogas produced. The latter method should be preferred when a limit in the existing concentration is desired.

Finally, no dynamics are designed for influent oxygen flow rate. Consequently, the results shown can be considered the setpoint value for this variable. This approach can lead to slightly misleading results in some cases. However, due to typical periods (fraction of hours or more) for control routines of AD systems, the error produced by this simplification is often negligible.

6.1.1. Non-predictive Injection

In this case, the ADOCS model is used to evaluate the impact of microaeration in that the amount of oxygen injected is increased only when the H_2S concentration is detected to be above the defined threshold. The simulation starts from stationary conditions where a constant O_2 addition is performed, providing an exciting sulfide concentration lower than the threshold. In this case, the maximum value for injected O_2 is defined as 1.5% of the total biogas flow rate, according to the rules of thumb of microaeration described in the dedicated section. To highlight the effects of microaeration, for H_2S are reported both the entering and the exiting compositions. As it is possible to see from figure 6.2, at

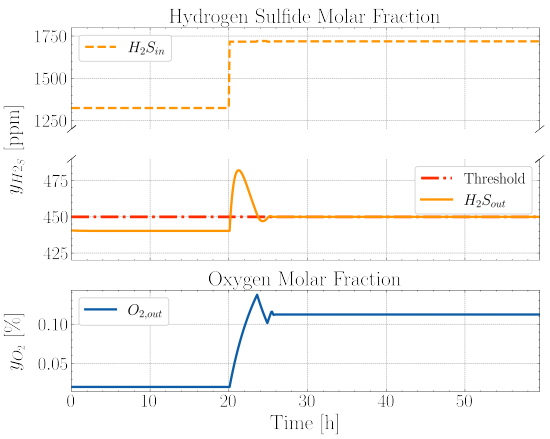

(a) Composition of gaseous stream, with the H_2S threshold highlighted.

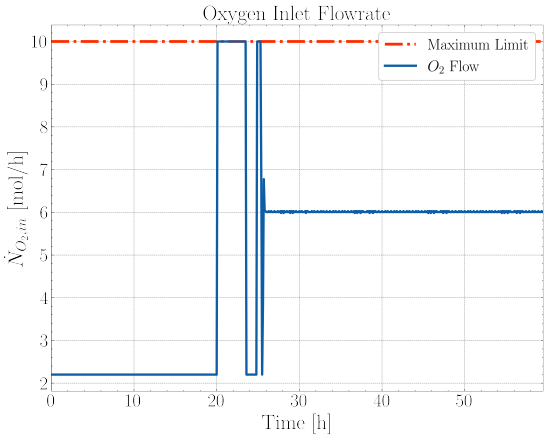

(b) Oxygen injection flow rate, with its maximum value.

Figure 6.2: Results of oxygen injection control based on a non-predictive control system.

$t = t^* = 20\ h$, it is assigned an increase in the headspace influent concentration of H_2S. This step increase in the influent results in a value of measured - calculated - concentration in the exiting stream $y_{H_2S,out}$ $[-]$ above the threshold. Consequently, the amount of oxygen injected is increased to return the $y_{H_2S,out}$ to an acceptable value. The way by which the entering oxygen flow rate is adjusted can be described as follows:

- A constant value is defined as the minimum flow rate possible (in this case, it is 2.2 $mol\,h^{-1}$).
- When this value is not enough to produce a concentration lower than the threshold, it is raised by a certain amount Δn (in this case, by 0.1 $mol\ h^{-1}$). In the present case, it occurs at the time $t = t^*$ when the deviation is assigned. The value obtained by adding Δn to the starting value corresponds to the possible regulations which can be provided to the injecting system.

- The resulting value will produce a new result for exiting sulfide concentration. If this value is acceptable, the next time step can be evaluated. Otherwise, the loop is repeated by increasing the oxygen dosage rate again by Δn.
- If the maximum influent flow rate is reached, but the $y_{H_2S,out}$ is still higher than its threshold, the loop is also broken, and the next time step $t = t^*_{+1}$ is evaluated. This situation means that microaeration for that system needs to reduce the sulfide concentration more.

Microaeration succeeds in finalizing the control action yielding outlet concentrations lower than the defined threshold. However, this approach leads to some criticalities.

The H_2S outlet concentration is lowered to an acceptable value with an oscillatory behavior. Consequently, the biogas contains a too high amount of sulfide for a certain time range. In some cases, this is unacceptable since the threshold must be strictly respected to avoid critical issues in the later phases of biogas processing. Moreover, in a real scenario, the critical value of $y_{H_2S,out}$ triggering the control action is detected only at the moment when the biogas leaves the digester, producing a further delay in the injection and consequently a more extensive time with impure biogas. It can be noted that no limits are given to the oscillatory behavior of the entering flow rate. That is done to allow the algorithm to detect the exact amount of oxygen dosage for each time unit considered, but of course, such frequent changes are rare to be seen in an actual application. Again, this is an ideal first approach to a possible control system subjected to additional physical boundaries in a defined application.

6.1.2. Predictive Injection

A *predictive* oxygen injection can limit and avoid the overshoot in exiting sulfide concentration when the control action is performed, keeping its value consistently below the defined threshold of acceptability. The term predictive means that the control scheme can estimate what will occur in the system and act consequently. This method allows anticipating the control action accordingly to what a deviation to system conditions will create, keeping its effect consistently below the acceptable range. The basis upon which a predictive control system lies is the mathematical model of the process examined, which should give the representative prediction of the system behavior.

A better explanation of what occurs when predictive oxygen injection is done is given by applying it to the examples presented in section 6.1.1 for a non-predictive injection. In that case, the $y_{H_2S,out}$ shows an oscillatory behavior after the control action, bringing values above the threshold for a certain period.

The resulting example, with a predictive oxygen control action, is reported in figure 6.3. From a quick view, it is possible to see that the control action, triggered by the not acceptable $y_{\mathrm{H_2S},out}$, is anticipated by a certain time. This anticipation allows acting previously on the system and preparing it for the upcoming deviation. As a result, the value of the exiting sulfide concentration is always below the defined threshold.

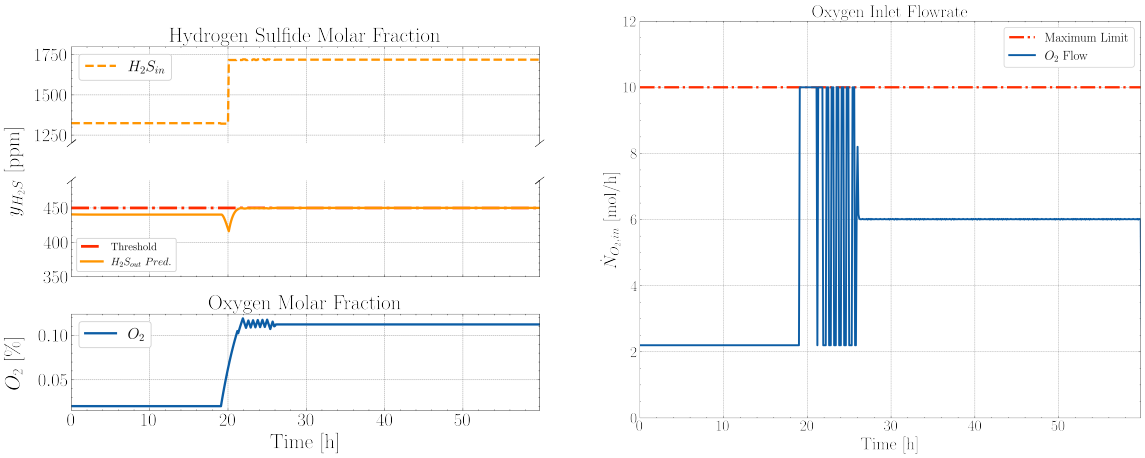

(a) Composition of gaseous stream, with the H_2S threshold highlighted.

(b) Oxygen injection flow rate, with its maximum value.

Figure 6.3: Results of oxygen injection control based on a predictive control system.

The logic behind the anticipation, obtained by upgrading the non-predictive one of the control action, is explained as follows:

- When the simulation reaches the time $t = t^*$ at which a critical H_2S concentration is obtained, at first, the control action is the same as in the non-predictive approach. Consequently, the influent flow is increased step-by-step when either an acceptable value of the exiting H_2S fraction is obtained or the influent flow reaches its maximum. At this point, the non-predictive control shows its limit, and the next time step ($t = t^*_{+1}$) is evaluated. In the predictive approach, a different procedure is instead performed.

- The value of the influent oxygen flow rate is increased up to its maximum (i.e., fully open valve) at the previous time step ($t = t^*_{-1}$). The simulation is then repeated between that instant and the actual time $t = t^*$ to assess the impact of the new condition.

- The resulting $y_{\mathrm{H_2S},out}(t^*)$ new value is then compared with the threshold. If it is below, thus acceptable, the anticipation is enough, and it is possible to proceed to the next time instant $t = t^*_{+1}$. On the contrary, if the new sulfide concentration is

still too high, the anticipation is not enough. Consequently, the algorithm returns one step more to $t = t^*_{-2}$.

- The loop is then repeated until the anticipation allows to have an acceptable value for $y_{\mathrm{H_2S},out}(t^*)$. It is possible that the anticipation goes back to the initial time of the simulation $t = t_0$, and an acceptable value for the considered concentration still needs to be obtained. In this case, the initial conditions and the system design cannot sufficiently reduce the sulfide quantity. An example of this situation is given in figure 6.6.

The schematic view of the described algorithm is provided in figure 6.4. In a non-predictive solution, after reaching the maximum flow rate for the current time, the next time step is evaluated instead of entering the larger loop. The efficacy and the robustness of the

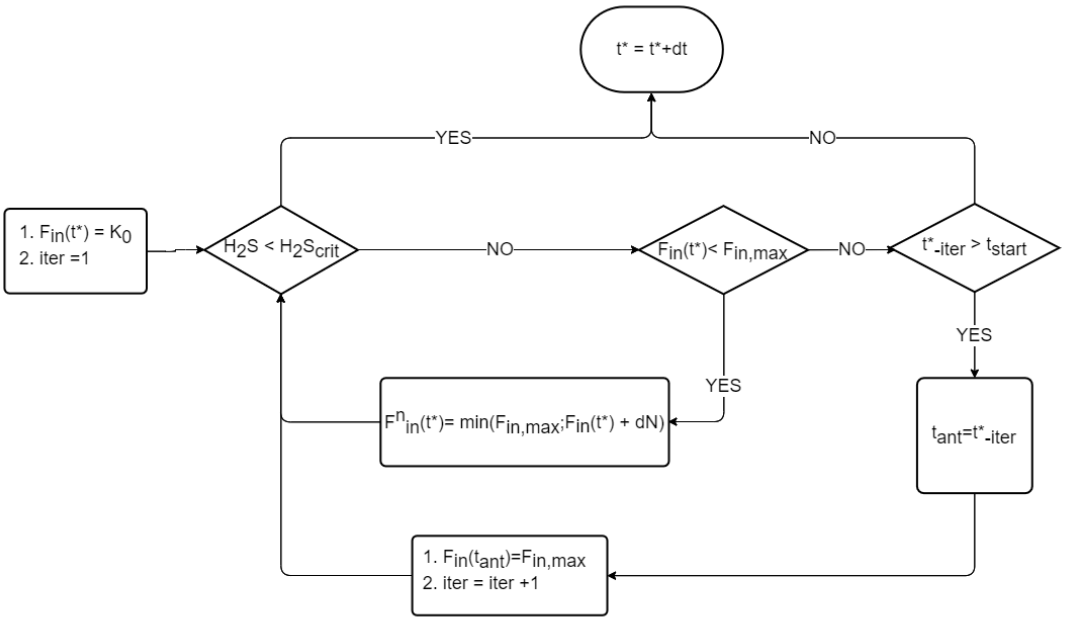

Figure 6.4: Schematic of the proposed algorithm for the control action in the predictive control system.

method established are also evaluated in two other examples. The first one is derived from the previous example by including a negative deviation; the second aims to estimate the system response to a larger number of deviations instead. Figure 6.5 shows how the system behaves when a lower value enters the headspace after a period with a rich H_2S influent. If the entering oxygen is not modified, a lower sulfide concentration also results in a low concentration at the headspace outlet. However, the aim of the control action is not to reduce as much as possible the sulfide concentration, but to keep it below a given threshold.

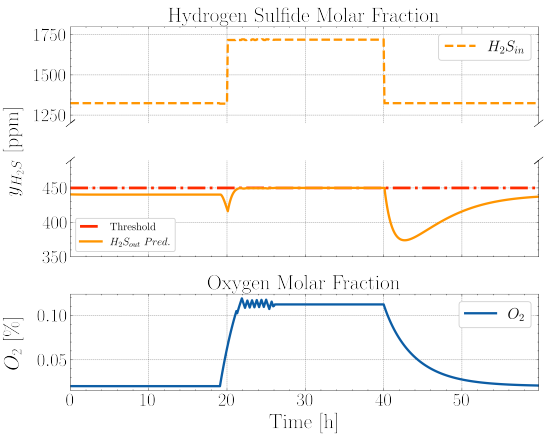

(a) Composition of gaseous stream, with the H_2S threshold highlighted.

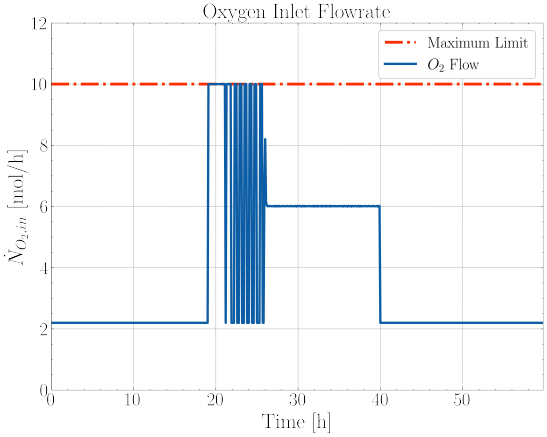

(b) Oxygen injection flow rate, with its maximum value.

Figure 6.5: Results of oxygen injection control based on a predictive control system.

In this case, the previous oxygen flow rate is too large and unnecessary to reach this target since a minor quantity could be utilized, reducing the associated operating costs. As a result, when the algorithm detects this kind of situation, the minimum amount of oxygen is injected. This situation occurs, in the example, at $t = 60\ h$, and the influent is set back to one, which is the minimum arbitrarily assigned. Eventually, this minimum can also be set to zero to avoid unnecessary oxygen consumption.

The last example provided, which results are shown in figure 6.6, aims at simulating a scenario with a large number of deviations in the headspace influent concentration of sulfide. Consequently, a large variability is obtained for the oxygen injection flow rate. This practical example provides two important considerations previously anticipated from the theoretical point of view. At first, it is possible to see a case in which microaeration fails to satisfy the requirements of sulfide reduction. In fact, as a consequence of the large H_2S influent concentration between hours 10 and 20, the anticipation of the control action goes back to the initial time. There needs to be more, and the exiting sulfide concentration is still above the threshold for a certain period. This issue can be tackled either by increasing the allowed flow rate of oxygen or by going further back in anticipating the full opening of the injecting valve (clearly, in the example proposed, this is only possible after the start of the simulation is reached).

The other important consideration emerging from this example is that it minimizes the injected oxygen quantity. The starting point for oxygen dosage quantity is null, and the injection will occur only when needed. As it is possible to see, between hours 20 and 30, the exiting sulfide concentration is lower than the threshold, and thus the injection

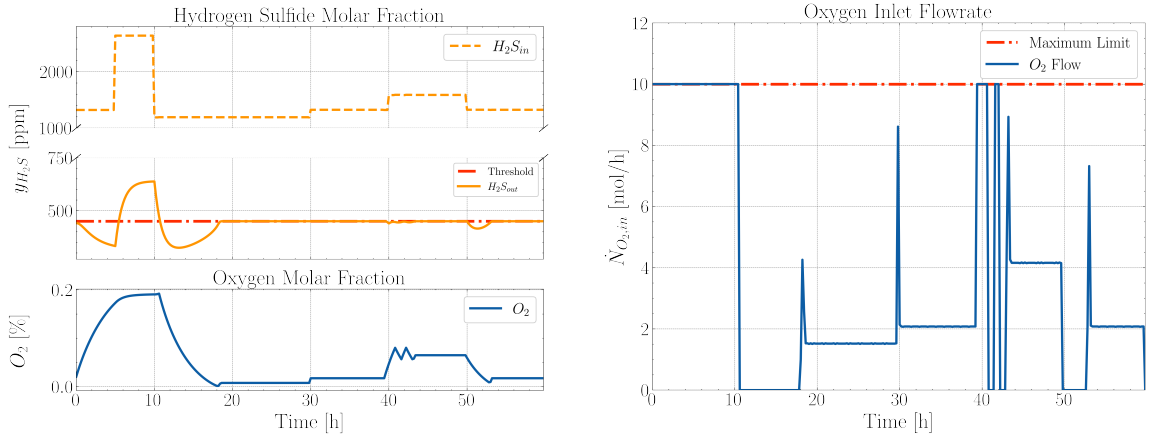

(a) Composition of gaseous stream, with the H_2S threshold highlighted.

(b) Oxygen injection flow rate, with its maximum value.

Figure 6.6: Results of oxygen injection control based on a predictive control system.

is stopped. Also, the oxygen concentration within the headspace gradually lowers. Since that is directly responsible for the amount of sulfide converted when it is too low, the reaction occurs too slowly. The sulfide concentration will rise again even if the entering is constant. As a result, at a certain point, more oxygen is to be added to the system to reestablish acceptable conditions.

6.2. Application to the *Base Case*

The predictive control action is finally presented compared to a scenario with an uncontrolled microaeration. The example shows how intermittent and controlled oxygen is beneficial for the system in avoiding an excessive oxygen dosage.

The base case is presented with an oxygen injection proportional, at each moment, to the total biogas flow rate. In particular, it is considered that $Q_{in,O2} = 0.03 \cdot Q_{tot,biogas}$. Such value is coherent to commonly applied standards and can almost always keep the sulfide concentration under the threshold defined. That maximum amount is arbitrarily set to 500 *ppm* to guarantee a reasonable removal efficiency (around 80%) without overloading the control action requirements. An arbitrary value of maximum influent flow rate for predictive addition is also defined and set equal to 10% of total biogas. The minimum injection is set to 0.1 $m^3\,h^{-1}$ to guarantee always a minimum amount of oxygen and to avoid any numerical issue in the simulation.

Figure 6.7a shows how the uncontrolled injection of oxygen leads to exceeding the threshold when the influent amount of sulfide is higher, which is never reached in the controlled

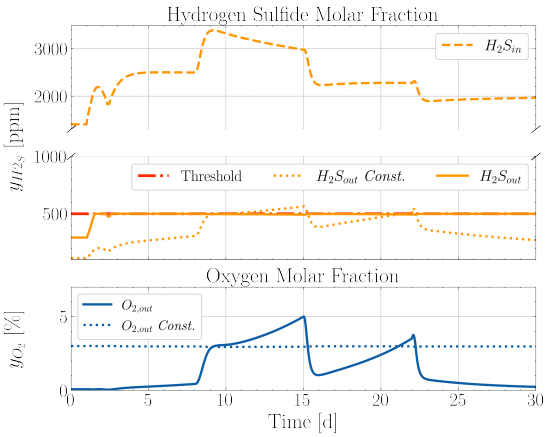

(a) Composition of gaseous stream, with the H_2S threshold highlighted.

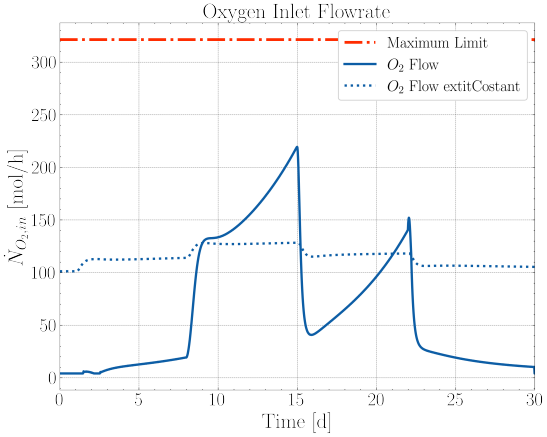

(b) Oxygen injection flow rate, with its maximum value.

Figure 6.7: Results of controlled and comparison with uncontrolled injection for base case scenario.

case. On average, it is possible to note that during specific periods the uncontrolled scenario leads to a lower amount of sulfide in the treated biogas. This behavior is a result of the optimization approach chosen, which, as discussed before for the case, does not aim at providing the minimum amount of sulfide. The target is to keep the H_2S concentration in the treated biogas below the defined threshold with the minimum amount of oxygen.

When an entering peak is present, there is also an increase in the inlet oxygen flow in order to bring the final sulfide below the critical zone. This situation is confirmed by figure 6.7b, which presents the injected flow rate. In fact, during the first days, a minimal injection is enough to keep the sulfide concentration below 500 *ppm*. These results also highlight that, in a *close-to-reality* scenario, the oscillations of the influent observed before are not present, and neglecting the dynamics of the control action is a reasonable assumption. Furthermore, within the thirty days of the simulation, the automatic control action guarantee a saving of more than 900 m^3 of oxygen.

7 | Conclusions

The present work aims to provide a preliminary quantitative assessment of microaeration for sulfide removal in practical contexts. A first lumped model describing sulfate reduction processes and sulfide oxidation is presented. That model is ultimately applied in a complete control algorithm for oxygen injection.

Overall, it is possible to conclude that the proposed model can adequately predict the sulfide fraction in biogas. Applying the model in the control algorithm satisfies the expectations regarding the intermittence of the oxygen injection, providing it only when required.

7.1. Limitations of the Work

Despite the tentatives done to describe the effects of microaeration within anaerobic digestion completely, the present work is subject to significant limitations. Those will be therefore explained in this section.

The interest in ADOCS application is to get good results for ADM1 steady-state variables, which are easier to predict with a limited number of parameters than more complex models. The model parameters are estimated according to ADM1 results. Consequently, ADOCS can be accurate only if ADM1 provides data accurate enough to obtain a successful calibration. According to ADM1 required inputs, this situation can take much work to be obtained in some cases. However, continuous improvements and increasing applications are enlarging ADM1's range of use, with validated results and parameters for more and more substrates. Thus, it can be reasonable to assume that the present limitation will be reduced with time.

The complete control algorithm is built on several inter-dependencies between the input data, the model, and the control action definition. Consequently, its real-time application may suffer instability if the data are not managed correctly or if the periods are not defined carefully. Moreover, the ultimate definition of acceptability for the H_2S concentration prediction relies on the representation of oxidation reaction. It has already been

highlighted the fact that the lack of detailed information about its kinetic parameters is a relevant constraint.

For a possible application of the ADOCS model in an industrial context, which is its ultimate purpose, a complete acceptance of the mentioned limitations is needed. The model is valid enough if its results are compared to referenced literature values. However, every single real case shows a large variability in its conditions. Sometimes it is easy to convert the influent available data to model inputs. The reactor design can only sometimes be compared to the one assumed by the ADOCS model (i.e., CSTR-cylindrical tank reactor type, with headspace varying accordingly to the level of liquid phase). The oxidation kinetics, expressed with power-law kinetics, may largely depend on bacteria concentration. Thus, avoiding their representation by a proper microbial kinetic equation may only sometimes be correct. The industrial scenario presented highlights traits that must be assessed for such an application. However, in that case, acceptable results have been obtained by reconciling the available data to the results arising.

The definition of the control system presented does not include any consideration of the characteristics of the dynamics of the practical controller implemented. This choice is made because it is impossible to know *a priori* which type of actuator is going to be used. Furthermore, the dynamics may not be impacting since, in a real-case scenario, the control action is evaluated with a relatively significant time step (10-30 minutes). The difference between the set-point values is slight, considering that typically axial pumps are used for oxygen injection, and these can perform step variations of flow rates quite quickly. It is thus reasonable to assume that the manipulated variable, at every time step considered, is not strongly affected by the control dynamics.

7.2. Further Research

The current work aims to serve as a startig point for further investigation into optimizing microaeration effectively in anaerobic digestion systems. Therefore, it is noteworthy to highlight some possible modifications that could increase the current work's accuracy and robustness while reducing the influence of the previously indicated limitations.

More attention must be paid to the identification procedure. It is necessary to look more closely at the stability of the proposed method employing ADM1, which may only sometimes be coherent. More precisely, it is critical to understand how to estimate ADM1 steady-state outcomes simply when only limited information is provided. Furthermore, a possible generalization of the reactor scheme proposed should be investigated, including the addition of non-idealities in the evaluation of phase equilibrium.

In general, extra experimental validation should be carried out for practical applications. The development of more precise parameters for the kinetics of sulfide oxidation and the validation of those used in the sulfate reduction models can thus benefit from more on-the-field data. It can also be of interest to add the control system dynamics for completeness and to verify the magnitude of the error eventually arising from the assumption.

A | Appendix A

A.1. Steady-state Data for Identification

This section collects the steady state data resulting from ADM1 simulations (or obtained from the literature) for the three cases presented.

- Dataset 1: AM2HN Simulation comparison and reference for the *base-case*
- Dataset 2: Second set used for further validation of the identification procedure presented
- Dataset 3: Industrial case used to validate the ADOCS model

Table A.1: Dataset 1

HRT	X_T	S_1	S_2	X_1	X_2	C	Z	CO_2	B	pH	P_C	q_C	q_{CH4}
[day]	**[gCOD/L]**	**[gCOD/L]**	**[mmol/L]**	**[gVS/L]**	**[gVS/L]**	**[mmol/L]**	**[mmol/L]**	**[mmol/L]**	**[mmol/L]**	**[-]**	**[atm]**	**[mmol/L/d]**	**[mmol/L/d]**
5	1.3	0.92	82.6	1.42	1.12	75	145	12.4	63	7.01	0.41	42.8	62.4
8	0.92	0.34	31.89	1.39	1.19	123	144	10.9	112	7.32	0.37	27.9	46.9
10	0.78	0.25	15.3	1.35	1.19	139	144	10.5	129	7.4	0.36	22.6	39.6
12	0.68	0.2	8.9	1.32	1.17	146	144	10.3	136	7.43	0.36	19	33.8
15	0.58	0.15	5.4	1.27	1.13	150	145	10.1	140	7.45	0.36	15.3	27.5
17	0.53	0.13	4.3	1.24	1.1	151	146	10	141	7.46	0.36	13.6	24.4
20	0.47	0.12	3.4	1.19	1.06	153	146	9.9	143	7.47	0.36	11.7	20.9
22	0.44	0.11	3	1.16	1.04	153	147	9.8	144	7.47	0.36	10.6	19.1
25	0.4	0.1	2.6	1.15	1	154	147	9.8	145	7.48	0.36	9.4	16.9
30	0.35	0.08	2.1	1.05	0.94	155	148	9.7	146	7.48	0.36	7.9	14.2
50	0.24	0.06	1.4	0.86	0.77	159	150	9.6	149	7.5	0.36	4.8	8.7
70	0.19	0.05	1.2	0.72	0.65	160	152	9.5	151	7.51	0.36	3.5	6.3
90	0.15	0.05	1	0.62	0.56	162	153	9.5	152	7.51	0.36	2.8	4.9

Table A.2: Dataset 2

HRT	X_T	S_1	S_2	X_1	X_2	C	Z	CO_2	B	pH	P_C	q_C	q_{CH4}
[day]	**[gCOD/L]**	**[gCOD/L]**	**[mmol/L]**	**[gVS/L]**	**[gVS/L]**	**[mmol/L]**	**[mmol/L]**	**[mmol/L]**	**[mmol/L]**	**[-]**	**[atm]**	**[mmol/L/d]**	**[mmol/L/d]**
5	11.31	1.05	8.74	0.73	0.63	53.94	52.38	10.30	43.64	6.93	0.38	19.80	36.15
8	8.38	0.36	3.64	0.85	0.75	67.91	61.71	9.83	58.07	7.08	0.36	15.50	29.41
10	7.16	0.26	2.74	0.88	0.77	72.85	65.90	9.69	63.16	7.12	0.36	13.53	25.77
12	6.26	0.20	2.24	0.89	0.79	76.45	69.10	9.59	66.86	7.15	0.36	12.11	23.05
15	5.27	0.16	1.80	0.89	0.79	80.43	72.74	9.49	70.94	7.18	0.35	10.16	19.40
17	4.78	0.14	1.61	0.89	0.79	82.47	74.65	9.44	73.04	7.20	0.35	9.29	17.72
20	4.19	0.12	1.41	0.88	0.78	84.95	76.98	9.38	75.57	7.21	0.35	8.13	15.52
22	3.87	0.11	1.31	0.86	0.77	86.32	78.28	9.34	76.97	7.22	0.35	7.55	14.41
25	3.48	0.10	1.19	0.85	0.75	88.06	79.94	9.31	78.75	7.23	0.35	6.83	13.03
30	2.98	0.09	1.05	0.81	0.72	90.37	82.16	9.26	81.11	7.25	0.34	5.86	11.18
50	1.91	0.06	0.78	0.69	0.61	95.87	87.49	9.16	86.71	7.28	0.34	3.76	7.15
70	1.42	0.05	0.67	0.59	0.52	98.78	90.33	9.12	89.66	7.30	0.34	2.81	5.33

Table A.3: Dataset 3: Industrial Case Study

HRT	X_T	S_1	S_2	X_1	X_2	C	Z	CO_2	B	pH	P_C	q_C	q_{CH4}
[day]	**[gCOD/L]**	**[gCOD/L]**	**[mmol/L]**	**[gVS/L]**	**[gVS/L]**	**[mmol/L]**	**[mmol/L]**	**[mmol/L]**	**[mmol/L]**	**[-]**	**[atm]**	**[mmol/L/d]**	**[mmol/L/d]**
10	8.2	0.3	2.1	1.11	0.79	43.5	35	10.6	33	6.8	0.39	14.9	25.4
12	7.1	0.2	1.6	1.13	0.81	46.8	38	10.5	36	6.8	0.39	13.2	22.4
13	6.6	0.2	1.4	1.14	0.81	48.3	39	10.5	38	6.8	0.39	12.4	21.1
14	6.3	0.2	1.3	1.14	0.82	49.6	41	10.5	39	6.9	0.39	11.8	20.0
15	5.9	0.2	1.2	1.14	0.82	51.0	42	10.4	41	6.9	0.39	11.2	18.9
16	5.6	0.2	1.1	1.14	0.82	52.2	43	10.4	42	6.9	0.38	10.7	18.0
17	5.3	0.2	1.1	1.14	0.82	53.4	44	10.4	43	6.9	0.38	10.2	17.2
18	5.1	0.1	1.0	1.14	0.82	54.6	45	10.3	44	6.9	0.38	9.7	16.4
20	4.6	0.1	0.9	1.14	0.83	56.7	47	10.3	46	6.9	0.38	9.0	15.1
22	4.3	0.1	0.8	1.14	0.83	58.7	49	10.3	48	7.0	0.38	8.3	14.0
24	4.0	0.1	0.8	1.14	0.83	60.6	51	10.2	50	7.0	0.38	7.7	13.0
26	3.7	0.1	0.7	1.13	0.83	62.3	53	10.2	52	7.0	0.38	7.3	12.2

A.2. Model Inputs

Table A.4: Base Case Operating Conditions

D [1/d]	T [°C]	P [atm]	D_r [m]	$V_{reactor}$ [m^3]	$V_{headspace}$ [m^3]
0.5	35	1	20	3400	350

Table A.5: Industrial Case Operating Conditions

D [1/d]	T [°C]	P [atm]	D_r [m]	$V_{reactor}$ [m^3]	$V_{headspace}$ [m^3]
0.0725	42.5	1	30	4050	350

Table A.6: Base Case Influent Conditions

$S_{1,in}$ [gCOD/L]	$S_{2,in}$ [mmol/L]	C_{in} [mmol/L]	Z_{in} [mmol/L]	$X_{T,in}$ [gCOD/L]	Q_{in} [m3/d]	pH_{in} [-]	$\gamma_{S,in}$ [-]	$x_{W,in}$ [-]
0.012	0.000499	40	10	32	170	6.78	0.02	0.97

Table A.7: Industrial Case Study Influent Conditions

$S_{1,in}$ [gCOD/L]	$S_{2,in}$ [mmol/L]	C_{in} [mmol/L]	Z_{in} [mmol/L]	$X_{T,in}$ [gCOD/L]	Q_{in} [m3/d]	pH_{in} [-]	$\gamma_{S,in}$ [-]	$x_{W,in}$ [-]
0.00	0.00	0.1	0.0026	41.08	290.7	6.5	0.0024	0.053

Table A.8: Base Case Influent Deviations

Dev. time [day]	$S_{1,in}$	$S_{2,in}$	C_{in}	N_{in}	$X_{T,in}$	Q_{in}	$\gamma_{S,in}$	$x_{W,in}$
1	1	1	1	1	1	1.1	1	1
8	1	1	1	1	1.1	1.1	1	1
15	1	1	1	1	1	1.1	1	1
22	1	1	1	1	1	1	1	1

Table A.9: Industrial Case Study Influent Deviations

Dev. time [day]	$S_{1,in}$	$S_{2,in}$	C_{in}	N_{in}	$X_{T,in}$	Q_{in}	$\gamma_{S,in}$	$x_{W,in}$
1	1	1	1	1	0.998	0.993	0.982	0.89
2	1	1	1	1	0.996	0.985	0.963	0.77
3	1	1	1	1	0.996	0.985	0.963	0.77
4	1	1	1	1	0.996	0.985	0.963	0.77
5	1	1	1	1	0.996	0.985	0.963	0.77
6	1	1	1	1	0.997	0.989	0.972	0.83
7	1	1	1	1	0.997	0.989	0.972	0.83
8	1	1	1	1	1.000	1.000	1.000	1.00
9	1	1	1	1	1.000	1.001	1.002	1.01
10	1	1	1	1	1.001	1.004	1.011	1.07
11	1	1	1	1	1.001	1.004	1.011	1.07
12	1	1	1	1	1.001	1.004	1.009	1.06
13	1	1	1	1	1.001	1.004	1.009	1.06
14	1	1	1	1	1.002	1.007	1.018	1.11
15	1	1	1	1	1.002	1.007	1.018	1.11
16	1	1	1	1	1.002	1.007	1.018	1.11
17	1	1	1	1	1.000	1.044	1.005	1.08
18	1	1	1	1	1.000	1.044	1.005	1.08
19	1	1	1	1	1.000	1.044	1.005	1.08
20	1	1	1	1	1.001	1.047	1.014	1.13
21	1	1	1	1	1.002	1.051	1.023	1.18
22	1	1	1	1	1.002	1.051	1.023	1.18
23	1	1	1	1	1.002	1.051	1.023	1.18
24	1	1	1	1	1.006	0.979	1.050	1.26
25	1	1	1	1	1.006	0.979	1.050	1.26
26	1	1	1	1	1.009	0.906	1.082	1.36
27	1	1	1	1	1.009	0.906	1.082	1.36
28	1	1	1	1	1.009	0.906	1.082	1.36
29	1	1	1	1	1.009	0.906	1.082	1.36
30	1	1	1	1	1.009	0.906	1.082	1.36
31	1	1	1	1	1.009	0.906	1.082	1.36

B | Appendix B

B.1. Identification

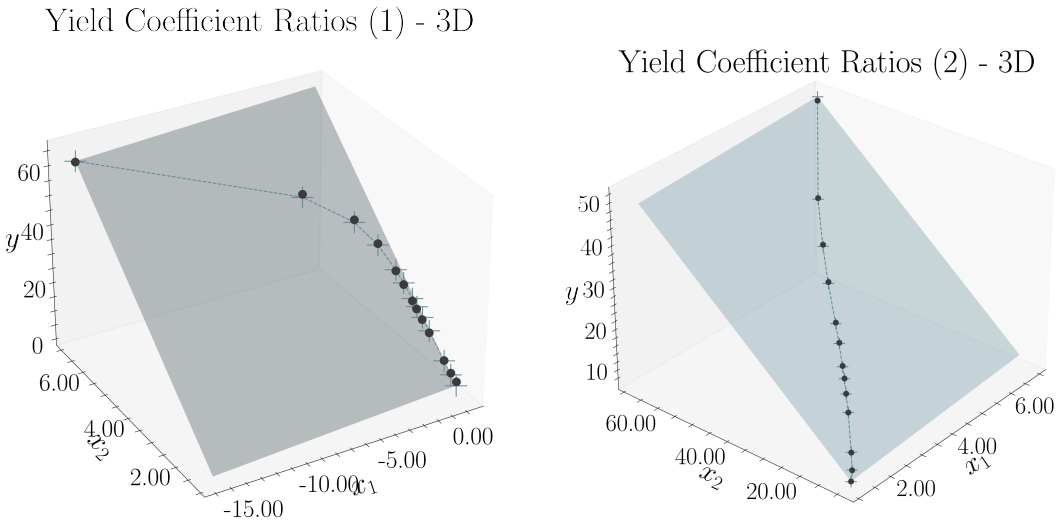

(a) Equation on methane molar flow.

(b) Equation on carbon molar flow.

Figure B.1: Tri-dimensional visualization for results on multi-variable regressions on equations 4.18 and 4.19.

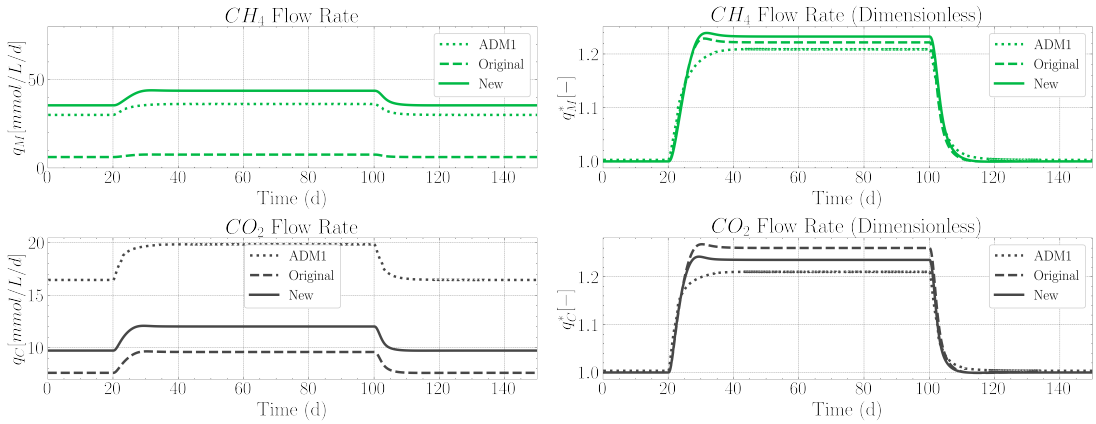

Figure B.2: Gaseous Variables for Dataset 2

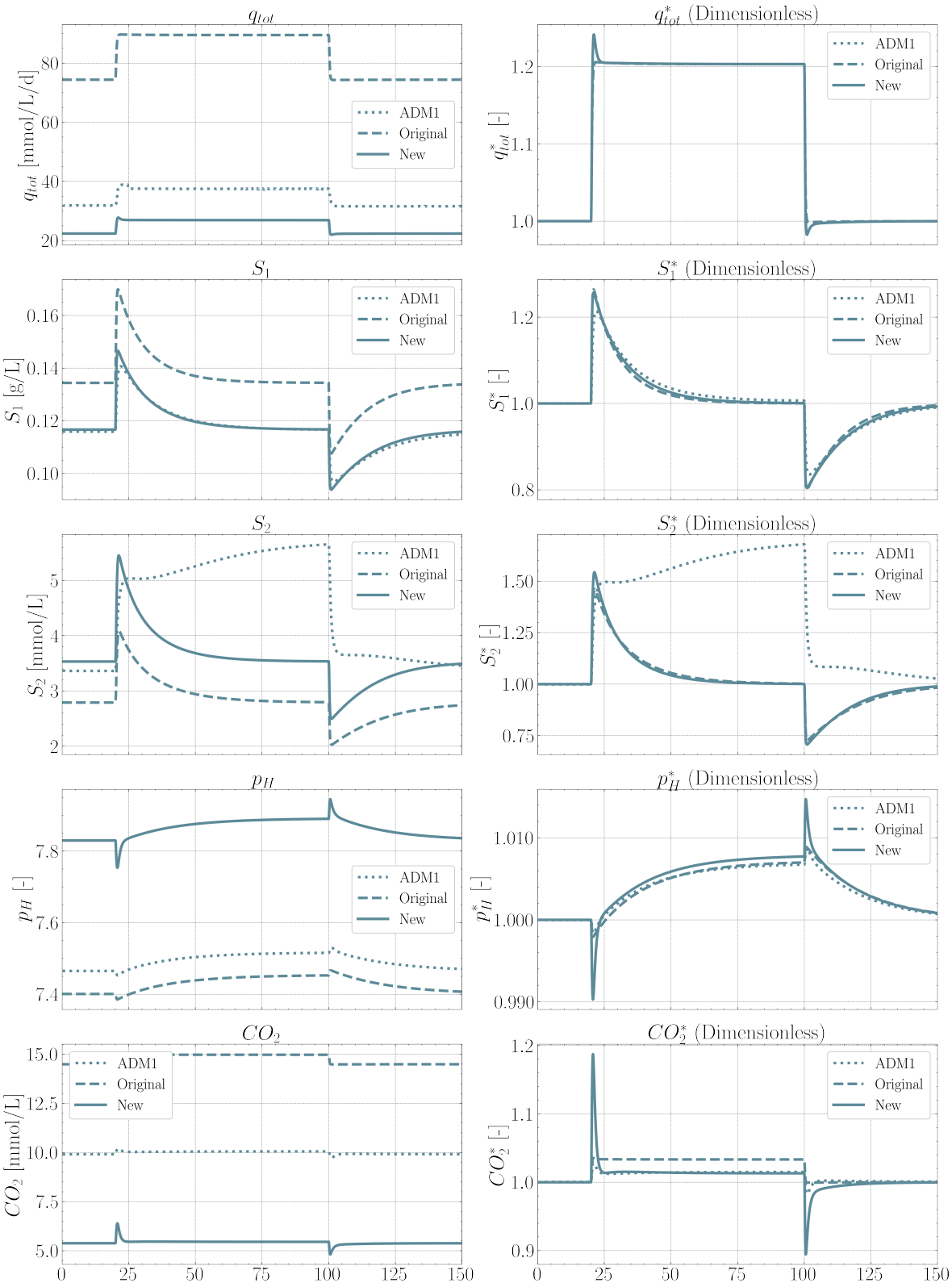

Figure B.3: Process Variables results for Dataset 1

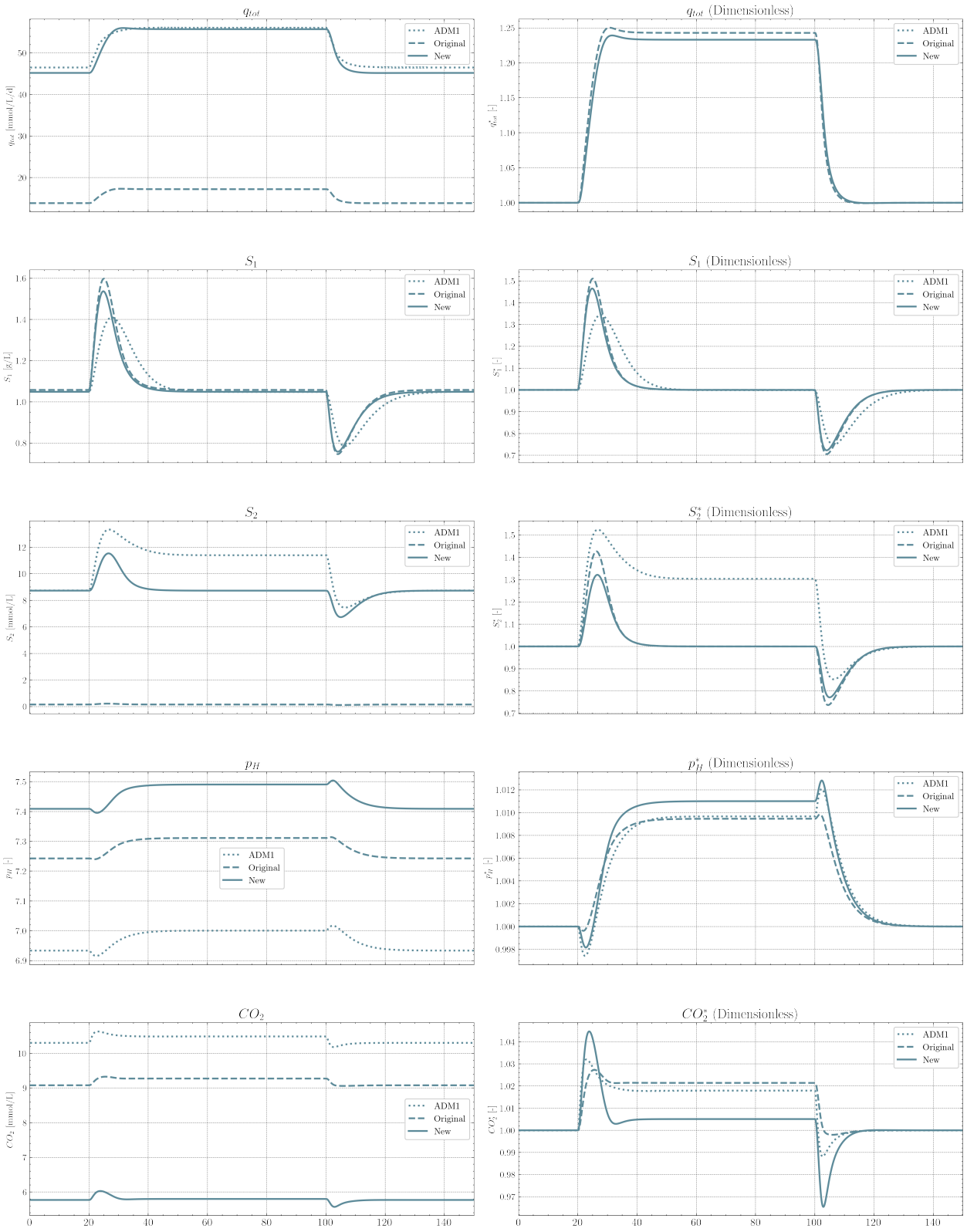

Figure B.4: Process Variables results for Dataset 2

B.2. ADOCS Model

Relevant results for comparison

Bibliography

[1] M. S. Schäfer, "Climate change and the media," in Elsevier Inc., Mar. 2015, pp. 853–859, ISBN: 9780080970875. DOI: 10.1016/B978-0-08-097086-8.91079-1.

[2] *Time* vol. 167, 14 Apr. 3, 2006, *Special Report Global Warming*: *Special Report Global Warming*. [Online]. Available: http://content.time.com/time/magazine/0,9263,7601060403,00.html.

[3] *Adoption of the Paris Agreement*, U.N. Doc. FCCC/CP/2015/L.9/Rev/1, UNFCC - Conference of the Parties, Paris, Dec. 12, 2015. [Online]. Available: https://unfccc.int/resource/docs/2015/cop21/eng/l09r01.pdf.

[4] *Transforming Our World: The 2030 Agenda for Sustainable Development*, Resolution adopted by the General Assembly on 25 September 2015 - A/RES/70/1, UN General Assembly, Oct. 21, 2015. [Online]. Available: https://www.un.org/ga/search/view_doc.asp?symbol=A/RES/70/1&Lang=E.

[5] B. Obama, "Statement by the President on the Paris Climate Agreement," The White House, Office of the Press Secretary, Dec. 12, 2015. [Online]. Available: https://obamawhitehouse.archives.gov/the-press-office/2015/12/12/statement-president-paris-climate-agreement.

[6] "The Paris Agreement," UNFCCC. (2015), [Online]. Available: https://unfccc.int/process-and-meetings/the-paris-agreement/the-paris-agreement.

[7] "Key aspects of the Paris Agreement," UNFCCC. (2015), [Online]. Available: https://unfccc.int/process-and-meetings/the-paris-agreement/the-paris-agreement/key-aspects-of-the-paris-agreement (visited on 09/02/2022).

[8] "Transforming our world: The 2030 agenda for sustainable development | department of economic and social affairs," United Nations. (2015), [Online]. Available: https://sdgs.un.org/2030agenda.

[9] "THE 17 GOALS | Sustainable Development," United Nations. (2015), [Online]. Available: https://sdgs.un.org/goals (visited on 09/02/2022).

[10] H. Ritchie, M. Roser, E. Ortiz-Ospina, and J. Mispy. "Measuring progress towards the Sustainable Development Goals." (2018), [Online]. Available: SDG-tracker.org (visited on 09/05/2022).

[11] *The Sustainable Development Goals Report 2022*, United Nations, Jul. 7, 2022. [Online]. Available: https://unstats.un.org/sdgs/report/2022/The-Sustainable-Development-Goals-Report-2022.pdf.

[12] U. von der Leyen, "Speech by president-elect von der leyen in the european parliament plenary on the occasion of the presentation of her college of commissioners and their programme," European Commission, Strasbourg, Nov. 27, 2019. [Online]. Available: https://ec.europa.eu/commission/presscorner/detail/en/SPEECH_19_6408.

[13] *The European Green Deal*, European Commission Communication COM(2019) 640 final. European Commission, Brussels, Dec. 11, 2019.

[14] *Europe's moment: Repair and Prepare for the Next Generation*, European Commission Communication COM(2020) 456 final, European Commission, Brussels, May 27, 2020.

[15] "Recovery plan for Europe," European Commission. (2020), [Online]. Available: https://ec.europa.eu/info/strategy/recovery-plan-europe_en.

[16] *"Fit for 55": delivering the EU's 2030 Climate Target on the way to climate neutrality*, European Commission Communication COM(2021) 550 final. European Commission, Brussels, Jul. 14, 2021.

[17] *Fit for 55 package: Council reaches general approaches relating to emissions reductions and their social impacts*, Council Press Release 619/22. Council of the EU, Jun. 29, 2022.

[18] *REPowerEU Plan*, European Commission Communication COM(2022) 230 final. European Commission, Brussels, May 18, 2022.

[19] "REPowerEU actions," European Commission, 2022. DOI: 10.2775/23837.

[20] A. Gili and A. Rizzi. "From the Green Deal to REPowerEU: The Green Transition in Europe and Beyond | ISPI." (), [Online]. Available: https://www.ispionline.it/it/pubblicazione/green-deal-repowereu-green-transition-europe-and-beyond-35902 (visited on 08/26/2022).

[21] *Italia Domani, il Piano Nazionale di Ripresa e Resilienza*, Governo Italiano - Presidenza del Consiglio dei Ministri, 2021. [Online]. Available: https://www.governo.it/sites/governo.it/files/PNRR_0.pdf.

[22] "Factsheet: Italy's recovery and resilience plan," European Commission, 2021. DOI: 10.2775/941269. [Online]. Available: https://ec.europa.eu/info/system/files/italy-recovery-resilience-factsheet_en.pdf.

[23] *Piano Nazionale Integrato per l'Energia e per il Clima*, Ministero dello Sviluppo Economico, Ministero dell'Ambiente e della Tutela del Territorio e del Mare, Min-

istero delle Infrastrutture e dei Trasporti, Dec. 2019. [Online]. Available: https://www.mise.gov.it/images/stories/documenti/PNIEC_finale_17012020.pdf.

[24] "Policy Brief: Bioenergy Landscape, Statistical report 2021," Bioenergy Europe, 2021.

[25] European Commission - Joint Research Centre, *How the bioeconomy contributes to the European Green Deal*. Publications Office, 2020. DOI: doi/10.2777/67636.

[26] S. P. Andersen, B. Allen, and G. C. Domingo, "Biomass in the EU Green Deal: Towards consensus on sustainable use of biomass for EU bioenergy," Institute for European Environmental Policy (IEEP), Policy Report, 2021.

[27] European Biogas Association (EBA), *Biogas Basics*. 2019. [Online]. Available: https://www.europeanbiogas.eu/wp-content/uploads/2019/09/Biogas-Basics-EBA.pdf.

[28] S. Alberici, M. Moultak, and J. Peters, *Gas for Climate/The future role of biomethane*. Guidehouse, Dec. 2021.

[29] N. Scarlat, J.-F. Dallemand, and F. Fernando, "Biogas: developments and perspectives in Europe," *Renewable Energy*, vol. 129, pp. 457–472, 2018, ISSN: 0960-1481 (online). DOI: 10.1016/j.renene.2018.03.006.

[30] J. Giuntoli, A. Agostini, R. Edwards, and L. Marelli, *Solid and gaseous bioenergy pathways: input values and GHG emissions. Calculated according to the methodology set in COM(2016) 767*. EUR 27215 EN, 2017. DOI: :10.2790/27486.

[31] "Policy brief: Biogas, Statistical report 2021," Bioenergy Europe, 2021.

[32] "The contribution of the biogas and biomethane industries to medium-term greenhouse gas reduction targets and climate neutrality by 2050, Background paper," European Biogas Association (EBA), Apr. 2020.

[33] *Implementing the REPowerEU action plan: investment needs, hydrogen accelerator and achieving biomethane targets*, Commission Staff Working Document SWD(2022) 230 final, European Commission, Brussels, May 18, 2022.

[34] S. Alberici, W. Grimme, and G. Toop, *Biomethane production potentials in the EU, Feasibility of REPowerEU 2030 targets, production potentials in the Member States and outlook to 2050*. Guidehouse, Jul. 2022.

[35] "Short-, mid- and long-term strategies to speed up biomethane deployment in Europe," European Biogas Association (EBA), Jun. 2022.

[36] "How to achieve the sustainable development goals through biogas, Factsheet 3," World Biogas Association (WBA), Jul. 2018. [Online]. Available: https://www.worldbiogasassociation.org/wp-content/uploads/2018/07/WBA-SDGs-Biogas-factsheet-3.pdf.

[37] K. Obaideen, M. A. Abdelkareem, T. Wilberforce, *et al.*, "Biogas role in achievement of the sustainable development goals: Evaluation, Challenges, and Guidelines," *Journal of the Taiwan Institute of Chemical Engineers*, vol. 131, p. 104 207, 2022. DOI: 10.1016/j.jtice.2022.104207.

[38] (), [Online]. Available: europeanbiogas.eu.

[39] F. Xu and Y. Li, "Biomass Digestion," in *Encyclopedia of Sustainable Technologies*, M. A. Abraham, Ed., Oxford: Elsevier, 2017, pp. 197–204, ISBN: 978-0-12-804792-7. DOI: https://doi.org/10.1016/B978-0-12-409548-9.10108-3. [Online]. Available: https://www.sciencedirect.com/science/article/pii/B9780124095489101083.

[40] P. Uçkun Kiran, K. Stamatelatou, G. Antonopoulou, and G. lyberatos, "Production of biogas via anaerobic digestion," in *Handbook of Biofuels Production*, ser. Woodhead Publishing Series in Energy, R. Luque, J. Campelo, and J. Clark, Eds., Woodhead Publishing, 2011, pp. 266–304, ISBN: 978-1-84569-679-5. DOI: https://doi.org/10.1533/9780857090492.2.266. [Online]. Available: https://www.sciencedirect.com/science/article/pii/B9781845696795500127.

[41] F. Moretta, A. Goracci, F. Manenti, and G. Bozzano, "Data-driven model for feedstock blending optimization of anaerobic co-digestion by BMP maximization," *Journal of Cleaner Production*, vol. 375, pp. 134–140, 2022, ISSN: 0959-6526. DOI: https://doi.org/10.1016/j.jclepro.2022.134140. [Online]. Available: https://www.sciencedirect.com/science/article/pii/S095965262203712X.

[42] R. Steffen, O. Szolar, and R. Braun, "Feedstocks for anaerobic digestion," *Institute of Agrobiotechnology Tulin, University of Agricultural Sciences, Vienna*, 1998.

[43] J. Van Lier, N. Mahmoud, and G. Zeeman, "Biological wastewater treatment: Principles, modelling and design. chapter 16: Anaerobic waste water treatment," *Biological wastewater treatment: principles, modelling and design*, 2008.

[44] O. W. Awe, Y. Zhao, A. Nzihou, D. P. Minh, and N. Lyczko, "A review of biogas utilisation, purification and upgrading technologies," *Waste and Biomass Valorization*, vol. 8, pp. 267–283, 2 Mar. 2017, ISSN: 1877-2641. DOI: 10.1007/s12649-016-9826-4.

[45] K. Rajeshwari, M. Balakrishnan, A. Kansal, K. Lata, and V. Kishore, "State-of-the-art of anaerobic digestion technology for industrial wastewater treatment," *Renewable and Sustainable Energy Reviews*, vol. 4, no. 2, pp. 135–156, 2000, ISSN: 1364-0321. DOI: https://doi.org/10.1016/S1364-0321(99)00014-3. [Online]. Available: https://www.sciencedirect.com/science/article/pii/S1364032199000143.

[46] M. Zupančič, V. Možic, M. Može, F. Cimerman, and I. Golobič, "Current Status and Review of Waste-to-Biogas Conversion for Selected European Countries and Worldwide," *Sustainability*, vol. 14, no. 3, 2022, ISSN: 2071-1050. DOI: 10.3390/su14031823. [Online]. Available: https://www.mdpi.com/2071-1050/14/3/1823.

[47] A. Converti, A. D. Borghi, M. Zilli, S. Arni, and M. D. Borghi, "Anaerobic digestion of the vegetable fraction of municipal refuses: Mesophilic versus thermophilic conditions," *Bioprocess Engineering 1999 21:4*, vol. 21, pp. 371–376, 4 1999, ISSN: 1615-7605. DOI: 10.1007/S004490050689. [Online]. Available: https://link.springer.com/article/10.1007/s004490050689.

[48] C. Mao, Y. Feng, X. Wang, and G. Ren, "Review on research achievements of biogas from anaerobic digestion," *Renewable and Sustainable Energy Reviews*, vol. 45, pp. 540–555, 2015, ISSN: 1364-0321. DOI: https://doi.org/10.1016/j.rser.2015.02.032. [Online]. Available: https://www.sciencedirect.com/science/article/pii/S1364032115001203.

[49] E. L. Barrera, H. Spanjers, J. Dewulf, O. Romero, and E. Rosa, "The sulfur chain in biogas production from sulfate-rich liquid substrates: A review on dynamic modeling with vinasse as model substrate," *Journal of Chemical Technology & Biotechnology*, vol. 88, pp. 1405–1420, 8 Aug. 2013, ISSN: 02682575. DOI: 10.1002/jctb.4071.

[50] G. F. Parkin, N. A. Lynch, W.-C. Kuo, E. L. V. Keuren, and S. K. Bhattacharya, "Interaction between sulfate reducers and methanogens fed acetate and propionate," *Research Journal of the Water Pollution Control Federation*, vol. 62, no. 6, pp. 780–788, 1990, ISSN: 10477624. [Online]. Available: http://www.jstor.org/stable/25043913 (visited on 11/10/2022).

[51] A. Robles, S. Vinardell, J. Serralta, *et al.*, "Anaerobic treatment of sulfate-rich wastewaters: Process modeling and control," in *Environmental Technologies to Treat Sulphur Pollution: Principles and Engineering*, vol. 2, IWA Publishing, 2020, pp. 277–317.

[52] M. Mahesh, K. V. Arivizhivendhan, K. Nivetha, S. Swarnalatha, and G. Sekaran, "Anaerobic digestion of sulphate-rich post-tanning wastewater at different cod/sulphate and f/m ratios," *3 Biotech*, vol. 8, p. 130, 2 Feb. 2018, ISSN: 2190-572X. DOI: 10.1007/s13205-018-1154-x.

[53] S. Abanades, H. Abbaspour, A. Ahmadi, *et al.*, "A conceptual review of sustainable electrical power generation from biogas," *Energy Science & Engineering*, vol. 10, no. 2, pp. 630–655, 2022. DOI: https://doi.org/10.1002/ese3.1030. [Online]. Available: https://onlinelibrary.wiley.com/doi/abs/10.1002/ese3.1030.

[54] L. Pokorna-Krayzelova, J. Bartacek, I. Díaz, D. Jeison, E. Volcke, and P. Jenicek, "Microaeration for hydrogen sulfide removal during anaerobic treatment: A review," *Reviews in Environmental Science and Bio/Technology*, vol. 14, pp. 703–725, Dec. 2015. DOI: 10.1007/s11157-015-9386-2.

[55] M. Andreides, L. Pokorná-Krayzelová, J. Bartáček, and P. Jeníč, "Biological h2s removal from gases," *Environmental Technologies to Treat Sulphur Pollution: Principles and Engineering*, pp. 345–375, 2020. DOI: 10.2166/9781789060966_0345.

[56] C. Becker, M. Marder, E. Junges, and O. Konrad, "Technologies for biogas desulfurization - an overview of recent studies," *Renewable and Sustainable Energy Reviews*, vol. 159, pp. 112–205, 2022, ISSN: 1364-0321. DOI: https://doi.org/10.1016/j.rser.2022.112205. [Online]. Available: https://www.sciencedirect.com/science/article/pii/S1364032122001289.

[57] D. Nguyen and S. K. Khanal, "A little breath of fresh air into an anaerobic system: How microaeration facilitates anaerobic digestion process," *Biotechnology Advances*, vol. 36, no. 7, pp. 1971–1983, 2018, ISSN: 0734-9750. DOI: https://doi.org/10.1016/j.biotechadv.2018.08.007. [Online]. Available: https://www.sciencedirect.com/science/article/pii/S0734975018301459.

[58] S. Fu, S. Lian, I. Angelidaki, and R. Guo, "Micro-aeration: An attractive strategy to facilitate anaerobic digestion," *Trends in Biotechnology*, 2022, ISSN: 0167-7799. DOI: https://doi.org/10.1016/j.tibtech.2022.09.008. [Online]. Available: https://www.sciencedirect.com/science/article/pii/S0167779922002426.

[59] S. Kundu, J. Zanganeh, and B. Moghtaderi, "A review on understanding explosions from methane–air mixture," *Journal of Loss Prevention in the Process Industries*, vol. 40, pp. 507–523, 2016, ISSN: 0950-4230. DOI: https://doi.org/10.1016/j.jlp.2016.02.004. [Online]. Available: https://www.sciencedirect.com/science/article/pii/S0950423016300286.

[60] A. J. H. Janssen, R. Sleyster, C. van der Kaa, A. Jochemsen, J. Bontsema, and G. Lettinga, "Biological sulphide oxidation in a fed-batch reactor," *Biotechnology and Bioengineering*, vol. 47, no. 3, pp. 327–333, 1995. DOI: https://doi.org/10.1002/bit.260470307. [Online]. Available: https://onlinelibrary.wiley.com/doi/abs/10.1002/bit.260470307.

[61] I. Ramos and M. Fdz-Polanco, "Microaerobic control of biogas sulphide content during sewage sludge digestion by using biogas production and hydrogen sulphide concentration," *Chemical Engineering Journal*, vol. 250, pp. 303–311, Aug. 2014, ISSN: 13858947. DOI: 10.1016/j.cej.2014.04.027.

[62] D. Batstone, J. Keller, I. Angelidaki, *et al.*, "The IWA Anaerobic Digestion Model No 1 (ADM1)," *Water Science and Technology*, vol. 45, no. 10, pp. 65–73, May 2002,

ISSN: 0273-1223. DOI: 10.2166/wst.2002.0292. eprint: https://iwaponline.com/wst/article-pdf/45/10/65/425002/65.pdf. [Online]. Available: https://doi.org/10.2166/wst.2002.0292.

[63] H. Zhou, H. Li, and F. Wang, "Anaerobic digestion of different organic wastes for biogas production and its operational control performed by the modified," *Journal of Environmental Science and Health, Part A*, vol. 47, no. 1, pp. 84–92, 2012. DOI: 10.1080/10934529.2012.629585. [Online]. Available: https://doi.org/10.1080/10934529.2012.629585.

[64] D. Nguyen, V. Gadhamshetty, S. Nitayavardhana, and S. K. Khanal, "Automatic process control in anaerobic digestion technology: A critical review," *Bioresource Technology*, vol. 193, pp. 513–522, 2015, ISSN: 0960-8524. DOI: https://doi.org/10.1016/j.biortech.2015.06.080. [Online]. Available: https://www.sciencedirect.com/science/article/pii/S0960852415008718.

[65] D. Dochain and G. Bastin, "Adaptive control of fedbatch bioreactors," *Chemical Engineering Communications*, vol. 87, no. 1, pp. 67–85, 1990. DOI: 10.1080/00986449008940684.

[66] J. Lauwers, L. Appels, I. P. Thompson, J. Degrève, J. F. Van Impe, and R. Dewil, "Mathematical modelling of anaerobic digestion of biomass and waste: Power and limitations," *Progress in Energy and Combustion Science*, vol. 39, no. 4, pp. 383–402, 2013, ISSN: 0360-1285. DOI: https://doi.org/10.1016/j.pecs.2013.03.003. [Online]. Available: https://www.sciencedirect.com/science/article/pii/S0360128513000178.

[67] M. Heiker, M. Kraume, A. Mertins, T. Wawer, and S. Rosenberger, "Biogas plants in renewable energy systems—a systematic review of modeling approaches of biogas production," *Applied Sciences*, vol. 11, no. 8, 2021, ISSN: 2076-3417. DOI: 10.3390/app11083361. [Online]. Available: https://www.mdpi.com/2076-3417/11/8/3361.

[68] E. Gueguim Kana, J. Oloke, A. Lateef, and M. Adesiyan, "Modeling and optimization of biogas production on saw dust and other co-substrates using artificial neural network and genetic algorithm," *Renewable Energy*, vol. 46, pp. 276–281, 2012, ISSN: 0960-1481. DOI: https://doi.org/10.1016/j.renene.2012.03.027. [Online]. Available: https://www.sciencedirect.com/science/article/pii/S0960148112002145.

[69] J. F. Andrews, "A mathematical model for the continuous culture of microorganisms utilizing inhibitory substrates," *Biotechnology and Bioengineering*, vol. 10, no. 6, pp. 707–723, 1968. DOI: https://doi.org/10.1002/bit.260100602. [On-

line]. Available: https://onlinelibrary.wiley.com/doi/abs/10.1002/bit.260100602.

[70] J. F. Andrews, "Dynamic model of the anaerobic digestion process," *Journal of the Sanitary Engineering Division*, vol. 95, no. 1, pp. 95–116, 1969. DOI: 10.1061/JSEDAI.0000943. [Online]. Available: https://ascelibrary.org/doi/abs/10.1061/JSEDAI.0000943.

[71] J. F. Andrews and S. P. Graef, "Dynamic modeling and simulation of the anaerobic digestion process," in *Advances in Chemistry*, ACS Publications, 1970, ch. 8, pp. 126–162.

[72] J. Monod, "The growth of bacterial cultures," *Annual Review of Microbiology*, vol. 3, no. 1, pp. 371–394, 1949. DOI: 10.1146/annurev.mi.03.100149.002103.

[73] D. Hill and C. Barth, "A dynamic model for simulation of animal waste digestion," *Journal (Water Pollution Control Federation)*, pp. 2129–2143, 1977.

[74] W. Sanders, M. Geerink, G. Zeeman, and G. Lettinga, "Anaerobic hydrolysis kinetics of particulate substrates," *Water Science and Technology*, vol. 41, pp. 17–24, 3 Feb. 2000, ISSN: 0273-1223. DOI: 10.2166/wst.2000.0051.

[75] P. N. Hobson, "The kinetics of anaerobic digestion of farm wastes," *Journal of Chemical Technology and Biotechnology. Biotechnology*, vol. 33, no. 1, pp. 1–20, 1983.

[76] V. Vavilin, S. Rytov, and L. Lokshina, "A description of hydrolysis kinetics in anaerobic degradation of particulate organic matter," *Bioresource Technology*, vol. 56, pp. 229–237, 2-3 May 1996, ISSN: 09608524. DOI: 10.1016/0960-8524(96)00034-X.

[77] A. C. Duarte and G. K. Anderson, "Inhibition modelling in anaerobic digestion," *Water Science and Technology*, vol. 14, pp. 749–763, 6-7 Jun. 1982, ISSN: 0273-1223. DOI: 10.2166/wst.1982.0139.

[78] V. Vavilin, V. Vasiliev, S. Rytov, and A. Ponomarev, "Self-oscillating coexistence of methanogens and sulfate-reducers under hydrogen sulfide inhibition and the ph-regulating effect," *Bioresource Technology*, vol. 49, no. 2, pp. 105–119, 1994, ISSN: 0960-8524. DOI: https://doi.org/10.1016/0960-8524(94)90074-4. [Online]. Available: https://www.sciencedirect.com/science/article/pii/0960852494900744.

[79] S. Kalyuzhnyi, V. Fedorovich, P. Lens, L. H. Pol, and G. Lettinga, "Mathematical modelling as a tool to study population dynamics between sulfate reducing and methanogenic bacteria," *Biodegradation 1998 9:3*, vol. 9, pp. 187–199, 3 1998, ISSN: 1572-9729. DOI: 10.1023/A:1008339018423. [Online]. Available: https://link.springer.com/article/10.1023/A:1008339018423.

[80] A. Aboulfotoh, "ADM1 Simulation of the Mesophilic Anaerobic Digestion of Mixture of Primary and Secondary Sludge Treated by Effective Microorganisms," *International Journal of Engineering and Technology*, vol. 02, pp. 1582–1587, 10 2013.

[81] S. G. Pavlostathis and J. M. Gossett, "Preliminary conversion mechanisms in anaerobic digestion of biological sludges," *Journal of Environmental Engineering*, vol. 114, pp. 575–592, 3 Jun. 1988, ISSN: 0733-9372. DOI: 10.1061/(ASCE)0733-9372(1988)114:3(575).

[82] J. A. Eastman and J. F. Ferguson, "Solubilization of particulate organic carbon during the acid phase of anaerobic digestion," *Journal (Water Pollution Control Federation)*, vol. 53, no. 3, pp. 352–366, 1981, ISSN: 00431303. [Online]. Available: http://www.jstor.org/stable/25041085 (visited on 11/08/2022).

[83] IWA Task Group for Mathematical Modelling of Anaerobic Digestion Processes, *Anaerobic Digestion Model No.1 (ADM1)*. IWA publishing, 2002, ISBN: 9781900222785.

[84] A. Galí, T. Benabdallah, S. Astals, and J. Mata-Alvarez, "Modified version of adm1 model for agro-waste application," *Bioresource Technology*, vol. 100, pp. 2783–2790, 11 Jun. 2009, ISSN: 09608524. DOI: 10.1016/j.biortech.2008.12.052.

[85] K. Derbal, M. Bencheikh-lehocine, F. Cecchi, A.-H. Meniai, and P. Pavan, "Application of the IWA ADM1 model to simulate anaerobic co-digestion of organic waste with waste activated sludge in mesophilic condition," *Bioresource Technology*, vol. 100, pp. 1539–1543, 4 Feb. 2009, ISSN: 09608524. DOI: 10.1016/j.biortech.2008.07.064.

[86] W. Parker, "Application of the ADM1 model to advanced anaerobic digestion," *Bioresource Technology*, vol. 96, pp. 1832–1842, 16 Nov. 2005, ISSN: 09608524. DOI: 10.1016/j.biortech.2005.01.022.

[87] D. Batstone, J. Keller, and J. Steyer, "A review of ADM1 extensions, applications, and analysis: 2002–2005," *Water Science and Technology*, vol. 54, pp. 1–10, 4 Aug. 2006, ISSN: 0273-1223. DOI: 10.2166/wst.2006.520.

[88] R. Kleerebezem and M. van Loosdrecht, "Critical analysis of some concepts proposed in adm1," *Water Science and Technology*, vol. 54, pp. 51–57, 4 Aug. 2006, ISSN: 0273-1223. DOI: 10.2166/wst.2006.525.

[89] J. Copp, "The cost simulation benchmark-description and simulator manual," Jan. 2001.

[90] U. Jeppsson, C. Rosen, J. Alex, *et al.*, "Towards a benchmark simulation model for plant-wide control strategy performance evaluation of wwtps," *Water Science and Technology*, vol. 53, pp. 287–295, 1 Jan. 2006, ISSN: 0273-1223. DOI: 10.2166/wst.2006.031.

[91] C. Rosén and U. Jeppsson, "Aspects on ADM1 Implementation within the BSM2 Framework," *Department of Industrial Electrical Engineering and Automation, Lund University, Lund, Sweden*, 2006.

[92] D. Botheju and R. Bakke, "Oxygen effects in anaerobic digestion-a review," 2011, pp. 1–19.

[93] D. Botheju, B. Lie, and R. Bakke, "Oxygen effects in anaerobic digestion," *Modeling, Identification and Control*, vol. 30, pp. 191–201, 4 2009, ISSN: 03327353. DOI: 10.4173/mic.2009.4.1.

[94] D. Botheju, B. Lie, and R. Bakke, "Oxygen effects in anaerobic digestion - ii," *Modeling, Identification and Control*, vol. 31, pp. 55–65, 2 2010, ISSN: 03327353. DOI: 10.4173/mic.2010.2.2.

[95] V. Fedorovich, P. Lens, and S. Kalyuzhnyi, "Extension of anaerobic digestion model no. 1 with processes of sulfate reduction," *Applied Biochemistry and Biotechnology*, vol. 109, pp. 33–46, 1-3 2003, ISSN: 0273-2289. DOI: 10.1385/ABAB:109:1-3:33.

[96] E. L. Barrera, H. Spanjers, K. Solon, Y. Amerlinck, I. Nopens, and J. Dewulf, "Modeling the anaerobic digestion of cane-molasses vinasse: Extension of the anaerobic digestion model no. 1 (adm1) with sulfate reduction for a very high strength and sulfate rich wastewater," *Water Research*, vol. 71, pp. 42–54, Mar. 2015, ISSN: 00431354. DOI: 10.1016/j.watres.2014.12.026.

[97] W. Ahmed and J. Rodríguez, "Modelling sulfate reduction in anaerobic digestion: Complexity evaluation and parameter calibration," *Water Research*, vol. 130, pp. 255–262, Mar. 2018, ISSN: 00431354. DOI: 10.1016/j.watres.2017.11.064.

[98] L. Pokorna-Krayzelova, K. E. Mampaey, T. P. Vannecke, J. Bartacek, P. Jenicek, and E. I. Volcke, "Model-based optimization of microaeration for biogas desulfurization in uasb reactors," *Biochemical Engineering Journal*, vol. 125, pp. 171–179, Sep. 2017, ISSN: 1369703X. DOI: 10.1016/j.bej.2017.06.009.

[99] L. Pokorna-Krayzelova, D. Vejmelková, L. Selan, P. Jenicek, E. I. P. Volcke, and J. Bartacek, "Final products and kinetics of biochemical and chemical sulfide oxidation under microaerobic conditions," *Water Science and Technology*, vol. 78, pp. 1916–1924, 9 Dec. 2018, ISSN: 0273-1223. DOI: 10.2166/wst.2018.485.

[100] H. S. Jensen, P. N. Lens, J. L. Nielsen, *et al.*, "Growth kinetics of hydrogen sulfide oxidizing bacteria in corroded concrete from sewers," *Journal of Hazardous Materials*, vol. 189, pp. 685–691, 3 May 2011, ISSN: 03043894. DOI: 10.1016/j.jhazmat.2011.03.005.

[101] X. Xu, C. Chen, D.-J. Lee, *et al.*, "Sulfate-reduction, sulfide-oxidation and elemental sulfur bioreduction process: Modeling and experimental validation," *Bioresource*

Technology, vol. 147, pp. 202–211, Nov. 2013, ISSN: 09608524. DOI: 10.1016/j.biortech.2013.07.113.

[102] A. H. Nielsen, J. Vollertsen, and T. Hvitved-Jacobsen, "Kinetics and stoichiometry of aerobic sulfide oxidation in wastewater from sewers-effects of ph and temperature," *Water Environment Research*, vol. 78, pp. 275–283, 3 Mar. 2006, ISSN: 10614303. DOI: 10.2175/106143005X94367.

[103] F. Moretta, E. Rizzo, F. Manenti, and G. Bozzano, "Enhancement of anaerobic digestion digital twin through aerobic simulation and kinetic optimization for co-digestion scenarios," *Bioresource Technology*, vol. 341, p. 125 845, Dec. 2021, ISSN: 09608524. DOI: 10.1016/j.biortech.2021.125845.

[104] S. Weinrich and M. Nelles, "Critical comparison of different model structures for the applied simulation of the anaerobic digestion of agricultural energy crops," *Bioresource Technology*, vol. 178, pp. 306–312, Feb. 2015, ISSN: 09608524. DOI: 10.1016/j.biortech.2014.10.138.

[105] S. Weinrich and M. Nelles, "Systematic simplification of the anaerobic digestion model no. 1 (adm1) – model development and stoichiometric analysis," *Bioresource Technology*, vol. 333, p. 125 124, Aug. 2021, ISSN: 09608524. DOI: 10.1016/j.biortech.2021.125124.

[106] O. Bernard, Z. Hadj-Sadok, D. Dochain, A. Genovesi, and J.-P. Steyer, "Dynamical model development and parameter identification for an anaerobic wastewater treatment process," *Biotechnology and Bioengineering*, vol. 75, pp. 424–438, 4 Nov. 2001, ISSN: 0006-3592. DOI: 10.1002/bit.10036.

[107] E. Petre, D. Selişteanu, and D. Şendrescu, "Adaptive and robust-adaptive control strategies for anaerobic wastewater treatment bioprocesses," *Chemical Engineering Journal*, vol. 217, pp. 363–378, Feb. 2013, ISSN: 13858947. DOI: 10.1016/j.cej.2012.11.129.

[108] J. A. Arzate, M. Kirstein, F. C. Ertem, *et al.*, "Anaerobic digestion model (am2) for the description of biogas processes at dynamic feedstock loading rates," *Chemie Ingenieur Technik*, vol. 89, pp. 686–695, 5 May 2017, ISSN: 0009286X. DOI: 10.1002/cite.201600176.

[109] O. Bernard, M. Polit, Z. Hadj-Sadok, *et al.*, "Advanced monitoring and control of anaerobic wastewater treatment plants: Software sensors and controllers for an anaerobic digester," *Water Science and Technology*, vol. 43, pp. 175–182, 7 Apr. 2001, ISSN: 0273-1223. DOI: 10.2166/wst.2001.0418.

[110] A. Donoso-Bravo, M. Carballa, G. Ruiz-Filippi, and R. Chamy, "Treatment of low strength sewage with high suspended organic matter content in an anaerobic

sequencing batch reactor and modeling application," *Electronic Journal of Biotechnology*, vol. 12, no. 3, pp. 13–14, 2009.

[111] A. Donoso-Bravo, J. Mailier, C. Martin, J. Rodríguez, C. A. Aceves-Lara, and A. V. Wouwer, "Model selection, identification and validation in anaerobic digestion: A review," *Water Research*, vol. 45, pp. 5347–5364, 17 Nov. 2011, ISSN: 00431354. DOI: 10.1016/j.watres.2011.08.059.

[112] E. Ficara, S. Hassam, A. Allegrini, A. Leva, F. Malpei, and G. Ferretti, "Anaerobic digestion models: A comparative study," *IFAC Proceedings Volumes*, vol. 45, no. 2, pp. 1052–1057, 2012.

[113] S. Hassam, E. Ficara, A. Leva, and J. Harmand, "A generic and systematic procedure to derive a simplified model from the anaerobic digestion model no. 1 (adm1)," *Biochemical Engineering Journal*, vol. 99, pp. 193–203, Jul. 2015, ISSN: 1369703X. DOI: 10.1016/j.bej.2015.03.007.

[114] A. Allegrini, "Anaerobic digestion modelling : A comparison between adm1 and amoco," Politecnico di Milano, 2010.

[115] R. Rota, *Fondamenti di termodinamica dell'ingegneria chimica*, 2nd ed. Pitagora, 2015.

[116] D. W. Green and R. H. Perry, *Perry's Chemical Engineers' Handbook (8th edition)*. McGraw-Hill Professional Publishing, 2007.

[117] P. Sadrimajd, P. Mannion, E. Howley, and P. N. L. Lens, "Pyadm1: A python implementation of anaerobic digestion model no. 1," *bioRxiv*, 2021. DOI: 10.1101/2021.03.03.433746. [Online]. Available: https://www.biorxiv.org/content/early/2021/03/04/2021.03.03.433746.

[118] X. Flores-Alsina, C. K. Mbamba, K. Solon, *et al.*, "A plant-wide aqueous phase chemistry module describing ph variations and ion speciation/pairing in wastewater treatment process models," *Water Research*, vol. 85, pp. 255–265, Nov. 2015, ISSN: 00431354. DOI: 10.1016/j.watres.2015.07.014.

[119] M. H. Zwietering, I. Jongenburger, F. M. Rombouts, and K. van 't Riet, "Modeling of the bacterial growth curve," *Applied and Environmental Microbiology*, vol. 56, pp. 1875–1881, 6 Jun. 1990, ISSN: 0099-2240. DOI: 10.1128/aem.56.6.1875-1881.1990.

[120] K. M. C. Tjørve and E. Tjørve, "The use of gompertz models in growth analyses, and new gompertz-model approach: An addition to the unified-richards family," *PLOS ONE*, vol. 12, e0178691, 6 Jun. 2017, ISSN: 1932-6203. DOI: 10.1371/journal.pone.0178691.

[121] M. Celis-García, F. Ramírez, S. Revah, E. Razo-Flores, and O. Monroy, "Sulphide and oxygen inhibition over the anaerobic digestion of organic matter: Influence of

microbial immobilization type," *Environmental Technology*, vol. 25, pp. 1265–1275, 11 Nov. 2004, ISSN: 0959-3330. DOI: 10.1080/09593332508618367.

[122] H. H. Rachford and J. Rice, "Procedure for use of electronic digital computers in calculating flash vaporization hydrocarbon equilibrium," *Journal of Petroleum Technology*, vol. 4, no. 10, pp. 19–3, 1952.

List of Figures

List of Tables

Acknowledgements

The author would like to thank the company *Thöni Italia S.r.l.* for the courtesy of the data provided.

1-